12-2015

Application of Starch-Based Nanoparticle Colloidal Dispersion in Curtain Coating

Ting Chen
Western Michigan University, ting.chen3303@gmail.com

APPLICATION OF STARCH-BASED NANOPARTICLE COLLOIDAL DISPERSION IN CURTAIN COATING

by

Ting Chen

A dissertation submitted to the Graduate College
in partial fulfillment of the requirements
for the degree of Doctor of Philosophy
Chemical and Paper Engineering
Western Michigan University
December 2015

Doctoral Committee:

Margaret Joyce, Ph.D., Chair
Paul D. Fleming, Ph.D.
Steven Bloembergen, Ph.D.
Do Ik Lee Ph.D.

APPLICATION OF STARCH-BASED NANOPARTICLE COLLOIDAL DISPERSION IN CURTAIN COATING

Ting Chen, Ph.D.

Western Michigan University, 2015

In this research, a conventional petro-based latex was partially replaced with a biobased latex in a curtain coating. A common petro-based rheology modifier used in curtain coatings, which is relatively costly and difficult to disperse, was also replaced with two inorganic rheology modifiers. The influence of these materials on coating rheology and curtain stability was thoroughly examined.

In the rheological study, the interactions between biopolymer nanoparticles and inorganic rheology modifiers were found to improve the rheological properties of the biobased latex coatings. Changes in the rheological properties of the coatings were found to depend on the type of rheology modifier used and ratio of rheology modifier to biobased latex. The extensional viscosity of each coating was measured by two methods; Capillary Break-up Extensional Rheometry (CaBER) and Squeeze/Pull-off Test (SPOT). As a novel method, the results from SPOT correlated well with CaBER results demonstrating its usefulness as a new analytical tool.

In a stability study, the effects of biobased latex and rheology modifiers on curtain stability were examined. A correlation between the surface tension and CaBER filament lifetime was revealed. Curtain stability studies were performed on a slot die over a flow rate range of 20 to 65 mL/s. It was found that the curtain stability significantly improved

after adding petro-based rheology modifier, as well as the inorganic rheology modifiers when biobased latex was present. The relative importance of coating surface tension, shear rate dependence of viscosity, viscoelasticity, as well as extensional viscosity to curtain stability at different flow rates was learned.

As a final study, coating formulations were adjusted for the application on a slide die by changing the latex type and surfactant amount. Curtain stability was improved by increasing latex substitution in the presence of inorganic rheology modifier. The impacts of biobased latex and inorganic rheology modifier on the properties of coated linerboard were examined in terms of brightness, gloss, and dry pick strength. Coatings containing one of the two inorganic rheology modifier chemistries were found to be very promising. It is believed that this research advances the application knowledge for biobased latex in commercial curtain coating operations.

ACKNOWLEDGEMENTS

I would like to express my sincere appreciation to my advisor Dr. Margaret Joyce for all the efforts she made to teach, help and guide me throughout my graduate study. Not only did she teach me with her profound professional knowledge, but she also showed me how an excellent woman engineer as well as a good professor should be. I am also very grateful to Dr. Paul D. Fleming for his patient teaching and help during my study.

This research is a joint project between Western Michigan University and EcoSynthetix. Sincere thanks to everyone involved in making this happen. I especially would like to thank Dr. Steven Bloembergen for his time, guidance and support throughout my study and Dr. Do Ik Lee for his insight and advice on my research.

My special and deep appreciation goes to my parents, Linsheng Chen and Yuqiu Gong. Nothing I have achieved in my life would have happened without their love and support. Thank my mom for being strict with me and disciplining me when I was a child and thank my dad for believing in me and unconditionally supporting my dream even it was thought to be impossible at the time. Sorry for being so far away from you for years and not being able to take care of you as a daughter. Thanks to all my other families for helping my family whenever needed, especially my aunt Guizhen Gong and my cousin Tian Tian. At last, I want to thank all my friends for their company and support, including Yumeizhi Jia, Xiaomeng Bu, Ruoxi Ma, Chenying Liu, and Bilge Altay, etc.

Ting Chen

TABLE OF CONTENTS

ACKNOWLEDGEMENTS ii

LIST OF TABLES vi

LIST OF FIGURES viii

CHAPTER 1

I. LITERATURE REVIEW 1

Paper Coating Technology 1

Curtain Coating Technology 8

Curtain Stability and Operability 11

Sheet Forming Zone 12

Curtain Flow Zone 15

Impingement Zone 29

Stretchability of Coating Curtain 35

Thickeners in Paper Coating 46

Replacement of Latex with Biobased Latex Binder 48

Latex 48

Biobased Latex Binder 53

Objectives 60

References 60

II. PIGMENTED FORMULATIONS CONTAINING BIOBASED NANOPARTICLE BINDERS FOR CURTAIN COATING APPLICATIONS; PART 1: RHEOLOGICAL STUDY 71

Table of Contents −Continued

CHAPTER

Abstract 71

Introduction 72

Experimental 77

Materials 77

Methods 81

Results and Discussion 84

Shear Rheometry 85

Extensional Rheometry 99

Conclusions 104

References 105

III. PIGMENTED FORMULATIONS CONTAINING BIOBASED NANOPARTICLE BINDERS FOR CURTAIN COATING APPLICATIONS; PART 2: CURTAIN STABILITY STUDY 111

Abstract 111

Introduction 112

Experimental 118

Results and Discussion 121

Conclusions 134

References 135

IV. PIGMENTED FORMULATIONS CONTAINING BIOBASED NANOPARTICLE BINDERS FOR CURTAIN COATING APPLICATIONS; PART 3: COATABILITY STUDY 138

Abstract 138

Table of Contents –Continued

CHAPTER

Introduction 139

Experimental 141

Results and Discussion 145

Conclusions 150

References 151

V. CONCLUSIONS AND OUTLOOK.....154

APPENDICES 157

A. Data Obtained from SPOT Experiments 157

B. Data Obtained from the Analysis of Slot-fed Curtain Stability 161

LIST OF TABLES

1.1 Critical properties of coatings required in different processes 4

1.2 Characteristics and benefits of curtain coating 7

1.3 A summary of techniques for the measurement of static/dynamic surface tension coating 22

1.4 Critical parameters measuring the ratios of competing forces in the impingement zone 30

1.5 Comparison of conventional and associative thickeners 47

1.6 Comparisons of coating performance and coated paper properties imparted by different types of latex 50

1.7 Experimental determined effective volume factors of biobased latex and SB latex samples 55

2.1 Coating formulations of the controls 79

2.2 Coating formulations for petro-based extensional viscosity modifier 79

2.3 Coating formulations for the inorganic rheology modifier study 80

2.4 Basic properties of control and coatings with petro-based extensional viscosity modifier 84

2.5 Basic properties of coatings with inorganic rheology modifiers A and B 85

3.1 A list of symbols used in Chapter III 115

3.2 R^2 values of cubic regression fitting of the data in Figures 3.15, 3.17, 3.19 128

4.1 Coating formulations for the controls 143

4.2 Coating formulations for the petro-based extensional viscosity modifier study 143

4.3 Coating formulations for the inorganic rheology modifier study 144

4.4 Basic coating properties 146

LIST OF FIGURES

1.1 General sequence of addition during coating makedown 3

1.2 Blade coater 5

1.3 Air knife coater 5

1.4 Rod coater 5

1.5 A multilayer curtain coater 6

1.6 Coverage profile of blade coating 7

1.7 Coverage profile of curtain coating 7

1.8 Schematic diagram of a slot-fed curtain die 9

1.9 Schematic diagram of a modified slot-fed curtain die 9

1.10 Schematic diagram of a slide-fed die with feeding nozzle 10

1.11 Schematic diagram of a reversed slide-fed die 11

1.12 Schematic diagram of a two-merging slide-fed die 11

1.13 Flow zones in slot-fed curtain coating 12

1.14 Flow zones in slide-fed curtain coating 12

1.15 Teapot effect: migration of the contact line and its hysteresis 14

1.16 Forces at the free edge of a liquid curtain 16

1.17 Surface tension in front and back surfaces of a curtain generated by slide die 21

1.18 The corresponding relation of pressure and bubble growth 23

1.19 Formation of Mach wave and Mach angle α 25

1.20 Development of boundary layer along a simplified curtain guide 27

1.21 Vertical and horizontal velocity profiles along the width direction of the curtain .. 28

List of Figures−Continued

1.22 Local edge thinning (neck-in) of the curtain near an edge guide 29

1.23 Dynamic wetting of curtain impinging the web at different capillary numbers 31

1.24 A general operational window for the curtain coating process 33

1.25 Contraction of a pulled coating curtain 33

1.26 Heel formation and down-web striation 33

1.27 Heel formation and pulled film with the change of U/V or Re at Ca=100 34

1.28 Puddling pattern in the CD direction of a coated paper 34

1.29 Capabilities of different techniques for extensional viscosity measurement 38

1.30 A series of the filament stretching images from FISER 39

1.31 An example of the evolution of filament diameter as a function of time on the capillary breakup extensional rheometry (CaBER) 40

1.32 The evolution of normalized filament radius as a function of time for three fluids, Newtonian fluid, Boger fluid (a model elastic fluid), and a pressure sensitive adhesive 43

1.33 The change of apparent extensional viscosity as a function of Hencky strain for three fluids, Newtonian fluid, Boger fluid (a model elastic fluid), and a pressure sensitive adhesive 43

1.34 Influences of latex on the whole coating and converting process 48

1.35 Illustration of an internally crosslinked biobased latex nanoparticle 54

1.36 Schematics showing the deformation of water-swollen crosslinked biobased latex nanoparticles under high shear rates 56

1.37 Schematics showing the deformations of different particles in the paper coatings 56under high shear rates 56

1.38 An example of particle size of biobased latex nanoparticle colloidal dispersion measured by different technologies 59

1.39 Particle size comparison of biobased latex nanoparticles colloidal dispersion with 59the other conventional binders used in paper coatings 59

List of Figures−Continued

2.1 The evolution of coating sample during a SPOT test 82

2.2 Steady state flow results of all coatings 88

2.3 Steady state flow results of coatings with petro-based extensional viscosity modifier 92

2.4 Viscoelasticity (tan δ) of all coatings obtained from frequency sweeps 93

2.5 Viscoelasticity (tan δ) of coatings with and without petro-based extensional viscosity modifier changing with frequency 94

2.6 Elastic moduli (G') of coatings with and without petro-based extensional viscosity modifier changing with frequency 94

2.7 Viscoelasticity (tan δ) of the control coating XSB-3 and coatings containing inorganic rheology modifier A changing with frequency 96

2.8 Elastic moduli (G') of the control coating XSB-3 and coatings with inorganic rheology modifier A changing with frequency 96

2.9 Viscoelasticity (tan δ) of the control coating XSB-3 and coatings containing inorganic rheology modifier B changing with frequency 98

2.10 Elastic moduli (G') of the control coating XSB-3 and coatings with inorganic rheology modifier B changing with frequency 98

2.11 SPOT Results of all the coatings 100

2.12 The time dependence of filament midpoint diameter of control coatings 103

2.13 The time dependence of filament midpoint diameter of coatings containing petro-based extensional viscosity modifier 103

2.14 The time dependence of filament midpoint diameter of coatings with inorganic rheology modifier A 103

2.15 The time dependence of filament midpoint diameter of coatings with inorganic rheology modifier B 103

2.16 An example of the axial asymmetric initial liquid bridge formed and amplified during the initial stretching 104

3.1 Curtain stability tester with a slot-fed die 120

List of Figures−Continued

3.2 Dynamic surface tension of controls and coatings with petro-based extensional viscosity modifier 122

3.3 Surface tension of controls and coatings with petro-based extensional viscosity modifier at bubble lifetime of 9.0 s 122

3.4 Dynamic surface tension of controls and coatings with inorganic rheology modifier A 123

3.5 Surface tension of controls and coatings with inorganic rheology modifier A at bubble lifetime of 9.0 s 123

3.6 Dynamic surface tension of controls and coatings with inorganic rheology modifier B 124

3.7 Surface tension of controls and coatings with inorganic rheology modifier B at bubble lifetime of 9.0 s 124

3.8 Correlation of the surface tension and CaBER filament lifetime of the control coatings 125

3.9 Correlation of the surface tension and CaBER filament lifetime of coatings with biobased latex and petro-based extensional viscosity modifier 125

3.10 Correlation of the surface tension and CaBER filament lifetime of the coatings with biobased latex and inorganic rheology modifier A 125

3.11 Correlation of the surface tension and CaBER filament lifetime of the coatings with biobased latex and inorganic rheology modifier B 125

3.12 Coating density changing over time 126

3.13 Brookfield viscosity of coating changing over time 126

3.14 Correlation of pump setting and volumetric flow rate of curtain 127

3.15 Weber numbers of coatings XSB-1, XSB-3 and EX-1 changing with curtain volumetric flow rates 129

3.16 Comparison of shear thinning behavior of coatings XSB-1, XSB-3 and EX-1 130

List of Figures−Continued

3. 17 Weber numbers of coatings containing biobased latex and inorganic rheology modifier A, and control coating XSB-3 changing with curtain volumetric flow rates 131

3. 18 Comparison of shear thinning behavior of coatings EA-2 and EA-3 132

3. 19 Weber numbers of coatings with 35% latex replacement and inorganic rheology modifier B, and control coating XSB-3 changing with curtain volumetric flow rates 133

3. 20 Comparison of shear thinning behavior of coatings XSB-3 and EB-2 133

4.1 Curtain stability tester with a slide-fed die 145

4.2 The correlation between the pump setting/density and coat weight 147

4.3 The correlation between brightness and coat weights of all coated samples 148

4.4 The correlation between gloss (MD and CD) and coat weights of all coated samples.....149

4.5 The correlation between IGT dry pick strength and coat weights of all coated sample 150

CHAPTER I

LITERATURE REVIEW

Paper Coating Technology

It is well known that the properties of a paper have a great influence on print quality. The application of a coating improves the optical, print and functional properties of paper, such as gloss, brightness, smoothness, ink density, dot roundness, oil resistance and water resistance. Though about 80% of all coated paper properties depend on the properties of the base paper, a coating is still required to fill the voids in the paper in order to create a uniform surface for best print quality [1].

A coating is comprised of coating pigments, binders and additives. The weight fraction of each component in the dry coating varies according to the coated grade of paper being produced, but commonly 80%-95% of the coating is pigment, 5%-20% of the coating is binder and 2% of the coating is additives [1]. Water is also an essential component of the formulation, which makes it possible to mix all the components together, to transport the coating, and to apply the coating evenly on the base paper. The content of water can be up to 30 wt. %. After drying, the coating layer may contain up to 50% pigment, 20%-30% binder, 25%-35% air and 1%-3% additives (% by volume) [2].

Pigments used in paper coating can be grouped into two categories; main pigments and specialty pigments. The main pigments include clay/kaolin, ground calcium carbonate (GCC) and talc, while precipitated calcium carbonate (PCC), calcined clay,

plastic pigments, alumina trihydrate and titanium dioxide are specialty pigments. Specialty pigments are used to compensate for the lack of properties obtainable by the main pigments alone. They typically comprise a small fraction of the total pigment used in a coating formulation and as a rule of thumb, consist of no more than 10% of the total pigment used in a formulation [1].

Binders in a coating formulation bind the pigment particles with each other and to the base paper, while filling part of the voids between the pigment particles. They have a great impact on the overall runnability of the coatings (rheological properties, water retention, drying, etc.), the final properties of the coated paper (stiffness, strength and optical properties, etc.), and the printability of the coated paper (ink-coating interactions) [1].

There are two types of binders: natural binders (starch and protein) and synthetic binders (styrene butadiene and styrene acrylic latexes, PVAc and PVOH). The selection of binder should take into account the end-use requirements of the coated paper, the rheological properties of the coating, the drying capability on machine, and the other components present in the coating, especially the pigment type to assure that desired coating strength, optical properties and print properties are achieved.

Coating additives are used at relatively low dosage levels but are very important to the end-use performance and runnability of the coating on the coater. The most common types of additives are dispersants, lubricants, pH control agents, defoamers, water retention aids, rheology modifiers, optical brightening agents (OBA), dyes and

colorants, insolubilizers, biocides/preservatives, and other functional agents (anti-skin agents, special surfactants, etc.) [1].

A general sequence for the order of addition of coating components is shown in Figure 1.1 [1]. The sequence of addition is important to prevent or minimize the interaction between coating components, which may lower the efficiency of their properties.

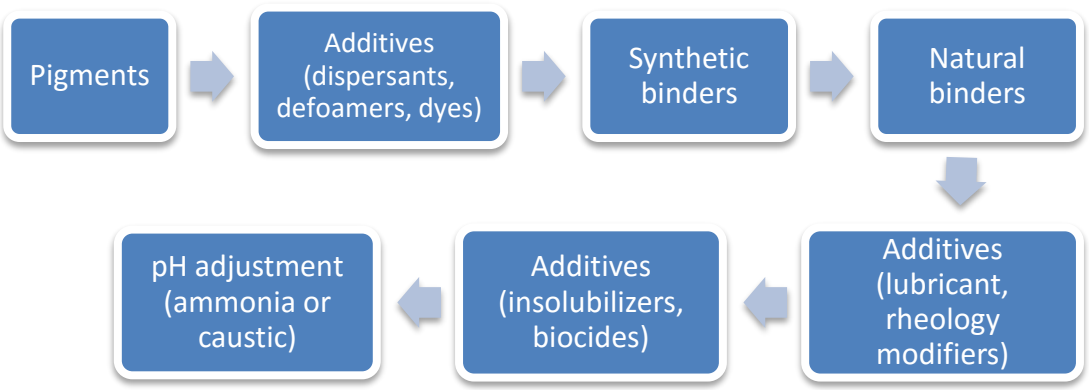

Figure 1.1: General sequence of addition during coating makedown.

The different units of operation involved in the coating and finishing of paper and paperboard, as well as a list of the important coating properties to each process, are provided in Table 1.1.

Table 1.1: Critical properties of coatings required in different processes.	
Processes	**Critical Coating Properties**
Coating	Rheology Water Retention
Drying	Film Formation Porosity
Finishing	Calenderability Structure Stability
Printing	Porosity Surface Energy Pick Strength Paper Gloss Printability

A coater station is generally comprised of an applicator and a metering element [1]. The applicator applies coating onto the basesheet and the metering element removes the excess coating to achieve a desired coat weight. These two actions can occur simultaneously or sequentially in any combination of orders determined by the basesheet properties, end product requirements and coating rheology. Various types of applicators are available for different paper coating processes, including pond/puddle, fountain, roll, short dwell or low angel jet, etc. Among metering systems, blade, rod and air knife are all categorized as post-metering systems (Figures1.2-1.4). A curtain coater is one of the most attractive pre-metering systems for its product uniformity and process productivity (Figure 1.5)

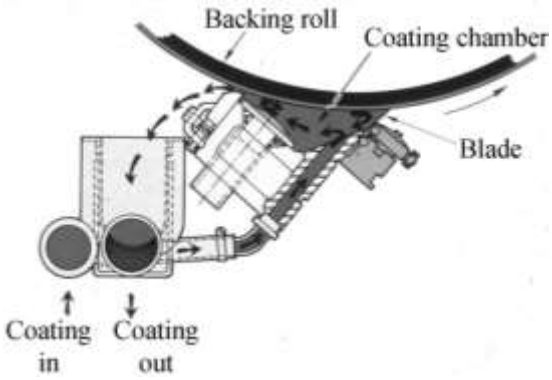

Figure 1.2: Blade coater [3].

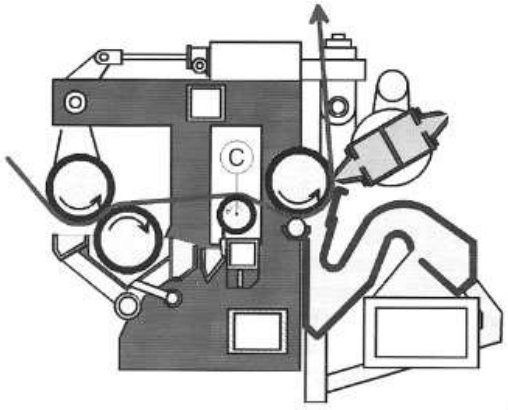

Figure 1.3: Air knife coater [1].

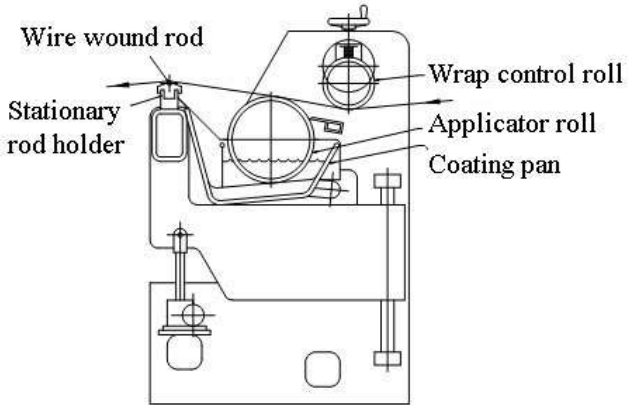

Figure 1.4: Rod coater [3].

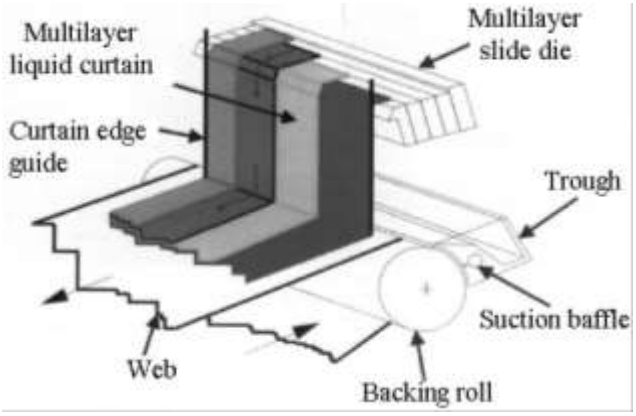

Figure 1.5: A multilayer curtain coater [4].

Different metering elements result in different coating coverage, which has a great impact on the surface and optical properties of the coated paper. Compared with blade or rod coated paper, curtain coated papers have a more uniform coating thickness, similar to that of air knife coated papers (Figures 1.6, 1.7) [5]. The uniform coating structure contributes to uniform ink absorption that improves the printability of the substrate. Due to the contoured coating profile, the surface properties of a curtain coated paper highly depend on the roughness of the basesheet. In addition, because no metering element directly contacts the basesheet, a curtain coater is not required to meet the higher strength requirements of a blade or rod coater for good runnability. This could also minimize streaking on the coated papers that is one of the common defects on a blade/film coater.

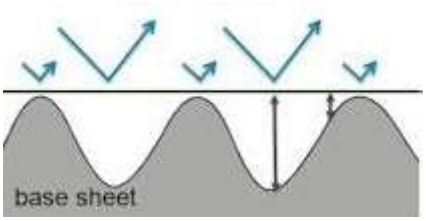

Figure 1.6: Coverage profile of blade coating [5].

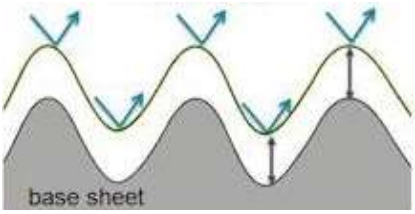

Figure 1.7: Coverage profile of curtain coating [5].

As another non-contact coating technology, air knife coating is very similar to curtain coating in terms of coating coverage. Air knife coaters have been the preferred coating application method in the paperboard industry for quite a while, but they are limited by multiple operational disadvantages including limited speed and coating solids, application amount, frequent cleaning required, poor runnability and noise [6]. Curtain coating is able to provide similar characteristics without these limitations (Table 1.2).

Table 1.2: Characteristics and benefits of curtain coating [6].

Characteristics	**Benefits**
Perfect coverage	Improved printability
Excellent runnability	Less break time
High solids contents	Reduced drying energy
Ease of operation	Lower coat weight
High efficiency	Higher content of recycled fibers
No wearing parts	
Excellent handling	
Optimum CD and MD coat weight profiles	

Curtain Coating Technology

Curtain coating is not a new technology. It has been used outside the paper industry for more than a century [7]. Up until the 1960s, it has been applied for the production of continuous webs, such as aluminum foil and corrugated paperboard [8]. Since the 1990s, it has found use in the production of specialty paper, such as thermal paper and carbonless paper. Nowadays, curtain coating has been adapted to produce a wide range of paper grades including printing paper, graphic paper, and paperboard, etc. [4].

In principle, curtain coating goes through a die to form a smooth curtain. The curtain falls freely onto the surface of a substrate where the coating creates a contour profile (Figure 1.7). As a result, it provides excellent coating coverage regardless of coat weight, and the thickness of the coating layer is independent of substrate roughness [3]. No coating recirculation is needed, which helps keep the system simple and clean and also helps to maintain a high quality of coating. Curtain coating can run at high speed with fewer web breaks and lower maintenance costs than other coating processes [9, 10]. Besides these advantages, it can also be designed to apply multiple coating layers simultaneously, which further improves productivity. In spite of these advantages, there are some inherent difficulties mainly related to the stability of the curtain. Much research has been done in this area over past decades [4, 9-20]. From these studies, some basic requirements were concluded, for example, low dynamic surface tension (30 mN/m), air

bubble free, good high shear stability, good wetting ability on the basesheet, a viscosity between 100-300 cP and so on [3].

The major component of a curtain coater is a die where the coating forms a curtain and falls onto the moving substrate. There are two basic die designs, slot-fed and slide-fed. Modern curtain coaters have been modified which allows the application of multiple coating layers simultaneously onto the continuous web at high speed [4].

The internal design of the curtain die is critical in supplying a uniformly distributed coating flow. A basic slot-fed curtain die is illustrated in Figure 1.8. The distribution system inside is comprised of a distribution chamber and a feed slot, both of which guarantee the uniformity of curtain thickness across the width of the paper machine. A modified slot-fed die is shown in Figure 1.9, where two layers of coating merge in the internal manifold before being extruded through the slot.

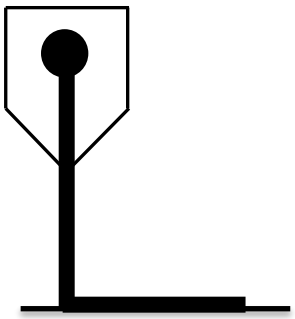

Figure 1.8: Schematic diagram of a slot-fed curtain die.

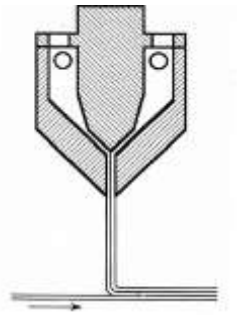

Figure 1.9: Schematic diagram of a modified slot-fed curtain die [11].

A main limitation of the slot-fed curtain die is that it is difficult to apply more than two coating layers simultaneously, while the slide-fed curtain theoretically allows an unlimited number of layers to be coated at the same time [11].

An example of a multilayer slide-fed die is shown in Figure 1.10. Coating is precisely metered by pumps and then fed through the feeding nozzles at a constant flow rate. After it is distributed uniformly in the cavities in the lateral direction, coating is discharged onto the slides where one layer is stacked on top of the next. When the coating accelerates on the elongated slide and flows along the lips, each layer forms a uniform falling film that is guided to a desired width by the edge guides. To keep the curtain stable, air shields are used to protect it from air currents [11].

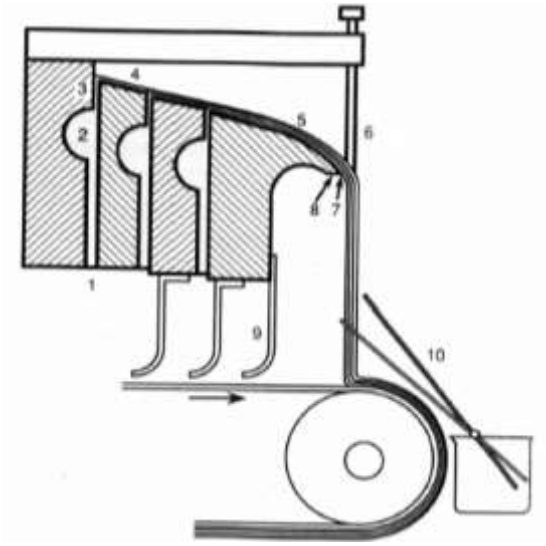

Figure 1.10: Schematic diagram of a slide-fed die with feeding nozzle (1); cavity (2); slot (3); slide (4); elongated slide (5); edge guide (6); lip (7); underside of lip (8); air shield (9); and catch pan for start-up (10) [11].

To optimize the stability and operability of the curtain, various designs of curtain dies have been invented, such as the reversed slide-fed die and the two-merging slide-fed die (Figures 1.11, 1.12). Different designs inherently generate different flow profiles, which together with the different adsorption time of surfactants in the coating, require different process control conditions [11].

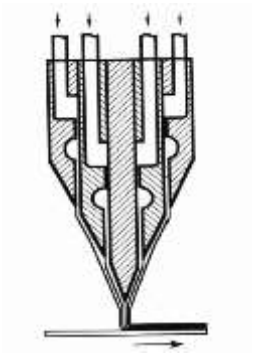

Figure 1.11: Schematic diagram of a reversed slide-fed die [11].

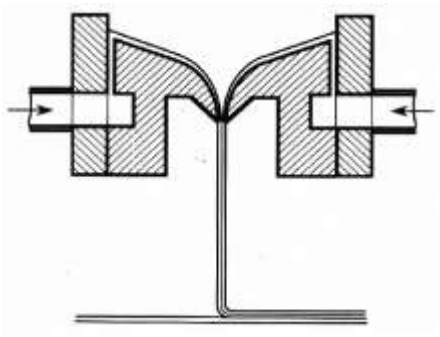

Figure 1.12: Schematic diagram of a two-merging slide-fed die [11].

Curtain Stability and Operability

Curtain stability is the ability of a curtain die to form and maintain a stable curtain over a certain period of time [11]. It is very critical because of its susceptibility to the operational conditions. The successful operation of a curtain coater requires multiple critical parameters to be met in order to guarantee a smooth process. Extensive studies have been conducted in this field from the aspects of flow mechanisms to the operability in production [4, 11, 12]. It has been well accepted that inertial, viscous, capillary and

external forces act on the curtain together and their interactions must be properly managed to maintain curtain stability.

In the analysis of curtain flow, a curtain is usually divided into three zones, i.e. sheet forming zone, curtain flow zone and impingement zone (Figures 1.13, 1.14) [12]. The static contact line is the position where a free surface separates from the solid surface. Depending on the design, there are different static contact lines at the slot exit.

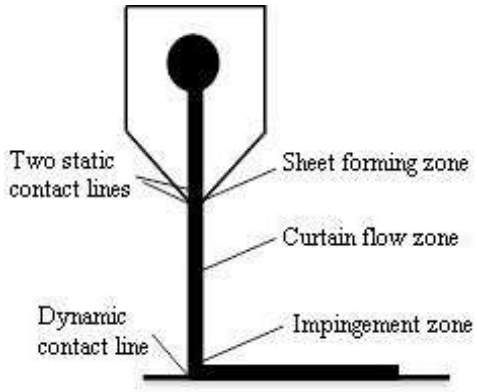

Figure 1.13: Flow zones in slot-fed curtain coating [modified from 12].

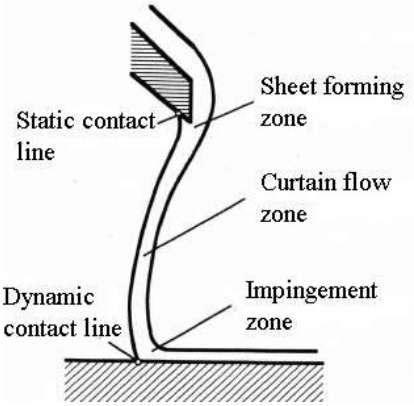

Figure 1.14: Flow zones in slide-fed curtain coating [12].

Sheet Forming Zone

In the sheet forming zone, the topic of most interest is the so-called “teapot effect”, a set of phenomena in which the static contact lines spontaneously advance, retreat, and seemingly attach at the sharp edge of the lip [13]. It is of more concern on slide-fed dies than on slot-fed ones because the lip design of slot-fed die has been optimized [12]. Important studies in this field were conducted and three basic mechanisms related to this were stated. They are the deflection of the liquid sheet by

hydrodynamic forces, contact-angle hysteresis, and purely hydrodynamic hysteresis caused by multiple steady states [13]. These mechanisms were demonstrated experimentally and analyzed theoretically by finite-element methods of analysis [13].

By studying the flow fields in the sheet forming zone, it was revealed that the flow transitions from a shear flow to an extensional flow within a rather small range of $-1< x <3$, where x is the distance from the die exit in the units of half the slot clearance [12]. The interactions of forces at the static contact line give rise to an uneven distribution of stress that sometimes causes a deflection of the falling curtain towards the underside of the lip [12, 13]. The flow rate per unit width Q, or equivalently the Reynolds number ($\mathrm{Re} \equiv \rho Q/\mu$, where ρ is the fluid density; μ is the fluid viscosity), is the key variable in this phenomenon and the deflection exhibits a distinct maximum at an intermediate flow rate [13]. This kind of deflection happens when the static wetting line remains pinned at the sharp corner so it is not a result of the wetting and spreading associated with the static contact line, but purely from hydrodynamic effects [13].

Whether and, if so, how far the liquid wets the lip past the sharp corner is referred to as the contact-angle hysteresis [13]. The conventional contact-angle hysteresis is caused by the differences in advancing and receding contact angles that originate from the surface roughness and inhomogeneity. It was shown that the wetting and movement of the static contact line depends on the static contact angle, the cut-back angle, the separation angle of the interface, the flow parameters Re and Po ($\mathrm{Po} \equiv \sigma(\rho/\mu^4\, g)^{1/3}$, where σ is the fluid surface tension; g is the gravitational acceleration) and the inclined

angle of the slide β [13]. Because of such dependence, hydrodynamic hysteresis exhibits multiple steady states at the same parameter value shown in Figure 1.15.

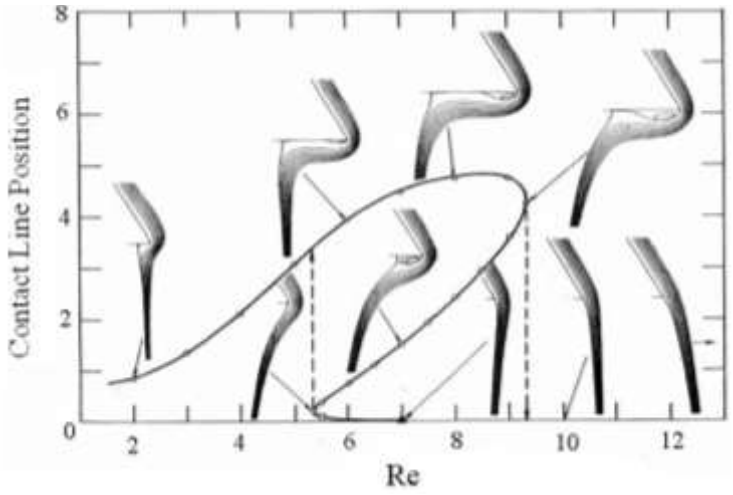

Figure 1.15: Teapot effect: migration of the contact line and its hysteresis (for the purpose of simplicity, the effects of contact angle hysteresis are ignored here) [12, 13].

It was also emphasized that much of the hysteresis seen in the teapot effect is purely hydrodynamic hysteresis in nature, even though it is influenced by contact angle, which exhibits hysteresis itself [12]. The influence of contact angle on the hydrodynamic hysteresis of contact line position was investigated and it was revealed that the hysteresis becomes less and less sensitive to flow rate as the contact angle increases and above a critical angle wetting no longer occurs over the entire range of flow rates as the Gibbs' inequality is satisfied [13]. In addition, it is worth noting that both types of hysteresis make the position of contact line strongly dependent on the history of the preceding back-and-forth movement of the line.

In actual production, especially on slide-fed curtain coaters, undesired teapot effects are associated with down-web striations and streaks on the coated layer, because the uneven wetting underneath the lip may form dried-out deposits in the dead flow zone and cause deviation of curtain from the vertical trajectory [12]. However, it was also claimed that the small deflection by teapot effects is beneficial at a high flow rate, because it forms a bowed-shape dynamic contact line that actually drives small bubbles toward the edges and thereby reduces the air entrainment downstream [14].

Curtain Flow Zone

In the curtain flow zone, curtain stability is most important. Early studies conducted by Brown and Taylor laid the fundamentals for this [15, 16]. Two ways to approach the curtain stability criterion with the concept of Weber number were introduced. It is not hard to tell that the principle behind these two approaches is the same and they both suggest that the curtain maintains stability when We >2.

In the first approach, curtain stability is determined by comparing the propagation velocity of a free edge with the main velocity of the falling curtain. A hole caused by a disturbance can create a free circular edge, which evolves and propagates in the curtain till the curtain ruptures. Thus, it is required that the main velocity of a stable curtain V_c be larger than the propagation velocity V_d of the free edge, which can be obtained through equation (1.1)

$$V_d = \sqrt{\frac{2\sigma}{\rho H_c}} \tag{1.1}$$

where

σ is the surface tension of the fluid;

ρ is the density of the fluid;

H_c is the local thickness of the curtain;

V_d is the propagation velocity of the free edge in the curtain. It could be in any direction.

Thus, the curtain stability criterion can be expressed as:

$$We = \frac{\rho {V_c}^2 H_c}{\sigma} > 2 \tag{1.2}$$

The Weber number (We) is a dimensionless number in fluid mechanics. In the second way, it can be considered as a measure of the relative importance of the fluid's inertial forces compared to its surface tension. ${\rho V_c}^2 H_c$ is the momentum that needs to be destroyed at the boundary, so the resultant force ${\rho V_c}^2 H_c$ has to be larger than the surface tension, i.e. ${\rho V_c}^2 H_c > 2\sigma$ (Figure1.16) [15].

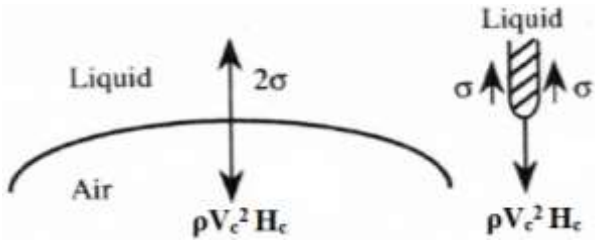

Figure 1.16: Forces at the free edge of a liquid curtain [11].

Furthermore, by substituting the volumetric flow rate Q, the web velocity U, the wet film thickness on the web H_{wet}, and the length of the curtain x measured from the die lip into equation (1.2), the following expression can be attained:

$$We = \frac{\rho {V_c}^2 H_c}{\sigma} = \frac{\rho V_c Q}{\sigma} = \frac{\rho \sqrt{2gx}\, H_{wet} U}{\sigma} > 2 \quad (1.3)$$

Some guidelines that can be concluded from equation (1.3) are; that the curtain stability can be improved with a thicker curtain, faster curtain velocity, higher volumetric flow rate per unit width, and lower surface tension [15]. For instance, surfactants are often added to a curtain coating to reduce the surface tension and propagation velocity, and increase the surface elasticity [11]. According to practical experience, two rules of thumb that have been summarized are: (a) volumetric flow rate per width should be above a minimum of 1.0 cm^2/s and (b) the surface tension needs to be below a maximum of 40 mN/m [4].

However, the criteria introduced above do not take into account the contribution of fluid viscosity to curtain stability. Experimental results suggest that there is an optimum range for liquid viscosity. The stability can be improved by dampening disturbances enhanced by increasing the viscosity. Meanwhile, it accelerates the growth of the boundary layer along the edge guides where the curtain breaks more easily [11, 17]. However, the propagation velocity of the free edge calculated from equation (1.1) is limited for low-viscosity fluids and the curtain of high-viscosity fluids can be stable with We < 2 if the curtain is shorter than a critical length [18]. The critical length increases with the increment of viscosity but it is rather short, which makes this finding lacking in

practical importance [18]. Other research reported that in some circumstances, e.g. spatial or temporal, 2-D or 3-D disturbances where placed, determined if the falling curtains were linearly stable regardless of the Weber number [19-22].

In the curtain flow zone, the other parameter of significance is the final curtain velocity at which the curtain impinges onto the substrate. Several empirical formulas were conjectured to estimate it, but none has succeeded due to the complicated curtain flow arisen from the complex interactions of inertial, viscous, capillary and external forces. For example, viscous forces in the transition zone inhibit the curtain velocity, which is a very short distance from the exiting lip of the curtain. As discussed before, the length of the transition zone is critical for the Weber number rule. To estimate the curtain velocity V_c, Brown proposed an empirical formula the result of which agreed with the velocity measured by his rotating mirror method when the vertical distance X is larger than two or three times X_0 (where X is the vertical distance from the beginning distance X_0, somewhere below the slot) [15]. For curtains with curved trajectories, Kistler obtained a set of integro-differential equations that consists of Reynolds number Re, Stokes number St ($\mathrm{St} = \rho g W^3/\mu Q$) and Capillary number Ca ($\mathrm{Ca} = \rho Q/W\sigma$), where 2W is the slit clearance [12]. These empirical equations are considered important as starting points for various approximations as they were applicable to all sorts of two-dimensional liquid sheets, but they are also very complicated and can only provide exact solutions in special cases [11].

Last but not least, it is worth noting that the relative difference of the final curtain velocity and the web velocity has a significant impact on the curtain behavior and the properties of the coated substrate once it hits the substrate. The ratio of the final curtain velocity and web velocity is usually one of the parameters used to define the operational window of a curtain coater.

Surface tension is the tension at the interface of a gas and a liquid. Its magnitude depends on the effort required to bring the molecules in the volume phase to the surface to achieve a specific surface size. Surfactants, also called surface-active agents, are a group of chemicals capable of reducing the surface tension at the interface by orienting their hydrophilic parts towards the aqueous phase and their hydrophobic parts towards the non-polar phase. By doing this, surfactants are able to reduce the interfacial tension and free energy of the system, which stabilizes the system. The existence of surfactants also promote wetting on the solid surface, which is important to the coating process. For the fact that this adsorption process is not spontaneous but diffusion-controlled, it requires some time to reach its equilibrium state, where the static surface tension is achieved. The time from the beginning of forming a surface or interface to the time of the measurement is called surface age [23]. Obviously, the surface tension of a surfactant-free fluid is independent of the surface age, but the surface tension of fluids with surfactants depends on the surface age. The rate of surfactant adsorption is determined by the surfactant mobility.

Industrial coating processes generally run at very high speed, such that the static surface tension is seldom reached there. Instead, dynamic/non-equilibrium surface tension, which is the local tension measured or estimated, in a flowing solution or on a deforming surface is of more interest. Depending on the time for surfactant adsorption, or the rate of surface deformation, the dynamic surface tension could range from the static surface tension or even lower, to the highest – the surface tension of the solvent. For curtain coating, the surface age of interest is from the time that the curtain exits the slot till it impinges onto the substrates. It is therefore dictated by the height of the curtain. In practice, curtain height is usually 100-300 mm, which gives a falling time on the order of 100-200 ms, accordingly [4]. Obviously, it requires a curtain coating to achieve the optimum surface tension before the surface age of surfactant is reached. The effectiveness of a surfactant in the curtain coating cannot be predicted, so must be determined experimentally. Ideally, the most effective surfactant needs to be chosen and applied at an appropriate concentration to obtain the desired flow conditions. According to the curtain stability guidelines, a low and stable surface tension allows a thinner coating curtain to be coated at a given web speed. However, low surface tension can either prevent the contraction of the curtain by improving the wettability of the edge guide or induce the contraction via Marangoni effect (a mass transfer along an interface between two fluids due to surface tension gradient), which adversely reduces the curtain stability [11].

For the curtain formed in a slide die, the tension of the front and back surfaces is asymmetrical as they start at different positions and flow down on an inclined plane. Figure 1.17 is an example of the surface tension of front and back surfaces of a curtain changing with surface age. The decreasing surface tension is caused by the diffusion and adsorption of surfactant molecules. The temporary increase of surface tension in front is resulted from the lack of surfactant molecules when the front surface reaches the lip where the flow changes [4].

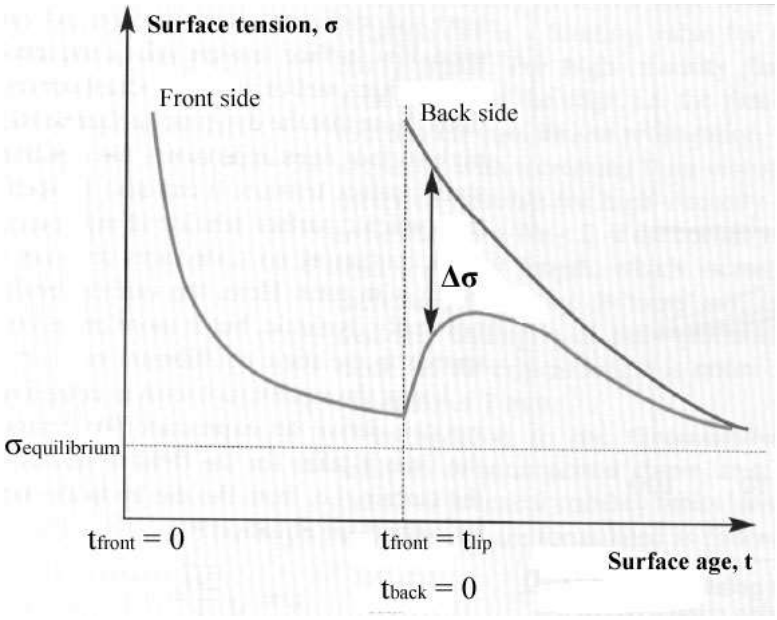

Figure 1.17: Surface tension in front and back surfaces of a curtain generated by slide die [4].

Compared with the curtain formed in a slide die, the surface tension of the coating going through a slot die is more critical, because both curtain surfaces start at the die lip

at the same time with high local surface tension. Hence, the dynamic surface tension of the coating must be estimated experimentally to ensure good curtain stability.

There are various techniques commonly used to measure the static/dynamic surface tension (Table 1.3). Two of them, maximum bubble pressure and falling curtain/Mach angle, were used in this project.

Table 1.3: A summary of techniques for the measurement of static/dynamic surface tension coating [24].

Static Surface Tension	**Dynamic Surface Tension**
Wilhelmy plate	Maximum bubble pressure
Du Nouy ring	Falling curtain (Mach angle)
Capillary rise	Inclined plane
Sessile or pendant drop	Oscillating or vibrating jet
	Overflowing funnel

In the method of maximum bubble pressure, a capillary is immersed with one end in the testing liquid introducing air bubbles at a certain rate. The surface tension can be calculated with the bubble pressure using the Young-Laplace law for any time where the corresponding radius is known [25, 26].

$$\Delta P = \frac{2\sigma}{r} \tag{1.4}$$

where

ΔP is the bubble pressure difference;

σ is the surface tension of the fluid;

r is the bubble radius.

The corresponding relation of pressure and bubble growth is illustrated in Figure 1.18. It shows that the pressure of a bubble reaches its maximum when the radius of the bubble equals that of the capillary. Before or after this point, the radius of the bubble is larger than that of the capillary. The time between the minimum and the maximum pressure is called bubble lifetime (t_l) during which surfactants orient to the surface of the bubble and affect the surface tension reading, accordingly. The remaining time with bubble expansion, inflation and break away is summed up in the dead time (t_d). Hence, the full time cycle is $t_b = t_l + t_d$.

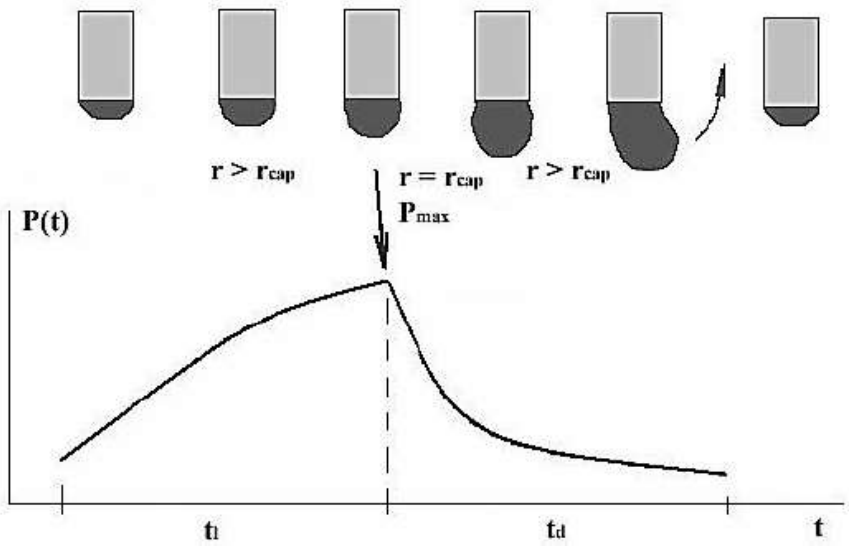

Figure 1.18: The corresponding relation of pressure and bubble growth (modified from [26]).

In the classic bubble pressure method, the surface tension is directly calculated with the maximum pressure in the gas system and the dead time (t_d) is overlooked. Not

only the surface tension but also the capillary radius, which makes the estimation of true surface age even more complicated, determine the dead time [27]. Moreover, this method requires a system volume much larger than the volume of a single separating bubble, while a precise measurement of the bubble lifetime can be performed only if the system volume is relatively small [28]. Therefore, some new methods have been proposed to distinguish bubble lifetime and dead time more precisely in the measurement. For example, instead of using the pressure signal directly, the oscillation of the airflow from the system to the capillary is detected to indicate the interval between two bubbles [29]. In this way, the determination of bubble dead time and lifetime can be more precise and additional errors arising from the system volume can be avoided as well. Other modifications regarding this method can be found in multiple references [24, 30]. Regarding the application of this method in curtain coating, it should be noted that the surface tension of a liquid with a surface age shorter than 200 ms cannot be attained if the low shear viscosity is higher than 120 mPa. s [4]. In other words, it is not recommended to use this method to measure the dynamic surface tension of a curtain coating.

Mach angle, also called falling curtain method, is the most commonly used technique to measure the dynamic surface tension of a curtain coating. In this method, a perturbation is introduced in the curtain flow at a certain height in order to generate a so-called Mach wave as shown in Figure 1.19. Half of the angle formed by the Mach wave is defined as the Mach angle (α) [15].

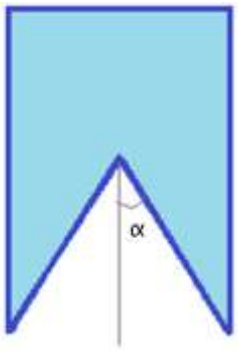

Figure 1.19: Formation of Mach wave and Mach angle α.

In accordance to the aforementioned guidelines for curtain stability, the critical condition of a stable curtain is where the fluid's inertial forces equal its surface tension, i.e. $\rho {V_c}^2 H_c = 2\sigma$ (5). Given the direction of velocity on the Mach wave, equation (5) becomes $\rho {V_c}^2 sin^2(\alpha) H_c = 2\sigma$ (6) [15]. Thus, the local dynamic surface tension can be calculated by the following equation (1.7):

$$\sigma = \frac{\rho H_c {V_c}^2}{2} sin^2(\alpha) \quad (1.7)$$

where

σ is the surface tension of the fluid;

ρ is the liquid density;

α is Mach angle;

V_c is the local curtain velocity;

H_c is the local curtain thickness.

Combining equations (1.2) and (1.7), the relation between Mach angle and Weber number at any given flow point in the curtain can be expressed as equation (1.8) which can be another way to obtain a Weber number on a curtain coater.

$$We = \frac{2}{sin^2(\alpha)} = \frac{\rho H_c {V_c}^2}{\sigma} \tag{1.8}$$

Also, it is worth noting that the accuracy of the Mach angle method is affected by whether the curtain is symmetric or asymmetric [24]. As introduced before, slot dies generate a symmetric curtain, while slide dies do not. The single surface age of the symmetric curtain makes the situation simpler than the asymmetric curtain where the lower surface tension of the front side of the curtain tends to be measured by this method. Extensive studies on this topic can be found in the literature [31, 32].

The function of edge guides on the curtain coater is to maintain the curtain along the width of the paper machine. The curtain stability is also highly affected by the flow fields along the edge guides. In the simplified case, if the edge guide is a stationary rod or plate, the viscous boundary layer grows from the die lip to the bottom of curtain as illustrated in Figure 1.20. Since the velocity within the boundary layer is more likely to be below the propagation velocity, the instability of the curtain close to the edge increases. In addition, the fact that the flow field in reality is three-dimensional incorporates more local variations to the case, let alone different designs of edge guides.

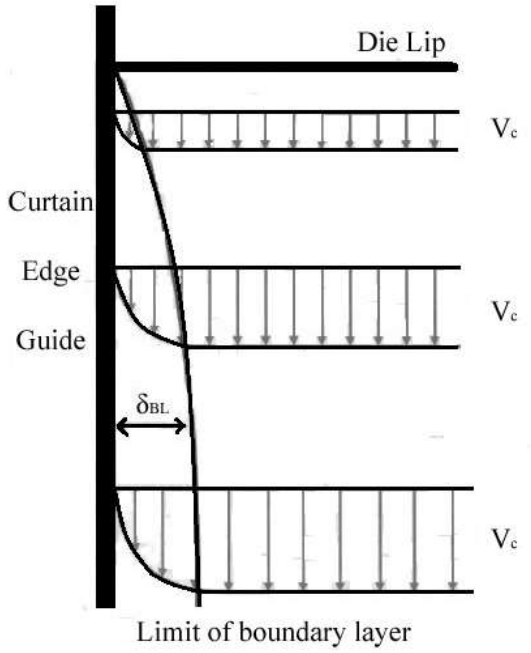

Figure 1.20: Development of boundary layer along a simplified curtain guide [4].

With the liquids having the same viscosity, the profiles of vertical and horizontal velocities as a function of the distance from the edge guide were studied by using a laser-Doppler velocimeter (Figure 1.21) [34]. It was observed that the velocities in the boundary layer accelerate faster than those of outside the layer in both vertical and horizontal directions as the curtain height increases. Moreover, Figure 1.21 (b) reveals that the horizontal velocity goes up to a maximum value before exiting the boundary layer and then decreases farther along the edge. Another study showed that the thickness of the boundary layer increases incrementally with curtain length as well as decreasing shear viscosity [35].

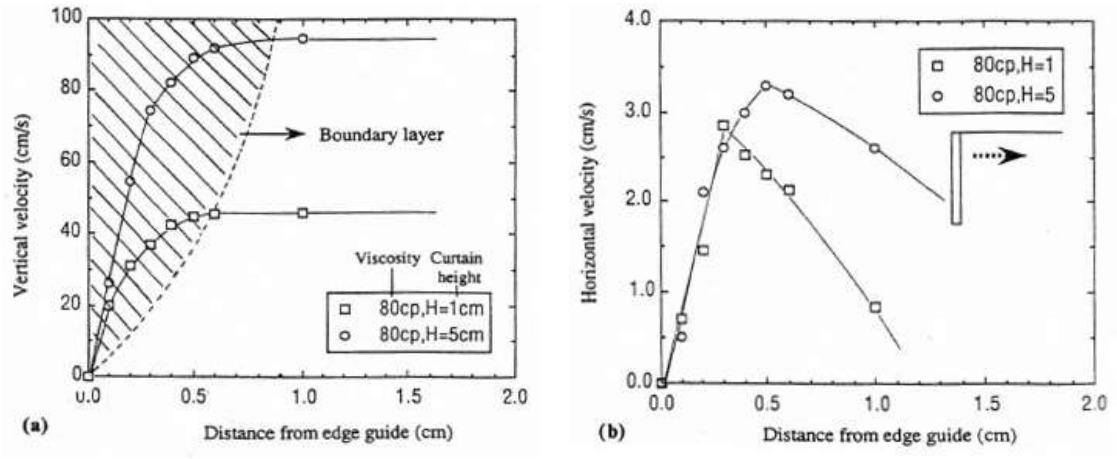

Figure 1.21: Vertical and horizontal velocity profiles along the width direction of the curtain: (a) vertical velocity profile; (b) horizontal velocity profile [34].

In the vicinity of the edge guides, variations of curtain thickness and velocities arise from the capillary force generated by the wetting action of the edge guides and the Marangoni effect caused by the surface tension gradient between the central and the edge regions [34, 36]. The liquid is attracted to the edge guide by capillary forces. Meanwhile, the surface tension gradient pulls it back toward the edge guide. If these actions are out of balance, edge thinning (neck-in) will occur, which increases the risk of curtain breakage (Figure 1.22) [35]. Hence, the local edge thinning can be avoided by adjusting the wetting properties of the liquid and edge guides. As a result, extra curtain fluid or an auxiliary fluid is often fed to the edge zone for this purpose [4].

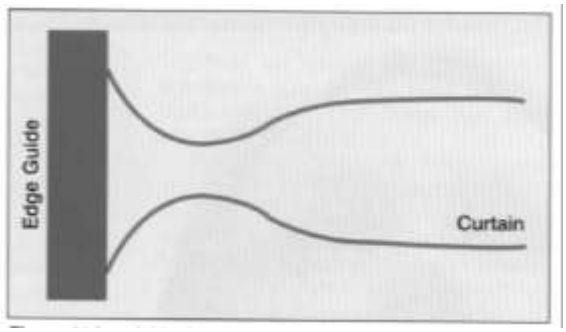

Figure 1.22: Local edge thinning (neck-in) of the curtain near an edge guide [4].

Impingement Zone

The impingement zone is the flow region where the curtain impinges onto the moving web. Curtain coating is usually considered as viscous free surface flows with dynamic wetting lines where the liquid/gas interface appears to intersect the substrate as the liquid continually lands on the solid substrate. Kistler did a profound study in this area, which built the basis for further research [4, 12, 17, 37]. Their findings help us not only solve runnability problems, such as heel formation and air entrainment, but also define the operational window for a curtain coating process. Given the interactions of inertial, viscous, capillary and external forces in the curtain flow, the following dimensionless numbers are usually considered as critically governing in this zone (Table 1.4).

Table 1.4: Critical parameters measuring the ratios of competing forces in the impingement zone.

Dimensionless Number	**Definition**	**Ratio of**
Reynolds number (Re)	$\mathrm{Re} = \rho Q/\mu$	inertial force (acceleration)/net viscous force
Capillary number (Ca)	$\mathrm{Ca} = \mu V/\sigma$	net viscous force/surface tension
Stokes number (St)	$\mathrm{St} = \rho g Q^2/\mu U^3$	gravity (acceleration)/net viscous force
Where, ρ is the fluid density; σ is the fluid surface tension; μ is the fluid viscosity; Q is the volumetric flow rate per unit width; V is the impinging velocity; and U is the web speed.		

In Kistler's studies [12], a curtain was treated as a viscous free surface of an incompressible fluid and the flows in it were considered as two-dimensional steady flows. The conservation equation was then applied in the form of the Reynolds number (Re), Stokes number (St) and speed ratio (U/V). The Re and St values were calculated using the zero-shear-rate viscosity value. The St (typically $St < 10^{-3}$) was found to be insignificant given the thickness of the curtain, which meant that the effect of gravity could be neglected in the impingement zone. The speed ratio (U/V) was used to compare the horizontal momentum outflow with the vertical momentum inflow. The phenomena of dynamic wetting with different capillary numbers (Ca) are illustrated in Figure 1.23. As shown, as the capillary number (Ca) varied, the dynamic wetting lines and apparent contact angle (θ_D) changed accordingly. These changes were suggested as possible triggers for runnability issues, such as heel formation.

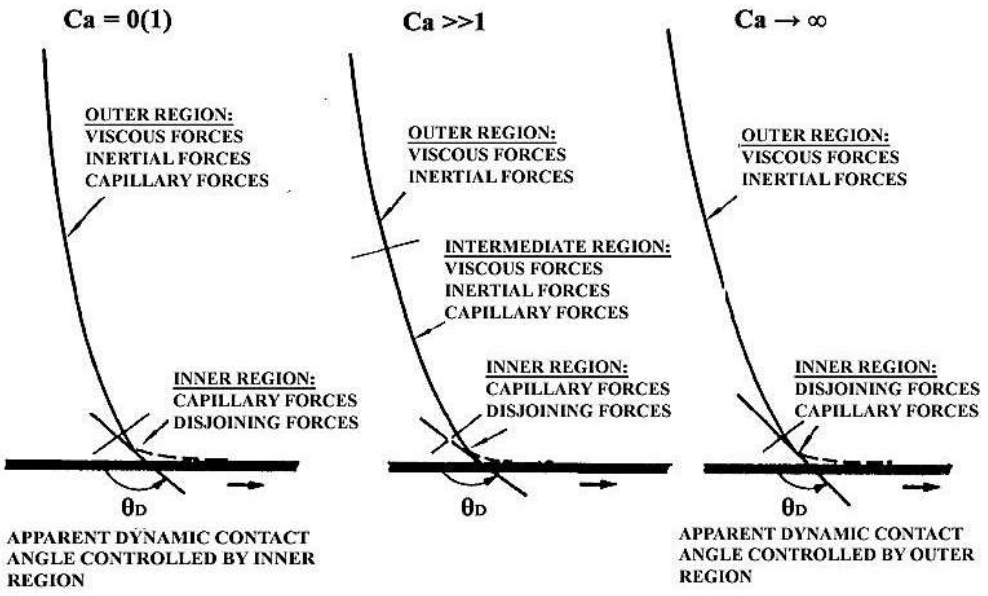

Figure 1.23: Dynamic wetting of curtain impinging the web at different capillary numbers (θ_D is the apparent contact angle) [12].

It was further revealed that for a high capillary number, the aforementioned correlation becomes so insensitive that "high-capillary-number theory" can be applied [12]. This theory accounts for the essential characteristics of curtain flow in the impingement zone and predicts hypothetical limits of coating operability at high capillary numbers. In other words, when viscous stresses overwhelm the capillary pressure, i.e. Ca >>1 (it is also the industrially relevant limit), the Reynolds number Re and speed ratio (U/V) are the only relevant parameters for macroscopic impingement flow. Accordingly, an operational window of the Reynolds number (Re) as a function of the speed ratio (U/V) can be drawn for a high-speed curtain coater.

In accordance to a general operational window summarized by previous studies (Figure 1.24), the phenomena limiting the operability of a curtain coater are [11, 12, 38]:

- At very low Re and U/V, the curtain is pulled by the viscous drag and starts to contract at the edge. It will eventually break as U/V continually increases (Figure 1.25);
- At low Re with U/V increasing, air is easily entrained in the V-shaped air pockets formed at the moving wetting line, which causes surface defects or even coating skips on the paper. In the worst case, the curtain will break;
- At high Re, a heel forms as the dynamic contact line migrates upstream (Figures 1.26, 1.27). The eddy caused by heel formation can trap bubbles, agglomerates, gels or other particles in the coating solution. The tendency of curvy dynamic contact line can also lead to various types of down-web striations (Figure 1.26);
- As U/V increases, the operational window narrows down and the control of the flow rate becomes more critical;
- At high Re and U/V reaching a certain high ratio (approximately $U/V \geq 15$), as a result of both air entrainment and heel formation, puddling occurs as CD-patterns on the coated paper (Figure 1.28). In the presence of a heel, air entrainment becomes massive.

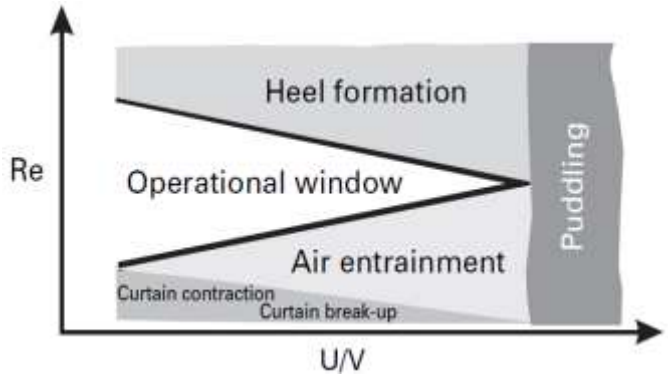

Figure 1.24: A general operational window for the curtain coating process [17].

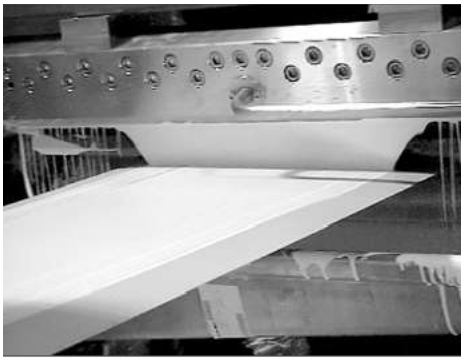

Figure 1.25: Contraction of a pulled coating curtain [38].

Figure 1.26: Heel formation and down-web striation [38].

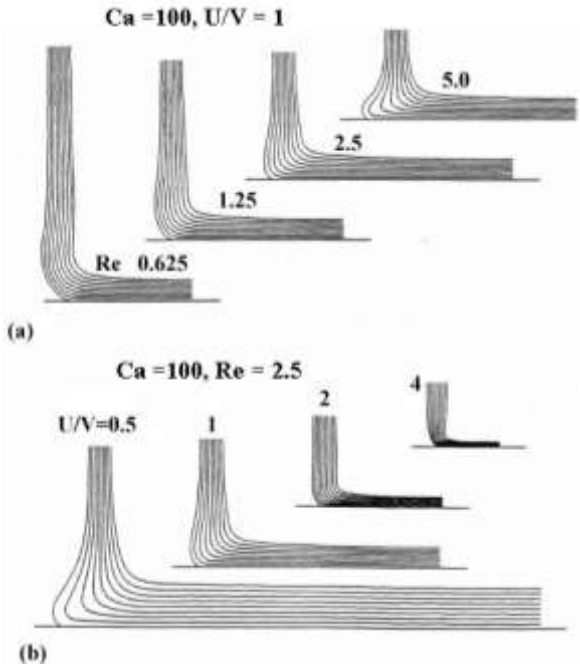

Figure 1.27: Heel formation and pulled film with the change of U/V or Re at Ca=100. (a) U/V=1; (b) Re=2.5 [12].

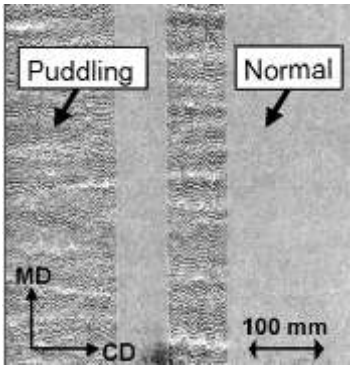

Figure 1.28: Puddling pattern in the CD direction of a coated paper [38].

Although the method to determine the operational window for a curtain coater with the viscosity measured under high shear stress has been proved practically feasible, it is worth mentioning that the dimensionless numbers in Kistler's studies were all

calculated with the zero-shear-rate viscosity, which is a theoretical value extrapolated from experimental results obtained at very low shear rates [11, 17, 38].

Stretchability of Coating Curtain

For a curtain coater, another requirement to ensure smooth operation is the curtain stretchability. Good stretchability means that the curtain can stand a certain degree of stretching or extension without oscillatory effects or breakage. The coating stretchability is a function of the extensional viscosity.

The concept of extensional viscosity was introduced first by Trouton in his paper where he coined a different term "coefficient of viscous traction (η_T)" to attain the shear viscosity η of an incompressible Newtonian fluid through the relationship $\eta_T = 3\eta$ [39]. This is also referred to as "Trouton's law" which was derived when the material is subjected to uniaxial extension. Among the types of extensional deformations, uniaxial extension is the simplest where homogeneous simple extensional flows are generated and the terms of "tensile viscosity" "elongational viscosity" "uniaxial extensional viscosity" or "Trouton viscosity" are all used to describe this type of viscosity. Since this type of extension can rarely be achieved, it is not the most useful material property. As well as uniaxial extension, the other two standard extensions, equibiaxial extension and planar extension, were studied. A general rate of strain tensor **D** for the extensional flows was given [40].

$$\mathbf{D} = \dot{\varepsilon}\begin{bmatrix} 1 & 0 & 0 \\ 0 & m & 0 \\ 0 & 0 & -(1+m) \end{bmatrix} \tag{1.9}$$

where

$\dot{\varepsilon}$ is the rate of strain;

m is the geometry parameter of the extensional flow. It is defined as $\mathrm{m} = \frac{\dot{\varepsilon}_{22}}{\dot{\varepsilon}_{11}}$ in a chosen Cartesian coordinate system $\dot{\varepsilon} = \dot{\varepsilon}_{11} \geq \dot{\varepsilon}_{22} \geq \dot{\varepsilon}_{33}$.

Two extensional viscosities under this general flow can be calculated as follows (τ is the stress) [40].

$$\eta_1^{(m)}(\dot{\varepsilon}, t) = \frac{\tau_{11}-\tau_{33}}{2(2+m)\dot{\varepsilon}} \tag{1.10}$$

$$\eta_2^{(m)}(\dot{\varepsilon}, t) = \frac{\tau_{22}-\tau_{33}}{2(1+2m)\dot{\varepsilon}} \tag{1.11}$$

Thus, for simple uniaxial extension, $\dot{\varepsilon}_{22} = \dot{\varepsilon}_{33} = -\dot{\varepsilon}_{11}/2$, so m= -1/2, $\tau_{22} = \tau_{33}$ and η_2=0; for equibiaxial extension, $\dot{\varepsilon}_{11} = \dot{\varepsilon}_{22}$ and $\dot{\varepsilon}_{33} = -2\dot{\varepsilon}_{11}$, so m=1, $\tau_{11} = \tau_{22}$ and η_1= η_2; for planar extension, $\dot{\varepsilon}_{11} = -\dot{\varepsilon}_{33}$ and $\dot{\varepsilon}_{22} = 0$, so m=0 and there are two extensional viscosities; in general, $-1/2 \leq \mathrm{m} \leq 1$ and two quantities needed to be measured [40- 42].

Theoretically, the extensional viscosity is defined for steady, spatially uniform extensional flows, but this can never be achieved in practical applications. The critical problems involved are [41, 42]:

- how to eliminate the shear stress caused by the flows over stationary boundaries;

- the difficulty in determining the role of strain in non-homogeneous flows;
- the strain required to reach the fluids' steady stress state is usually too large to cause sample ruptures or non-uniform deformation before the measurement takes place;
- the low controllability of flows generated by different geometries, etc.

As a result, no equilibrium extensional viscosity can be attained by using any of those different techniques, i.e. the results of them are all transient. Hence, the concept of "transient extensional viscosity" was brought up and a variety of approximations and averaging techniques were employed. Nevertheless, it seems that transient extensional flows can be achieved in reality, but it was also argued that the term of "transient extensional viscosity" may oversimplify the reality by giving a false indication that one might obtain the same dependence on time from different experimental techniques [42, 43]. The fact is that the "transient extensional viscosity" (as a function of the rates of strain) of one material obtained by different techniques exhibits a wide divergence with one another [44]. Each experiment reveals the deformation of the material to a different extensional flow (with different flow history) and none of them is actually incorrect, per se. It was also found that reporting the transient extensional viscosity as a function of strain instead of a function of the strain rate allowed to present those data more consistently [42]. Therefore, it is recommended that the use of a "transient extensional viscosity" expressed as a function of strain is acceptable when it is carefully defined for a specific experiment that is relevant to the actual flows with extensional deformations taking place for limited times [42].

The extensional rheometers currently used to measure the extensional viscosity of materials can be catalogued as follows [42, 44]:

- The tensile test and the filament rheometer;
- Fiber spinning;
- Stagnation point flows (four-roll mill, opposed jets);
- Converging and contraction flows.

Measuring the extensional viscosity of the low viscosity fluid (10-1000 mPa. s) has been a challenge for many years. Different techniques have been employed, but in general, none of them have succeeded in generating a pure extensional flow, i.e. the extensional viscosity attained from them is only an apparent value (Figure 1.29).

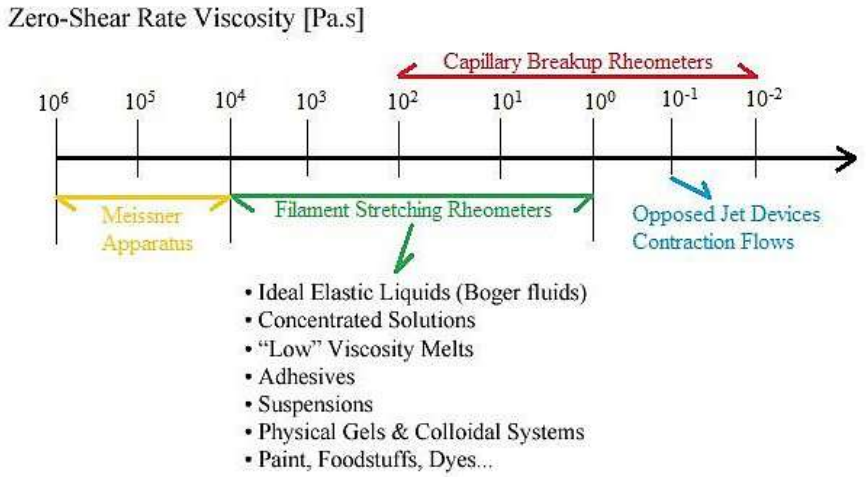

Figure 1.29: Capabilities of different techniques for extensional viscosity measurement (modified from [45]).

By approximating an ideal homogeneous uniaxial elongation, filament rheometry has been applied in this field in the past decades. Two kinds of rheometry are classified in

this category, one is filament stretching extensional rheometry (FISER) and the other is capillary break-up extensional rheometry (CaBER). A detailed comparison of them has been discussed in the reference [45].

Filament stretching extensional rheometry (FISER) generates a cylindrical filament, which is stretched out uniaxially (Figure 1.30). A constant strain rate is employed by imposing an exponential endplate displacement profile to the filament. The evolution of tensile force and the midpoint radius of filament are measured to compute the transient viscosity [45]. Due to the resolution of the force transducer, it is required that the viscosity of the liquid must be above 1 Pa. s [46, 47].

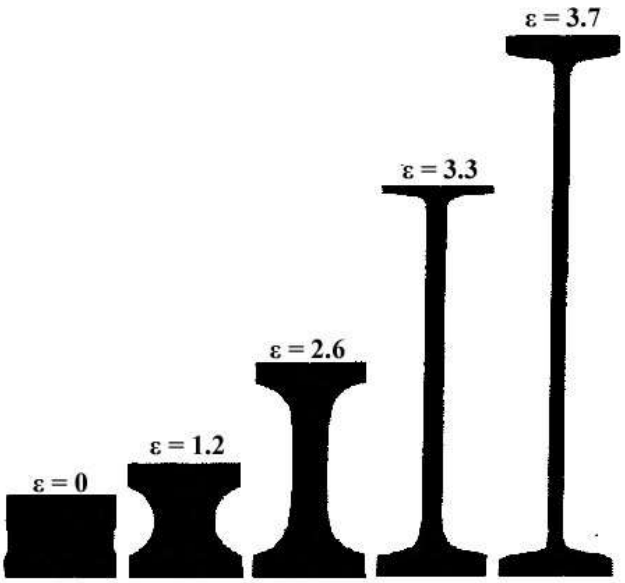

Figure 1.30: A series of the filament stretching images from FISER [45].

In the capillary break-up extensional rheometry (CaBER), the liquid sample is injected between two circular endplates. The endplates separate quickly over a short

distance, during which the initial axial deformation of the sample happens (see images at t = -1 s and t = 0 s in Figure 1.31). Immediately after the cessation of plate separation, a necked but axisymmetric liquid bridge is established and it further evolves until finally breaking (see images from t = 0 s to t/t_c = 1 in Figure 1.31). A laser micrometer monitors the change of the filament midpoint diameter with time (D_{mid} (t)) during the whole process. As a relatively new but low-cost technique, CABER has been gradually applied on the approximation of extensional viscosity of fluids with low zero-shear-rate viscosities ($\eta_0 \leq 100$ mPa. s) [48].

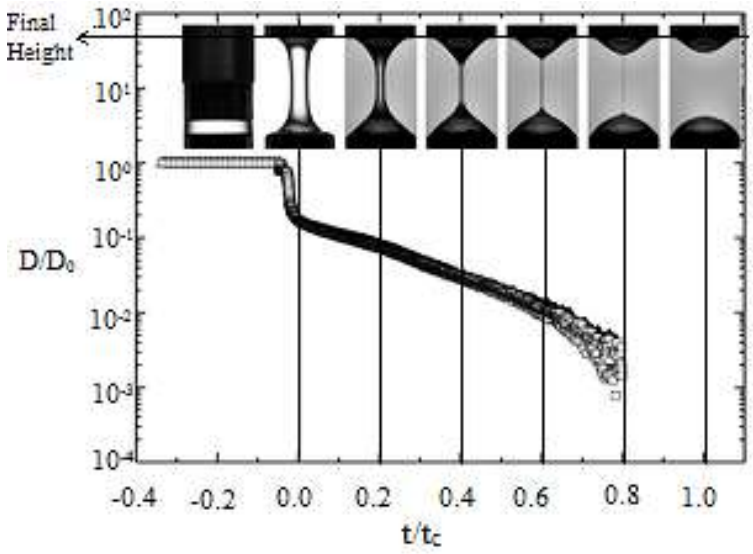

Figure 1.31: An example of the evolution of filament diameter (normalized by the plate diameter D_0) as a function of time (normalized by the breakup time, t_c) on the capillary breakup extensional rheometry (CaBER) (modified from [49]).

The evolution of the liquid filament, i.e. filament necking and thinning, is driven by the capillary pressure (which serves as an effective force transducer) and resisted by

the viscoelastic forces in the liquid. The filament imposed by a rapid prescribed axial step strain undergoes necking and thinning, and eventually breaks at large extensional strain. A generic model of the force balance in this process was proposed [50, 51].

$$\underbrace{3\eta_s\left(-\frac{2}{D_{mid}}\frac{dD_{mid}}{dt}\right)}_{\text{Viscous stress}} = 3\eta_s\dot{\varepsilon} = \underbrace{\frac{F_Z}{\pi(D_{mid}(t)/2)^2}}_{\text{Tensile stress}} - \underbrace{[\tau_{zz}-\tau_{rr}]}_{\text{Elastic/ Non-Newtonian stress}} - \underbrace{\frac{\sigma}{(D_{mid}(t)/2)}}_{\text{Capillary pressure}} \quad (1.12)$$

where

σ is the fluid surface tension;

F_z is the tensile force acting on the column ends;

τ_{ij} denotes the non-Newtonian stresses in different directions;

η_s is the Newtonian viscosity of the solvent.

In equation (1.12), different terms represent different stress components. It is obvious that the solution to this equation depends on how these stress components vary with the deformation rates for different materials [52-54]. Transient apparent extensional viscosity (η_{app}) obtained from CaBER is defined in equation (1.13) [56]

$$\bar{\eta}_{app}(\varepsilon) \equiv \frac{[\tau_{zz}-\tau_{rr}]_{total}}{\dot{\varepsilon}(t)} \quad (1.13)$$

With the fluid surface tension σ and the change of filament diameter as a function of time ($D_{mid}(t)$), the apparent extensional viscosity can be calculated in the following simplified way [54]:

$$\tau_E = \frac{2\sigma}{D_{mid}(t)} \quad (1.14)$$

$$\dot{\varepsilon} = -\frac{2}{\mathrm{D}_{mid}(\mathrm{t})}\frac{dD_{mid}(t)}{dt} \tag{1.15}$$

$$\bar{\eta}_{app} = -\frac{\sigma}{\frac{dD_{mid}(t)}{dt}} \tag{1.16}$$

The total strain accumulated in the material is a Hencky/Logarithmic strain, which is a measure of final strain when the deformation occurs in a series of increments. Knowing the beginning filament diameter D_0, one can calculate the Hencky strain $\varepsilon(t)$ using equation (1.17).

$$\varepsilon(\mathrm{t}) = 2\ln\left(\frac{D_0}{\mathrm{D}_{mid}(\mathrm{t})}\right) \tag{1.17}$$

Accordingly, CaBER provides the graphs of $D_{mid}(t)$ vs. t, η_{app} vs. $\varepsilon(t)$, and η_{app} vs. $\dot{\varepsilon}$ for each experimental analysis. In addition, the evolution of filament shape during the necking and thinning processes can be captured using a high-speed camera on the CaBER with high configuration. Examples of typical results from CaBER are shown in Figures 1.32-1.33.

The experimental data show that the filament diameter of a Newtonian fluid evolves linearly with time and its extensional viscosity approaches a constant in spite of strain, whereas the extensional viscosity of viscoelastic fluid increases as the strain goes up (Figures 1.32, 1.33) [56]. In polymer solutions, the growth of extensional viscosity depends on the concentration and molecular weight of the polymeric solute as well as the background viscosity and thermodynamic quality of the solvent [57].

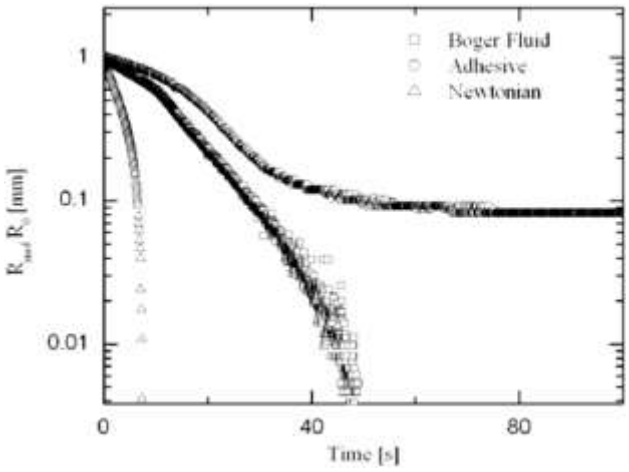

Figure 1.32: The evolution of normalized filament radius as a function of time for three fluids, Newtonian fluid, Boger fluid (a model elastic fluid), and a pressure sensitive adhesive [56].

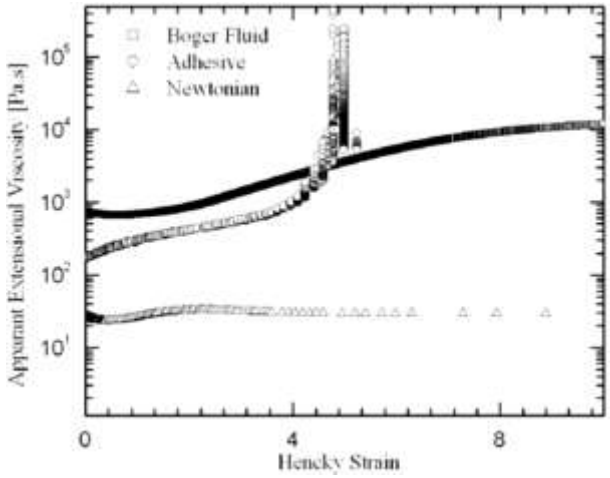

Figure 1.33: The change of apparent extensional viscosity as a function of Hencky strain for three fluids, Newtonian fluid, Boger fluid (a model elastic fluid), and a pressure sensitive adhesive [56].

To ensure the accuracy of CABER measurement, the requirements for multiple intrinsic or naturally occurring length and time scales should be met in order for their complex effects on the dynamics of the thinning and break-up process to be determined.

For instance, it is required that the viscous break-up timescale (t_v) must not be shorter than the plate's separation time (δt_0). This means that the liquid has to be sufficiently viscous to undergo the rapid capillary break-up process before the plates are completely separated. Moreover, for low viscosity non-Newtonian fluids, the effects of fluid inertia complicate the filament thinning process by possibly leading to an inertial oscillation or "beads-on-a-string" morphology [57, 58]. In other words, the studies of the dynamics of capillary break-up rheometry help us to understand and optimize the measurements performed on a CaBER.

Much attention has been given to the investigation of the role of extensional viscosity on curtain stability and operability. On the curtain coater, the curtain is deflected and undergoes extreme extension because of the velocity difference of the curtain and the moving web in the impingement zone. The extension ratio, along with the volume stream of the coating, determines the coat weight. Thus, the way to improve the surface quality of coated paper,, while achieving the desired coat weight, is of great concern in this flow zone. Unfortunately, it is usually overlooked by researchers that a certain stretchability is required to maintain a stable curtain before impingement. It has been stated that the transition from a shear flow to an extensional flow in the sheet forming zone is restricted to a rather small range of $-1<x<3$, where x is the distance from the die exit in units of half the slot clearance [11, 12]. Given the slot clearance and curtain height (100-300 mm [4]) of industrial interest, the height of the curtain undergoing shear flow in the sheet forming zone is actually so short that the significance of curtain stability in extension flow rises in

this area. If the extensional force is too high, the curtain may break or split, and interfere with the impingement zone further. Therefore, more attention needs to be paid to the extensional viscosity in the sheet forming zone too.

Previous studies have shown that there is strong acceleration and stretching forces of the coating and a significant influence of shear thinning effects in the impingement zone [59]. The results further indicated that the stretching zone becomes longer and the acceleration becomes gentler as the coating shear viscosity increases [59]. In other research, it was shown that the coating with low viscoelasticity does not require extensional viscosity to withstand the high shear stress in the impingement zone and the coating actually flows undisturbedly onto the substrate [37]. On the contrary, when a coating with high viscosity and viscoelasticity is running, the extensional viscosity needs to be at certain level to maintain a uniform coating film [37].

Defined as the ratio of extensional viscosity to shear viscosity, Trouton ratio was introduced to the cases where their relative importance needs to be compared. According to Trouton's law, the Trouton ratio of Newtonian fluids is 3 [39]. The Trouton ratio of the paper coating with limited effective thickener was reported to range from 3 to 6 and the ratio around 10 was thought of as the insurance for defect-free curtain runnability [60].

It is clear that the shear viscosity, viscoelasticity and extensional viscosity of a coating, and their impact on the behavior of the coating curtain in the different flow zones are critical. Nevertheless, all the aforementioned criteria for curtain stability and operability only take into account the shear viscosity, such as Weber number >2 and the

determination of the operational window in the graph of Reynolds numbers vs. U/V, etc. Extensional viscosity is usually mentioned separately. It is therefore worth creating a bigger picture where influences of all these properties of interests, individually and together, on curtain stability and operability are discussed together.

Thickeners in Paper Coating

Thickeners are added to paper coatings for the purpose of adjusting their rheological and water retention characteristics. Thickeners must interact with water if the water retention of a coating needs to be increased. Thickeners can also interact with other coating components, especially binders and/or pigments, to provide thickening. Additionally, most thickeners impart pseudoplastic rheological features to the coating (i.e. low viscosity at high shear) in order to ensure good runnability on a coater. The nature and strength of these interactions are dependent of the chemical properties of thickeners. Common types of thickeners added in paper coatings are non-associative and associative thickeners based on natural and synthetic raw materials (Table 1.5).

Table 1.5: Comparison of conventional and associative thickeners [1].		
Functions	**Non-Associative Thickeners**	**Associative Thickeners**
Thickening Effect	high	very high • requires minimum addition level (cost saving) • especially suitable for low solids formulations
Water Retention	medium to high	low • not suitable for processes with critical water holding behavior • requires additional water retention aid
Rheology	pseudoplastic	highly pseudoplastic • low high-shear viscosity • good runnability • reduce blade pressure
Immobilization	slow	fast • bulk coating structure • better coverage

In a curtain coating formulation, adding the right thickener can tailor the stretchability to a desired level without altering the shear viscosity. It has been reported that standard thickeners, such as starch, CMC and synthetic acrylate thickeners (ASE), have very limited effects on extensional viscosity [61]. Thus, some special thickeners are recommended for this purpose in the application of curtain coating, such as polyacrylate-based Sterocoll from BASF.

Replacement of Latex with Biobased Latex Binder

Latex

Various latex polymers are widely used as binders in paper coatings, such as styrene-butadiene (SB), styrene-acrylate (SA), polyvinyl acetate (PVAc), vinyl acrylic (VA) and vinyl acetate-ethylene (VAE), etc. These polymers are usually milky white in appearance and consist of spherical hydrophobic particles with sizes from 20 to 1000 nm [62]. They form stable emulsions in which the particles are stabilized by their surface charge in water.

Although latex polymers only contribute 4%-25% weight in a paper coating [62], their properties have great effects on the quality of the coated product and the entire coating and converting process (Figure 1.34).

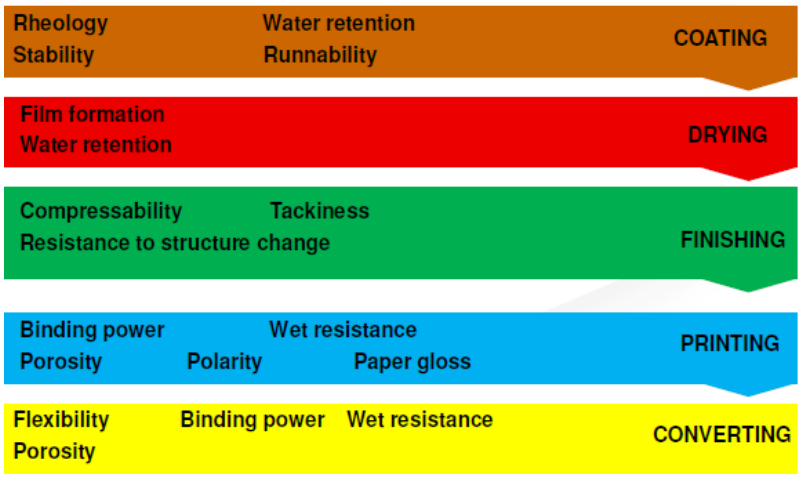

Figure 1.34: Influences of latex on different coating and converting processes [1].

The properties of latex are mainly determined by the ratio and individual properties of co-monomers, as well as carboxylation or other modifications if applied. For papermakers, the characteristics of latex of greatest interest are; particle size, polymer molecular properties (molecular weight, gel%, related to branching, crosslinking, swelling, etc.), glass transition temperature (Tg), minimum film formation temperature (MFFT), colloidal stability, and the mechanical properties of latex films, etc. Different types of latex polymers can be chosen according to the process and product requirements. Comparisons of coating performance and coated paper properties resulting from different latex polymers are summarized in Table 1.6.

Table 1.6: Comparisons of coating performance and coated paper properties imparted by different types of latex (1-best, 2-intermediate, 3-worse) [62].

Properties	**SB**	**SA**	**PVAc**	**VA**	**VAE**
Porosity	2	3	1	1	1
Strength	1	1	3	3	2
Stiffness	2	2	1	1	1
Wet strength	1	1	3	3	2
Blister Resistance	2	2	1	1	1
Board Glueability (AQ/Hot)	2-1	2-1	1-2	1-2	1-2
Light Stability	3	2	1	1	1
Gloss	1	1	2	2	2
Print Gloss	1	1	3	2	2
Brightness	3	2	1	1	1
Coverage/Opacity	2	2	1	1	1
Runnability	1	1	2	2	2
Economics	1-3	1-3	1	1	1

It is well accepted that the way that latex particles bind with each other, pigment particles, and cellulosic substrate in/on the coated paper is so-called “spot welding”. In this mechanism, particle size plays an essential part. By comparing the cross-sectional electron micrographs of coated papers with latex of exaggerated particle sizes (0.3 μm and 0.05 μm respectively), researchers found that the smaller the latex particles are,

greater the level of “spot welding” is in a given volume of coating [1]. Consequently, a less open coating structure is created with smaller particles.

Binding strength is one of the key characteristics of coating binders. Both chemical and structural features in the fiber-pigment-binder-air compositions affect the binding strength of latex polymers. The chemical features have much to do with the surface functionality of the latex polymers and the structural features are impacted by the particle size, viscoelastic properties and the properties of wet coating formulations [1]. For instance, it was found that decreasing particle size, increasing latex carboxylation, and increasing gel% can increase the dry pick strength, a measure of latex binding strength [1].

Through chemical bonding between polymer chains, ultra-high molecular weight polymer networks are developed, which are considered gel formation. In other words, the gel content of latex polymers is related to their internal crosslinking formation that greatly affects their swellability and molecular weight. It was found that latex polymers lose their binding strength with a decrease in gel content because they become cohesively relatively weaker. Reversely, at high gel content, the coalescence of latex is retarded, which diminishes the binding strength. On the other hand, low gel% of latex polymers leads to better blister resistance of coated paper, because the high melt-flow behavior allows them to flow under elevated temperatures and pressures during drying and let water vapor escape. In addition, it was reported that increasing gel% in the range of 40%-70% reduced the porosity of coated paper dramatically, while outside of this range, the

reduction of porosity was relatively minor [61]. It has been reported that typical gel contents in SB latex are in the range of 30%-100% [62].

The glass transition temperature (Tg) is the temperature below which the polymer chain loses segmental macromolecular motions and its freedom of motion causing them to, resist flow and film formation. This characteristic is determined by the types and ratios of co-monomers in the latex polymer. For a latex polymer, the Tg has the greatest impact on its film forming properties, which imparts various properties to the coated paper, such as wet and dry pick, varnish holdout, and gloss, etc. For example, with the increasing styrene content (rigid), gloss generally increases, but eventually SB latex can be expected to become too hard and rigid to form a complete film after drying. As a result, the coating structure on the coated paper becomes weak and porous.

The other critical property relative to the film formation of latex polymers is the minimum film formation temperature (MFFT). At this temperature, the latex starts forming a continuous film. In general, this temperature is near or slightly above the glass transition temperature of the polymer. Both temperatures are very critical when proper processing and drying conditions need to be determined in order to form a good latex film.

A detailed discussion of the influences of synthetic latex composition on the properties of coatings and coated paper is beyond the scope of this work. All in all, there are a large number of latex grades available in the market, meeting different processing

and product requirements. After being studied for many decades, latex binder technology is mature.

Biobased Latex Binder

As the popularity of biopolymers grows rapidly, starch-based nanoparticle colloidal dispersions (referred to as biolatex® emulsions) were introduced into the paper industry about ten years ago. It has been reported that a starch-based nanoparticle colloidal dispersion can replace up to 50% conventional latex binders in a paper coatings [63-70].

Biobased latex binder is available commercially as a dry powder, and is composed of clusters of internally crosslinked nanoparticles, which are produced from starch through the addition of an inorganic rheology modifier via a patented continuous extrusion process [71]. Upon dispersion the powder agglomerates release the individual nanoparticles to form a biobased latex dispersion [72]. The configuration of a biobased latex nanoparticle is illustrated in Figure 1.35. Owing to such unique configurations, biobased latex nanoparticles are water swollen and deformable. Varying the crosslink density, biobased latex nanoparticles have different swell ratios. Consequently, biobased latex emulsions exhibit distinct performance in the wet and dry states.

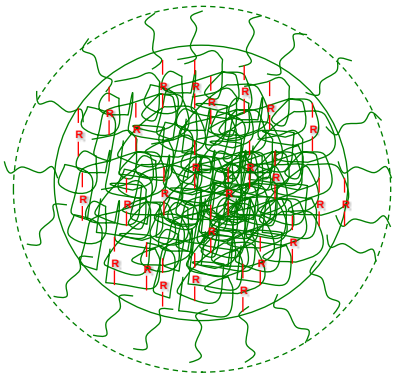

Figure 1.35: Illustration of an internally crosslinked biobased latex nanoparticle (—R— represents an intermolecular crosslink) [72].

So far, research has been conducted to reveal the characteristics of biobased latex binders and their contributions to paper coating properties. The swell ratio is one of the key characteristics. A method to determine the swell ratio of different biobased latex grades was proposed by measuring the relative viscosity using glass Cannon-Fenske and Ubbelohde viscometers [70]. In this method, the relative viscosity ($\eta_r=\eta/\eta_o$) of the biobased latex colloidal dispersion was determined by timing the flow between two demarcations of capillary viscometers for the diluted biobased latex emulsion (η) and the dispersion medium (η_o), which is water. Then using the modified Einstein equation: $\eta_r = 1+2.5f\varphi$ it is fitted to the curve of the relative viscosity (η_r) versus volume fraction (φ) to determine the effective volume factor (f) which implies the value of the volume swell ratio (SR (V)) of the biobased latex nanoparticle [70, 73, 74].

By this means, the effective volume factors, i.e. the volume swell ratios ($SR\ (V) \approx f = [V_{Core\text{-}swollen} + V_{Shell}]/V_{Core\text{-}unswollen}$) of three biobased latex samples were measured previously. Likewise, the volume swell ratio ($SR\ (V) \approx f = [V_{Core} + V_{Shell}]/V_{Core}$) of a SB

latex colloid system was determined with a commercial carboxylated SB latex product as well. The results of these comparisons are shown in Table 1.7 [73, 74].

Table 1.7: Experimental determined effective volume factors of biobased latex and SB latex samples [73, 74].

Sample	**Relative Crosslink Density**	**Effective Volume Factor**
Bio-A	Low	16.58
Bio-B	Medium	10.74
Bio-C	High	6.32
SB Latex		1.4

Further discussion was based on these results [70, 73, 74]: Because the hard-sphere system of SB latex contains virtually no water in the core, its mild swelling is primarily caused by the expansion of the electrical double-layer in the shell upon dilution. Consequently, its internal core volume swell ratio theoretically is $V_{Core\text{-}swollen}$ /$V_{Core\text{-}unswollen}$ = 1.0. By contrast, take the biobased latex sample with f = 6.32 as an example. Although the shell volume (V_{Shell}) of the biobased latex nanoparticle has not been experimentally determined because of the experimental difficulty, it is reasonable to assume $V_{Shell} \approx 2V_{Core\text{-}unswollen}$. Then, the internal core volume swell ratio of becomes 4.32 that corresponds to the unique configuration of biobased latex nanoparticle proposed before.

Owing to the swellability, biobased latex nanoparticles are able to deform and de-swell under high shear and pressure (Figures 1.36, 1.37).

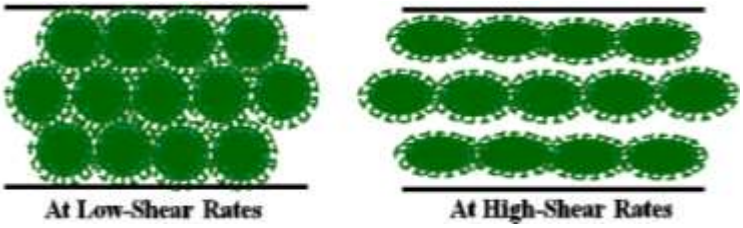

Figure 1.36: Schematics showing the deformation of water-swollen crosslinked biobased latex nanoparticles under high shear rates [70].

The deformation of biobased latex nanoparticle and that of the other hard particles in the paper coating under shearing is illustrated in Figure 1.37.

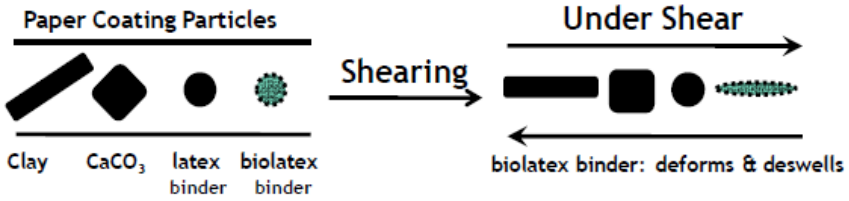

Figure 1.37: Schematics showing the deformations of different particles in the paper coatings under high shear rates [70].

Because of this unique behavior, the coating containing biobased latex binder manifests similar or even better coating performance than its conventional binder counterparts on high-speed coaters in the aspects of rheological properties, dynamic water retention, and wall slip properties, etc.

In the rheology study [74], different rheometers (Cannon-Fenske viscometer, TA AR-2000 stress rheometer, Hercules high shear rheometer, and ACAV A2 Ultra-High Shear capillary and slit rheometers) were used to generate composite rheograms over a

wide range of shear rates. The biobased latex colloids with higher crosslink density were found to behave much like the synthetic latex colloids in most of the range other than the ultra-high shear. Under the ultra-high shearing, biobased latex binders were found to be relatively more shear thinning than the hard particle systems, including synthetic latex and pigment particles that exhibited shear-thickening and dilatancy. At the end, it was concluded that controlling the crosslink density of biobased latex binder enabled the paper coating to meet low and high shear rheological requirements, which ensured its good runnability on a high-speed paper coater.

On the other hand, the dynamic water retention and wall-slip properties of the coating containing biobased latex nanoparticles were elucidated as well [75]. On paper coaters, the interaction between the base paper and the water phase of the coating has to be controlled to avoid an excessive material shift from the coating color to the base paper, otherwise it will cause poor machine runnability, unstable systems and uneven coating layers on the paper. By using gravimetric (lower shear) and dynamic (higher shear) water retention testers, researchers found that the biobased latex binder system helped limit coating dewatering under both low and high shear stresses [75]. The capillary wall-slip measurements using ultra-high shear ACA viscometer (ACAV) showed that biobased latex binders tended to generate higher apparent slip velocities, which indicate better slippage than the coating without it. This corresponds to the theory predicted in an early study where the act of de-swelling and releasing water helped the biobased latex nanoparticles to lubricate jammed solid particles and facilitate flow [70]. Therefore,

biobased latex binders can also function as a unique rheological lubricant in paper coatings.

In addition, the average molecular weight and particle size of biobased latex binders were studied too. It was stated that biobased latex binder is high molecular weight (>1,000,000 g/mole) internally crosslinked biopolymers that are “hidden” within the biobased latex colloid particles in the dispersion [76]. They are usually shipped as dry powders which are agglomerates having about 300 μm average diameters [72]. They are dispersed in water on site to release the nanoparticles. The size of nanoparticles in the colloidal dispersion is essentially determined by the crosslink density and is also affected by the concentration due to its water-swollen nature. This makes it difficult to measure the particle size of biobased latex dispersions. It was claimed earlier that the average size biobased latex nanoparticles in a dispersion is about 100 nm [73], but recent research reveals that this number can range from 20 to 150 nm [76]. Various technologies are being used to detect the particle size distribution of biobased latex dispersions, such as SEM, STEM, HELOS laser diffraction analysis and dynamic light scattering, etc. (Figure 1.38).

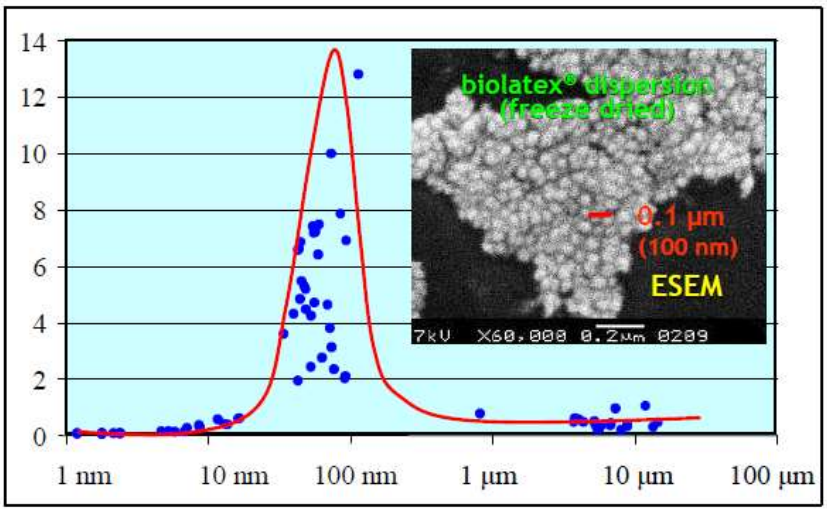

Figure 1.38: An example of particle size of biobased latex nanoparticle colloidal dispersion measured by different technologies [76].

It can still be concluded that the average particle size of the biobased latex binder emulsion is the smallest among all the paper coating binders (Figure 1.39), which contributes to its performance in paper coatings.

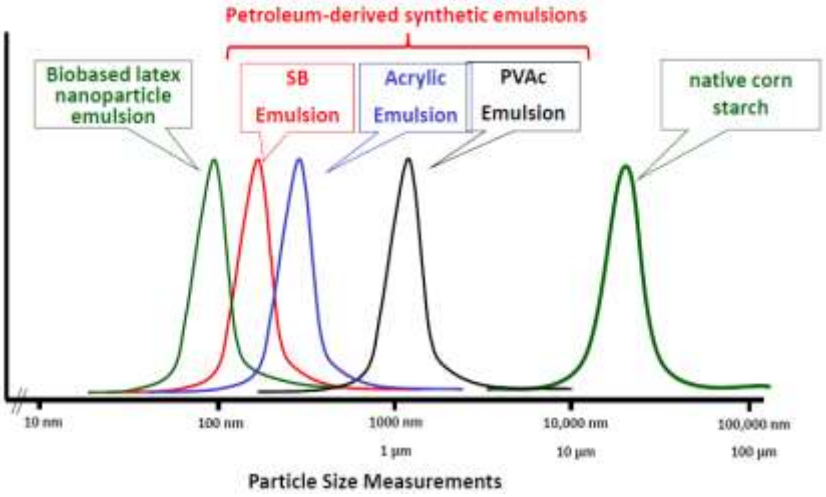

Figure 1.39: Particle size comparison of biobased latex nanoparticles colloidal dispersion with the other conventional binders used in paper coatings [76].

Objectives

To investigate the influences of a biobased latex binder on the coating properties that contribute to curtain stability and coatability, a series of coating formulations of different wt.% biobased latex binder, in replacement of petro-based latex, were studied. Given the special rheological properties required for good curtain stability, two types of inorganic rheology modifiers were added to the biobased latex coatings to determine if in combination they could replace a petro-based extensional viscosity modifier commonly used in curtain coatings. All coatings were characterized in terms of shear rate dependence of shear viscosity, viscoelasticity and extensional viscosity. By studying the effects of these rheology modifiers on coating rheology, the contributions of rheological properties and coating surface tension on curtain stability and coatability were to be clarified. Through insight gained, coating formulations containing biobased latex binders could be better optimized for commercial curtain coating operations resulting in a greener coating solution.

References

1. Esa Lehtinen (Ed.) (2000): “Pigment coating and surface sizing of paper”, Fapet Oy, Helsinki.
2. Rousu, S., Gane, P., Eklund, D. (2001): "Influence of coating pigment chemistry and

morphology on the chromatographic separation of offset ink constituents", 12th Fundamental Research Symposium, FRC-Oxford, UK.

3. Klass, C. (2013): “Blade, rod and contour coaters”, Coating Short Course, Western Michigan University.
4. Schweizer, P. (2003): “Curtain coating-stability a critical operating parameter”, 4th and 5th PITA Coating Conference, Edinburgh, UK.
5. Valmet: “Layering curtain coating”, retrieved on 11/14/2015, from http://www.valmet.com/products/board-and-paper-mills/coating/layering-curtain-coating/.
6. Schmid, M. (2011): “Curtain coater as air knife replacement”, TAPPI PaperCon, New Orleans, USA.
7. Taylor, L.H. (1903): “Machine for production of solidification forming nutriment with whole cover as confectionery and pie”, German Patent Publication DE145517.
8. Poirier, C.C. (1966): “Curtain coating of corrugated paperboard”, TAPPI J., 49(10): p. 66-67.
9. Tripathi, P., Joyce, M., Fleming, P.D. and Sugihara, M. (2009): “A statistical study of process variables to optimize a high speed curtain coater-Part I”, TAPPI J., 8(1): p. 20-26.
10. Tripathi, P., Joyce, M., Fleming, P.D. and Sugihara, M. (2009): “A statistical study of process variables to optimize a high speed curtain coater-Part II”, TAPPI J., 8(2): p. 29-32.

11. Miyamoto, K. and Katagiri, Y. (1997) “Curtain Coating”, Chapter 11c in “Liquid film coating: scientific principles and their technological implications”, ed. Kistler, S.F. and Schweizer, P.M., Chapman & Hall, London.
12. Kistler, S.F. (1983): “The fluid mechanics of curtain coating and related viscous free surface flows with contact lines”, PhD thesis, University of Minnesota, Minneapolis and University Microfilms International, Ann Arbor, MI.
13. Kistler, S.F. and Scriven, L.E. (1994): “The teapot effect: sheet-forming flows with deflection, wetting and hysteresis”, J. Fluid Mech. 263: p. 19-62.
14. Suga, Y., Kobayashi, K., Sasahara, T. and Miyamoto, M. (1991): “Coating method”, European Patent EP 426122 A2.
15. Brown, D.R. (1961): “A study of the behavior of a thin sheet of moving liquid”, J. Fluid Mech. 10: p. 297-305.
16. Taylor, G.I. (1959): “Disintegration of fluid sheets”, Part III in “The dynamics of thin sheets of fluid”, Proc. Roy Soc. A., p.253-313, London.
17. Triantafillopoulos, N., Grön, J., Luostarinen, I., and Paloviita, P. (2004): “Operational issues in high-speed curtain coating of paper, Part 1: The principles of curtain coating”, TAPPI J., 3(11): p.6-10.
18. Alleborn, N., Suenderhauf, G., Raszillier, H., and Durst, F. (2001): “Edge retraction on a planar liquid sheet”, Proceedings of the 4th European Coating Symposium, Bruxelles, Belgium.
19. Lin, S.P. (1981): “Stability of a viscous liquid curtain”, J. Fluid Mech.104, p. 111-

118.

20. Lin, S.P., Lian, Z.W. and Creighton, B.J. (1990): “Absolute and convective instability of a liquid sheet”, J. Fluid Mech. 220: p. 673-689.
21. Do, D.V. and Christodoulou, K.N. (1992): “Multilayer curtain coating flows: stability and sensitivity to small disturbances”, AIChE Spring National Meeting, New Orleans, LA.
22. Finnicum, D.S., Weinstein, S.J., and Ruschak, K.J. (1993): “The effect of applied pressure on the shape of a two-dimensional liquid curtain falling under the influence of gravity”, J. Fluid Mech. 255: 647-665.
23. KRŰSS: “Surface age”, retrieved on 10/29/2015 from http://www.kruss.de/services/education-theory/glossary/surface-age/
24. Tricot, Y.M. (1997): “Surfactants; static and dynamic surface tension”, Chapter 4 in “Liquid film coating: scientific principles and their technological implications”, ed. Kistler, S.F. and Schweizer, P.M., Chapman & Hall, London.
25. Simon, M. (1851): "Recherches Sur La Capillarité", Ann. Chim. Phys., 32: p.5-41.
26. SINTERFACE Technologies: “Bubble pressure analyser BPA-1P”, retrieved on 10/29/2015 from http://www.mpikg.mpg.de/4862784/BPA-1P-Info.pdf
27. Garrett, P.R. and Ward, D.R. (1989): “A reexamination of the measurement of dynamic surface tension using the maximum bubble pressure method”, J. Coll. Interf. Sci., 132: p. 475-490.
28. Fainerman, V.B. and Miller, R. (1998): “The maximum bubble pressure technique,

monograph in ‘Drops and Bubbles in Interfacial Science”, in “Studies of Interface Science”, ed. Möbius, D. and Miller, R., 6: p. 279–326. Elsevier, Amsterdam.

29. Fainerman,V.B., Miller, R. and Makievski, A.V. (2004): “Accurate analysis of the bubble formation process in maximum bubble pressure tensiometry”, Rev. Sci. Instruments, 75: p. 213-221.
30. Fainerman, V.B. and Miller, R. (2004): “Maximum bubble pressure tensiometry-an analysis of experimental constraints”, Advances in Colloid and Interface Science, 108-109: p. 287-301.
31. van Havenberg, J. and Joos, P. (1983): “The dynamic surface tension in a free-falling film”, J. Coll. Interf. Sci., 95: p. 172-182.
32. Balbaert, I., Bleys, G. and Joos, P. (1987): “Measurement of the dynamic surface tension in an asymmetric free-falling film”, J. Coll. Interf. Sci., 115: p. 362-371.
33. Katagiri, Y. (1992): “Analysis of edge effects in curtain coating”, AIChE Spring National Meeting, New Orleans, LA.
34. Nishida, S. (1990): “The formation of flow rate distribution near the edge guide of liquid curtain”, SCEJ 55th Meeting, Nagoya, Japan.
35. Durst, F., Koo, J.B., Wagner, H.G., and Walter, C. (1992): “Experimental study of the boundary layer development at the edge guides in curtain coating”, 2nd International Symposium on coating of Then Film, University of Bradford, UK.
36. Nishida, S., Katagiri, Y., and Suga, Y. (1992): “Coating method.” European Patent EP 0517170A2.

37. Kokko, A., Kettle J., Rautkoski, H., Shen, Y. (2010): “Characterization of curtain coating colors”, TAPPI 11th Advanced Coating Fundamentals Symposium, Munich, Germany.
38. Triantafillopoulos, N., Grön, J., Luostarinen, I., and Paloviita, P. (2004): “Operational issues in high-speed curtain coating of paper, Part 2: Curtain coating of lightweight coated paper”, TAPPI J., 3(12): p.11-16.
39. Trouton, F.T. (1906): “On the coefficient of viscous traction and its relation to that of viscosity”, Proc. Roy. Soc. A 77: p. 426-440.
40. Meissner, J. (1985): “Experimental aspects in polymer melt elongational rheology” Chem. Eng. Commun., 33: p. 159-180.
41. Macosko, C.W. (1994): “Extensional rheometry”, Chapter 7 in “Rheology: Principles, Measurements and Applications”, ed. Macosko, C.W., Wiley-VCH, New York.
42. Petrie, C.J.S. (2006): “Extensional viscosity: A critical discussion”, J. Non-Newtonian Fluid Mech., 137: p. 15-23.
43. Ferguson, J., Hudson, N.E. and Odriozola M.A. (1997): “The interpretation of transient extensional viscosity data” J. of Non-Newt. Fluid Mech., 68 (2-3): p. 241-257.
44. James, D.F. and Walters, K. (1994): “A critical appraisal of available methods for the measurement of extensional properties of mobile systems”, in: A.A. Collyer (ed.), Techniques of Rheological Measurement, Elsevier, New York.
45. McKinley, G.H. (2000): “A decade of filament stretching rheometry”, Proceedings

of the XIIIth International Congress on Rheology, Binding, D.M. et al. (eds.), p.15-22, Cambridge. Presentation slides can be found at "http://web.mit.edu/nnf/presentation/sld001.htm".

46. Tripathi, A., Tam, K.C. and McKinley, G.H. (2006): "Rheology and dynamics of associative polymers in shear and extension: theory and experiments", Macromolecules, 39: p. 1981-1999.
47. Bhardwaj, A. Richter, D., Chellamuthu, M. and Rothstein, J. P. (2007): "The effect of pre-shear on the extensional rheology of worm-like micelle solutions". Rheologica Acta, 46: p. 861-875.
48. Kheirandish, S., Guybaidullin, I, Wohlleben, W. and Willenbacher, N. (2008): "Shear and elongational flow behavior of acrylic thickener solutions. Part I: Effect of intermolecular aggregation", Rheologica Acta, 48(4): p. 397-407.
49. Haward, S. J., Ober, T. J., Oliveira, M.S.N., Alves, M.A., and McKinley, G.H. (2012): "Extensional rheology and elastic instabilities of a wormlike micellar solution in a microfluidic cross-slot device" Soft Matter, 8: p. 536-555.
50. Yarin, A.L.(1993): "Free liquid jets and films: hydrodynamics & rheology, Interaction of Mechanics and Mathematics Series, Longman, Wiley, New York.
51. Renardy, M. (1995): "A numerical study of the asymptotic evolution and breakup of Newtonian and viscoelastic Jets", J. Non-Newt. Fluid Mech., 59: p. 267-282.
52. Entov, V.M. and Hinch, E.J. (1997): "Effect of a spectrum of relaxation times on the capillary thinning of a filament of elastic liquid", J. Non-Newt. Fluid Mech., 72,

pp31-53.

53. Bazilevskii, A.V., Entov, V.M., Lerner, M.M. and Rozhkov, A.N. (1997): “Failure of polymer solution filaments”, Polymer Science Ser. A (translated from Vysokomolekulyarnye Soedineniya Ser. A, p. 474-482), **39**(3): p. 316-324.
54. McKinley, G.H. and Tripathi, A. (2000): “How to extract the newtonian viscosity from capillary breakup measurements in a filament rheometer”, J. Rheol., 44(3): p. 653-671.
55. Schümmer, P. and Tebel.K.H. (1983): “A new elongational rheometer for polymer solutions”, J. Non-Newt. Fluid Mech., 12: p. 331-347.
56. Cambridge Polymer Group, Inc.: “The Capillary Breakup Extensional Rheometer (CaBER™)”, Retrieved on 10/29/2015 from http://www.campoly.com/files/4513/5216/6043/007.pdf
57. Rodd, L.E., Scott, T.P., Cooper-White, J.J., and McKinley, G.H. (2005): “Capillary breakup rheometry of low-viscosity elastic fluids”, Appl. Rheol. 15(1): p. 12–27.
58. Oliveira, M.S.N., Yeh, R., and McKinley, G.H. (2006): “Iterated stretching, extensional rheology and formation of beads-on-a-string structures in polymer solutions”, J. Non-Newt. Fluid Mech., 137: p. 137-148.
59. Alleborn, N., Sünderhauf, H., and Rasziller, H. (2001): “High-speed curtain coating of paper”, PTS Coating Symposium Proceedings, Munich, Germany.
60. Voss, M. and Tadjbach, S. (2003): “Optimizing curtain-coating colours for graphic papers”, PTS Coating Symposium Proceedings, Baden, Germany.

61. Ojanen, M., Sinkko, T., and Kunnas, L. (2007): “Extensional viscosity measurement for curtain coating colours”, PTS Coating Symposium Proceedings, 27: p.1-24, Baden, Germany.
62. Vantresca, D. (2013): “Synthetic binders”, Coating Short Course, Western Michigan University.
63. van Leeuwen, J. (2006): “Paper coating - SBR latex replacement technology”, 2006 TAPPI Coating and Graphic Arts Conference, Atlanta, GA.
64. Klass, C. P. (2007): “New nanoparticle latex offers natural advantage”, Paper360°Magazine, p. 30-31.
65. van Leeuwen, J. (2007): “Update on biopolymer nanoparticle latex development and applications”, TAPPI Coating and Graphic Arts Conference, Miami, FL.
66. Bloembergen, S., McLennan, I., Lee, D.I., and van Leeuwen, J. (2008): “Paper binder performance with nanoparticle biobased latex™: EcoSynthetix develops EcoSphere® biobased latex for replacement of petroleum based latex binders”, ACFS, Montreal, Canada.
67. Bloembergen, S., McLennan, I. J., Lee, D. I., and van Leeuwen, J. (2008): “Paper binder performance with biobased nanoparticles. A starch-based biobased latex can replace petroleum-based latex binders in papermaking”, Paper360ºMagazine, p. 46-48.
68. Figliolino, F.C., Rosso, F., van Leeuwen, J. and Klass, C.P. (2009): “Mill experiences with biobased latex in Brazil”, TAPPI PaperCon Proceedings, Section

19-1.

69. Figliolino, F.C. and Rosso, F., (2009): “Reducing carbon footprint with biobased latex”, Paper360º Magazine, p. 25-28.
70. Lee, D. I, Bloembergen, S., van Leeuwen, J. (2010): “Development of new biobased emulsion binders”, TAPPI PaperCon, Atlanta, GA.
71. van Ballegooie, P., Greenall, P., Bloembergen, S. and DeJong, R., “EcoSphere® biobased latex® binders: Next generation solutions for today’s paper coating industry”, World Pulp & Paper, The International Review for the Pulp and Paper Industry, 2012, 100.
72. Bloembergen, S., McLennan, I.J., van Leeuwen, J., and Lee, D.I. (2010): “Specialty biobased monomers and emulsion polymers derived from starch”, PTS Advanced Coating Fundamentals Symposium, Munich, Germany.
73. Bloembergen, S., VanEgdom, E., Wildi, R., McLennan, I.J., Lee, D.I., Klass, C.P., and van Leeuwen, J. (2010): "Biobased latex binders for paper and paperboard applications", J. of Pulp and Paper Sci., 36(3-4), p. 1-11.
74. Shin, J.Y., Jones, N., Lee, D.I., Fleming, P.D., Joyce, M.K., DeJong, R. and Bloembergen, S. (2012): “Rheological properties of starch latex dispersions and starch latex-containing coating colors”, TAPPI PaperCon, New Orleans, LA.
75. Shin, J.Y., Jones, N., Lee, D.I., Fleming, P.D., Joyce, M.K., DeJong, R. and Bloembergen, S. (2013): “Dynamic water retention properties of biobased latex containing coating colors”, TAPPI PaperCon, Atlanta, GA.

76. Bloembergen, S. (2013): “Advances in Organic Based Binder Chemistries”, Coating Short Course, Western Michigan University.

CHAPTER II

PIGMENTED FORMULATIONS CONTAINING BIOBASED NANOPARTICLE BINDERS FOR CURTAIN COATING APPLICATIONS; PART 1: RHEOLOGICAL STUDY

Abstract

In this work, a conventional petroleum-based styrene-butadiene-acrylonitrile (XSB) latex binder was partially replaced with a biobased latex binder. In addition, a petro-based extensional viscosity modifier that is commonly used in curtain coating applications, which is relatively costly and difficult to disperse, was replaced with two different inorganic rheology modifiers. The results of this work demonstrate that the interaction between the biopolymer nanoparticles and the inorganic rheology modifiers can improve the rheological properties of biobased latex containing coatings in terms of shear rate dependence of viscosity, viscoelasticity, and extensional viscosity. Their functions not only depend on their type, but also the ratio of them *vs.* biobased latex in the coatings. This finding enables papermakers to eliminate the usage of the petro-based extensional viscosity modifier in coatings containing biobased latex. Moreover, in addition to analyzing the extensional viscosity of all the coatings using Capillary Break-up Extensional Rheometry (CaBER), a new and simple method called SPOT (Squeeze/Pull-off Test) was explored using a dynamic stress rheometer. This was demonstrated to be a convenient and effective alternative means of analyzing the extensional viscosity of coating formulations.

Introduction

Curtain coaters have been used by the paper industry for decades, but have recently regained popularity by advancements that enable their use in the high-speed production of various paper grades, such as paperboard, specialty, printing, and graphic papers, etc. [1, 2]. On a curtain coater, the coating goes through a slot-fed or slide-fed die to form a smooth curtain that falls freely onto the surface of a substrate where the coating creates a contour profile. The contour profile creates excellent coating coverage at low coat weights, and the thickness of the coating layer is independent of substrate roughness [3]. No coating recirculation is needed, which helps maintain a high quality of coating and a clean system. Curtain coaters can run at high speed with fewer web breaks and lower maintenance cost than the other coating processes (such as air knife coaters, etc.), and in the case of multi-slot coaters, multiple coating layers can be applied simultaneously to further improve productivity [4, 5].

In spite of these advantages, achieving acceptable curtain stability at high speeds has been a challenge. Curtain stability is the ability of a curtain die to form and maintain a stable curtain over a certain period of time [2]. Due to its susceptibility to operational conditions, a smooth running curtain coater requires multiple critical conditions to be met. Numerous studies have been conducted in this field from the aspects of flow mechanisms to the operability in production [1, 2, 4-12]. Usually, curtain flow is divided into three zones, i.e. a sheet forming zone, a curtain flow zone and an impingement zone (Figures

1.13, 1.14) [2]. In each zone, different parameters need to be controlled in order to achieve a stable curtain and high quality coated surface with desired coat weight.

As with other coaters, the rheological properties of the coating play an important role in the runnability and coatability of a curtain coater. Typically, the coating viscosity is measured using a Brookfield viscometer, which is an acceptable control tool but not capable of predicting the coating performance under high, low or extensional shear conditions. While coatings experience comparatively low shear stresses when passing through different conveying units, such as pumps and pipes, on a high-speed coater high shear stresses are the norm. Thus, the shear-dependent rheological performance of a coating is critical.

The curtain flow behavior of a coating also depends, to a certain extent, on its viscoelastic properties, which affect the extensional viscosity of the coating and its "stretchability". An elastic network structure is typically achieved using polymeric additives to induce particle-polymer interactions in concentrated coating dispersions. This structure influences the rheology through its proportional resistance to strain and recovery within a finite period after cessation of the externally applied stress or strain that deforms the structure [13]. Hence, the investigation of viscoelasticity can reveal the state and recovery of coating microstructure in a coating under different deformations, the state of coating flocculation/deflocculation, sensitivity to structural breakdown upon shearing, and after-shear memory of a coating [13]. It has also been shown that

viscoelasticity prevails during the consolidation of a wet coating after deposition onto a substrate [13].

On a curtain coater, the coating curtain should endure a certain degree of stretching or extension without oscillatory effects or breakage, i.e. sufficient extensional viscosity behavior in order to maintain a good coating stretchability. A number of studies have shown that extensional viscosity, as well as shear viscosity and viscoelasticity, greatly impacts the runnability and coatability of a curtain.

For theoretical considerations, the extensional viscosity is defined for steady, spatially uniform extensional flows, but in practice, the flows are more complex and therefore this can never be perfectly attained [14, 15]. Thus, a variety of approximations and averaging techniques are employed to measure the transient extensional viscosity. In fact, transient extensional viscosity (as a function of strain or strain rate) of one material obtained by different techniques can exhibit a wide divergence, because each experiment reveals the deformation of this material to different extensional flows (and with different flow history) and none of them being necessarily incorrect [16]. Especially for low viscosity fluids, measuring extensional viscosity has been a challenge for many years. There are various types of filament rheometry techniques, including Capillary Break-up Extensional Rheometry (CaBER) and Filament Stretching Extensional Rheometry (FISER). In this work we used a commercially available CaBER instrument, which is an automated and temperature controlled unit in which an applied fluid or semi-solid is gradually extended and the filament that is formed is traced using an imaging device the

output of which is used to create a plot of filament diameter *vs.* time. The technique is suitable for fluids with low zero-shear-rate viscosity from 0.01 to 100 mPa.s [17]. The thinning and break-up of a fluid or semi-solid filament provides valuable information on a material's physical properties. It has been used in the paper industry for coating formulation development and optimization.

With the help of different instruments, researchers have shown extensional viscosity to strongly influence the stability and operability of a curtain coater. Previous work has shown that the transition from a shear flow to an extensional flow in the sheet forming zone is restricted to a rather small range of $-1<x<3$, where x is the distance from the die exit in units of half the slot clearance [2, 6]. Given a slot clearance and curtain height (100-300 mm [1]) of industrial interest, the height of the curtain undergoing shear flow in this zone is so short that the significance of curtain stability in extensional flow dominates in this zone. If the extensional force is too high, the curtain may break or split, and interfere with the impingement zone further. Previous studies also verified that strong acceleration and stretching forces, as well as shear thinning effects, have significant influences on the curtain in the impingement zone [18]. The stretching zone becomes longer and the acceleration becomes gentler as the coating shear viscosity increases [18]. In the impingement zone, the ability of the curtain to endure extreme extension, because of the velocity difference between the curtain and the moving web, is also of great concern due to its direct effects on coat weight and the surface quality of the coated paper. In another study [19], it was reported that a coating of low viscoelasticity does not require

extensional viscosity to withstand the high stress shear of the impingement zone and the coating actually flows undisturbed onto the substrate. However, when a curtain coating formulation having a controlled viscosity and viscoelasticity is running at commercial speeds, the extensional viscosity needs to be at such a level so as to maintain a uniform coating film. Therefore, it is critical to consider the shear viscosity, viscoelasticity, extensional viscosity, and their impacts on the behavior of a curtain coating formulation in the different flow zones.

A biopolymer nanoparticle latex based binder system, which is typically supplied in dry form and then dispersed at the mill to form a biobased latex emulsion (referred to as biobased latex® emulsions), was introduced to the paper industry in 2006. These biobased latex polymers have been shown to be able to replace 25%-50% or more of the conventional latex binders in a paper coating [20-27]. In the dry powder form, the biobased latex binder is composed of clusters of internally crosslinked nanoparticles, which are produced from starch biopolymers and other components through the addition of an inorganic rheology modifier via a proprietary, patented continuous extrusion process [28]. Upon dispersion, the powder agglomerates release the individual nanoparticles to form a biobased latex dispersion [29]. The nanoparticles are swollen by water and are deformable. The swellability of the particles can be altered by their crosslink density. As a result, biobased latex nanoparticles deform and de-swell under high shear and pressure, which imparts unique properties to the coating in both wet and dry states (Figure 1.36).

Multiple studies have shown coatings containing biobased latex binder provide similar or better coating performance than conventional binder formulations on high-speed coaters with respect to rheological properties, dynamic water retention, and wall slip properties, etc. [30-33].

In this paper, coatings containing different levels of biobased latex binder and different types of rheology modifiers were formulated and their rheological properties were studied. Based on the results, some coating formulations were selected for further evaluation of their curtain stability and coatability [34].

Experimental

Materials

Coatings were formulated in accordance with Tables 2.1-2.3. The petroleum-based styrene-butadiene-acrylonitrile (XSB) latex binder used in this study was Prostar 5405 (formerly Dow, then Styron, now Trinseo), and the petro-based extensional viscosity modifier was Sterocoll DF 3 from BASF. The biobased latex used was EcoSphere® X202 from EcoSynthetix. The surfactant used was BASF Lumiten ISC and the dispersant was BASF Dispex N40. The GCC used was Hydrocarb 90 from OMYA. The clay used was KaMin Hydragloss 90. As shown, two control coatings containing all latex were prepared (Table 2.1). In addition, three groups of coatings were formulated with petro-based extensional viscosity modifier, inorganic rheology modifier A and B

respectively (Tables 2.2 and 2.3). The petro-based extensional viscosity modifier is a common additive used in conventional curtain coatings. To determine its effect on biobased latex binder, the first group of coatings was studied (Table 2.2). The two inorganic rheology modifiers were investigated to determine if their interactions with the biobased latex binder could be used to eliminate the need for the petro-based extensional viscosity modifier (Table 2.3). The weight percentages of latex replaced with biobased latex binder were 25%, 35%, and 45%, which are respectively denoted as EX-1, -2 and -3. The amount of inorganic rheology modifier added to each formulation was determined by matching the Brookfield viscosity for the control coating XSB-3. The target ranges of pH, %solids, and Brookfield viscosity of the coatings at 100 RPM were 8.5-9.0, 60.45-60.60%, and 200 - 300 cP, respectively. Note, the %solids were determined using a CEM Smart System 5 Microwave Analyzer.

Table 2.1: Coating formulations of the controls.		
	XSB-1	**XSB-3**
	pph	pph
GCC	70	70
Clay	30	30
Petro-based Latex	12	12
Petro-based Extensional Viscosity Modifier	0	0.25
Surfactant	0.2	0.2
Dispersant	0.2	0.2

Table 2.2: Coating formulations for petro-based extensional viscosity modifier.			
	EX-1	**EX-2**	**EX-3**
	pph	pph	pph
GCC	70	70	70
Clay	30	30	30
Petro-based Latex	9	7.8	6.6
Biobased Latex	3	4.2	5.4
Petro-based Extensional Viscosity Modifier	0.25	0.25	0.25
Surfactant	0.2	0.2	0.2
Dispersant	0.2	0.2	0.2

Table 2.3: Coating formulations for the inorganic rheology modifier study.						
	Inorganic Rheology Modifier A			Inorganic Rheology Modifier B		
	EA-1	**EA-2**	**EA-3**	**EB-1**	**EB-2**	**EB-3**
	pph	pph	pph	pph	pph	pph
GCC	70	70	70	70	70	70
Clay	30	30	30	30	30	30
Petro-based Latex	9	7.8	6.6	9	7.8	6.6
Biobased Latex	3	4.2	5.4	3	4.2	5.4
Inorganic Rheology Modifiers A/B (Proprietary)	13.3% dry weight of biobased latex	7.14% dry weight of biobased latex	2.78% dry weight of biobased latex	6.92% dry weight of biobased latex	3.0% dry weight of biobased latex	0.8% dry weight of biobased latex
Surfactant	0.2	0.2	0.2	0.2	0.2	0.2
Dispersant	0.2	0.2	0.2	0.2	0.2	0.2

Methods

1. Shear Rheometry

The shear rheometry of all coatings was investigated using an AR-2000 dynamic stress rheometer (TA Instruments). All measurements were performed at 21.5 °C. A Couette geometry was used for all steady state flow and small amplitude oscillatory shear and steady state flow experiments. Steady state flow experiments were performed over a shear range of 10^{-4} to 4355 s^{-1}. The latter were performed in a stress-control mode over an angular frequency range of 0.06285 to 628.3 rad/s, i.e. frequency from 0.01 to 100 Hz. In order to determine the linear viscoelastic regime (LVR) of each sample, stress sweeps were performed at a frequency of 1 Hz. From the stress sweep data, it was found that an oscillatory stress of 0.1 Pa was in the LVR range for all coatings. Hence, all frequency sweeps were performed at a constant stress of 0.1Pa in a stress-control mode over an angular frequency range of 0.06285 to 628.3 rad/s, i.e. frequency from 0.01 to 100 Hz. All measurements were repeated twice and the averages of these measurements are reported.

2. Squeeze/Pull-off Test (SPOT)

To estimate the extensional viscosity behavior of the coatings, the authors performed what we refer to here as “Squeeze/Pull-off” tests (SPOT) utilizing the dynamic stress rheometer used above. In this test, a known weight of coating was loaded onto the

bottom plate of the stress rheometer. After determining an appropriate stretching speed and distance to perform the test with a 20 mm-diameter-steel plate, the known weight of coating was squeezed and then quickly pulled to form a cylindrical liquid neck. Pulling continued until the filament formed broke (Figure 2.1). During the test, the instrument detected the changes of velocity and normal force and the gap distance at break was determined using a camera. The difference in gap was then normalized to the weight of sample applied to enable the stretchability of the coatings under extension to be directly compared. Although the deformation was not induced by pure extension, it is believed that the current method provides a sufficiently controlled and quantifiable method for estimating the extensional properties of a coating, and provides an alternative for those who do not have access to a CaBER, and per the authors' experience, provides a significantly better way of testing the extensional viscosity behavior of a coating than testing it with the infamous "finger test", i.e. extension of the coating between two fingers.

(a) (b) (c)

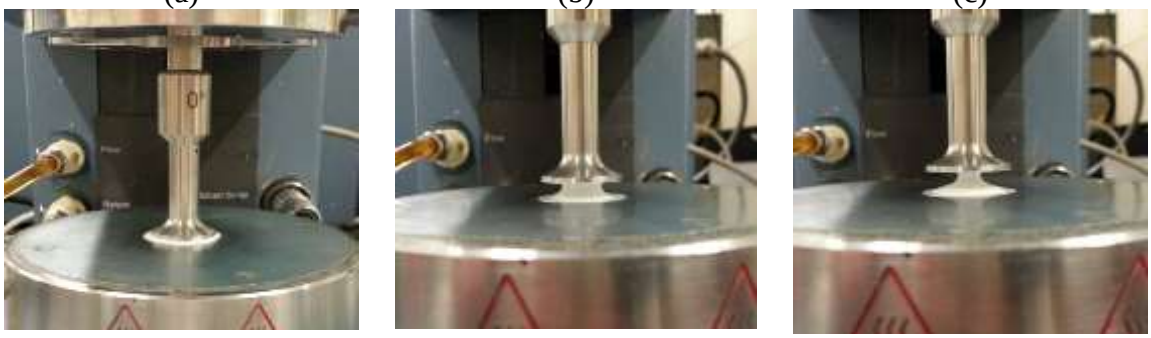

Figure 2.1: The evolution of coating sample during a SPOT test.

3. Capillary Breakup Extensional Rheometry (CaBER)

The extensional property of each coating was further characterized with a CaBER rheometer (Thermo Haake). To form a liquid filament, two plates with diameter d = 6 mm were separated from an initial gap h = 3.00 mm to a final height f = 11.68 mm at 21.5 °C, which resulted in the change of aspect ratio from 1.00 to 3.89 and a step strain (Hencky strain) $\varepsilon = 1.36$. With these geometric settings, the filament midpoint diameters of all tests after stretching were able to start at 1-1.5 mm, which ascertains that the subsequent necking of the liquid bridge was only controlled by the balance of capillary and viscoelastic forces [35]. In other words, the part of gravitational forces in this process can be neglected.

During the test, the change of filament midpoint diameter with time D(t) was monitored by a laser micrometer with a resolution down to 10 μm. In order to compare the data of D(t) *vs.* t from different samples, it is required to keep the settings of stretch profile constant. Hence, preliminary experiments with the control coating XSB-3 were conducted first. It was found that the plates separated within 60 ms at a constant speed 0.14 mm/ms with a linear stretch profile resulted in the smoothest curve of D(t) *vs.* t, which ensures no significant runnability issues (e.g. initial oscillation or beads-on-a-string problem). Afterwards, the same stretch profile was used for testing the other coatings. After measuring the density and surface tension of the coatings, the analysis software can also calculate the transient apparent extensional viscosity η_{app} at different strain ε or strain rates $\dot{\varepsilon}$, and consequently generate two graphs, η_{app} *vs.* ε and η_{app} *vs.* $\dot{\varepsilon}$.

Results and Discussion

The properties measured for the coatings are shown in Table 2.4. From the results, it is clear that the addition of petro-based extensional viscosity modifier increased the Brookfield viscosity of the coatings and the effect of its addition was greater for the coatings containing biobased latex binder.

Table 2.4: Basic properties of control and coatings with petro-based extensional viscosity modifier.

Sample	**XSB-1**	**XSB-3**	**EX-1**	**EX-2**	**EX-3**
pH	8.52	8.37	8.38	8.51	8.41
Solids%	60.48	60.57	60.51	60.44	60.50
Brookfield Viscosity (cP, 100 RPM, #5 spdl)	72	258	404	444	456

Knowing that the Brookfield viscosity of the coatings would also significantly increase as a result of the addition of inorganic rheology modifiers, formulations were adjusted to obtain coatings of similar Brookfield viscosities (200 – 300 cP) by varying the amount of each of the inorganic rheology modifiers added. Consequently, it was found that the incremental latex replacement reduced the amount of inorganic rheology modifier needed to achieve the target viscosity (Table 2.5). Of the two inorganic rheology modifiers used, type B had the greatest impact on coating pH (Table 2.5).

Table 2.5: Basic properties of coatings with inorganic rheology modifier A and B.						
Sample	**EA-1**	**EA-2**	**EA-3**	**EB-1**	**EB-2**	**EB-3**
pH	8.86	8.66	8.67	9.85	9.40	8.51
Solids%	60.49	60.47	60.53	60.51	60.46	60.52
Brookfield Viscosity (cP, 100 RPM, #5 spdl)	214	226	244	196	236	200

Shear Rheometry

1. Steady state flow tests

The results of steady state flow tests are shown in Figure 2.2. Over the selected range of shear rates, all coatings are shear thinning. Among the three rheology modifiers, the petro-based extensional viscosity modifier increased the viscosity of the coatings containing 35% and 45% latex replacement to the highest. Coatings with inorganic rheology modifier A exhibited similar viscosity and shear thinning behavior as found for the control (XSB-3), while coatings with inorganic rheology modifier B were lower in viscosity in comparison to the others (Figure 2.2 (b)-(d)).

(a)

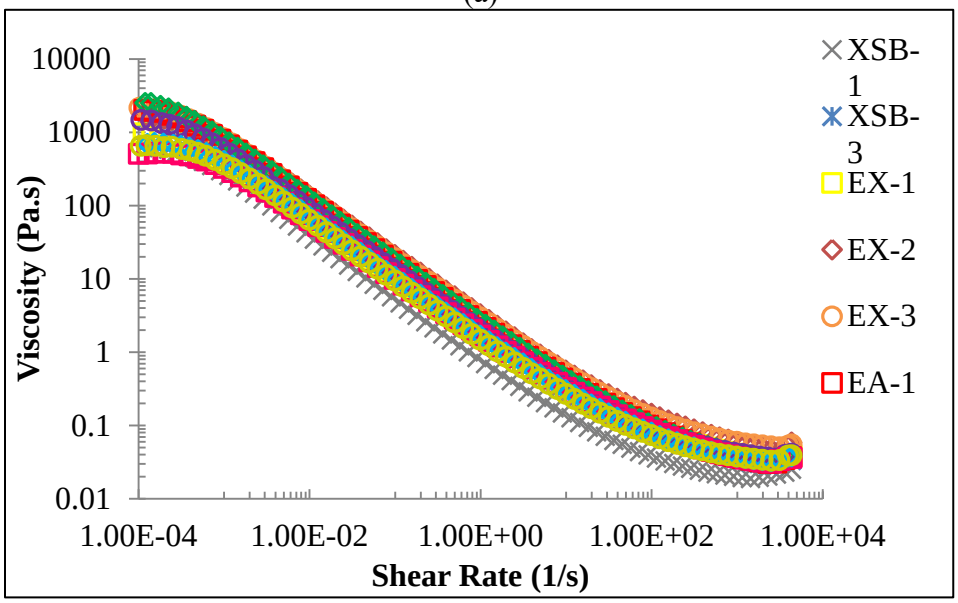
10000
1000
100
10
1
0.1
0.01
Viscosity (Pa.s)
1.00E-04
1.00E-02
1.00E+00
1.00E+02
1.00E+04
Shear Rate (1/s)
XSB-1
XSB-3
EX-1
EX-2
EX-3
EA-1

(b)

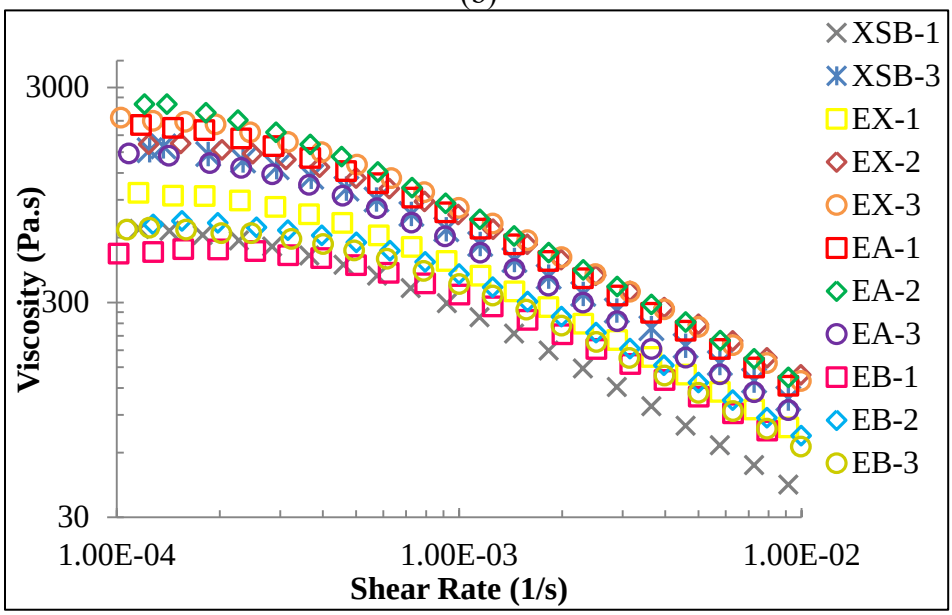
3000
300
30
Viscosity (Pa.s)
1.00E-04
1.00E-03
1.00E-02
Shear Rate (1/s)
XSB-1
XSB-3
EX-1
EX-2
EX-3
EA-1
EA-2
EA-3
EB-1
EB-2
EB-3

(c)

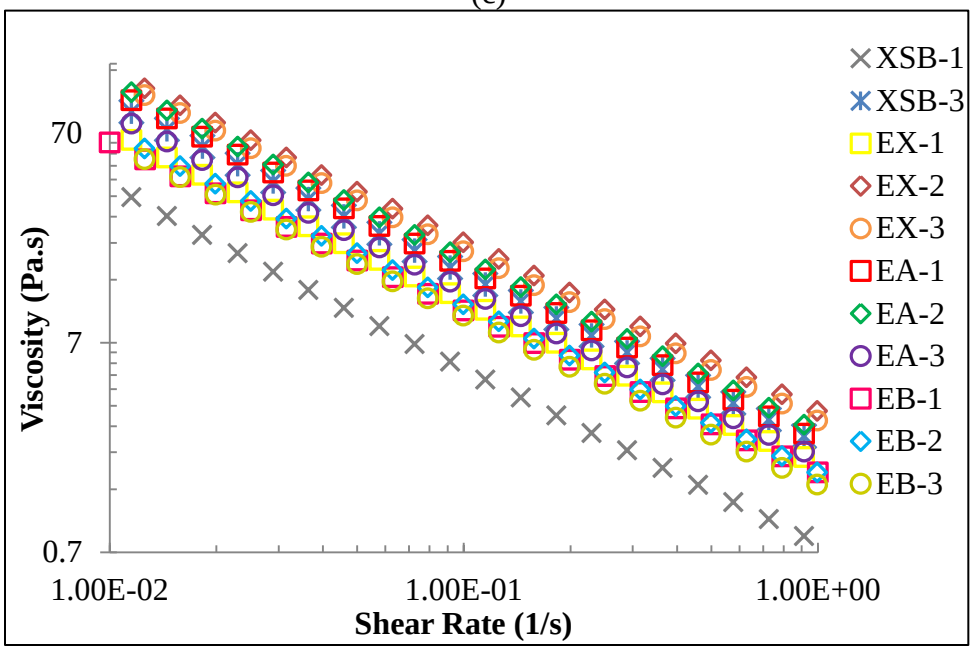
70
7
0.7
Viscosity (Pa.s)
1.00E-02
1.00E-01
1.00E+00
Shear Rate (1/s)
XSB-1
XSB-3
EX-1
EX-2
EX-3
EA-1
EA-2
EA-3
EB-1
EB-2
EB-3

(d)

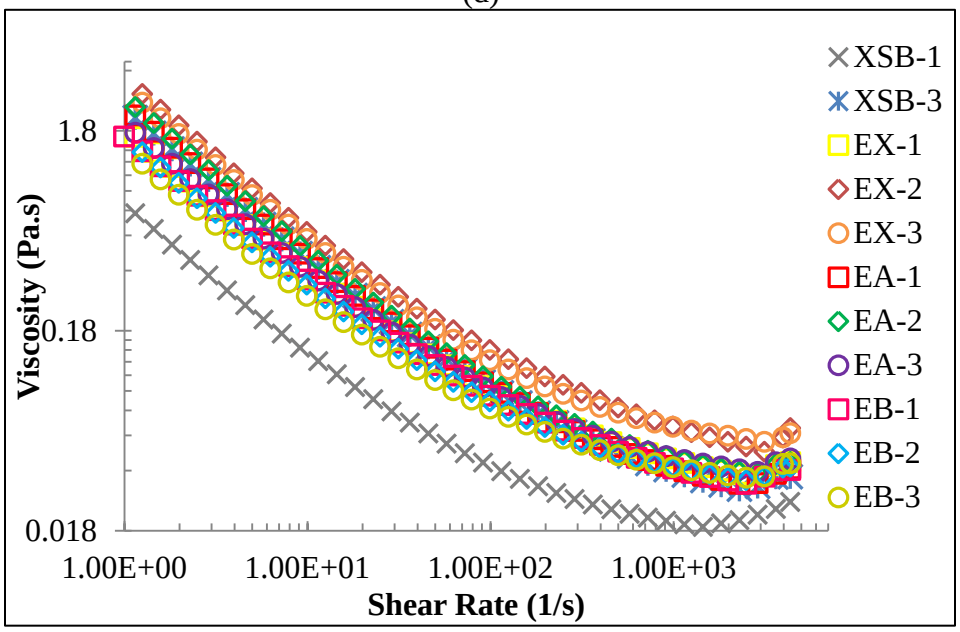

Figure 2.2: Steady state flow results of all coatings: a. viscosity changing with shear rates ranging from 10^{-4} to 10000 s^{-1}; b. viscosity changing under the shear rates from 10^{-4} to 10^{-2} s^{-1}; c. viscosity changing under the shear rates from 10^{-2} to 1 s^{-1}; d. viscosity changing under the shear rates from 1 to 10000 s^{-1}.

It is well accepted that the petro-based extensional viscosity modifier functions in the coating by participating in the association of petro-based latex that contributes to the changes of coating rheological properties. The situation is complicated by replacing petro-based latex with biobased latex. Obviously, the decrease in the amount of petro-based latex reduces its concentration, which can weaken the agglomeration. However, the swelling of biobased latex nanoparticles also reduces the amount of free water in the coating, which can increase the concentration of the petro-based latex. In addition, the effective volumes of biobased latex particles become much larger than those of the petro-based latex due to their swelling [30, 31]. Thus, the coating may become more elastic

when the volumetric concentration of the sterically stabilized biobased latex particles increase beyond the point where steric layers overlap [13]. As a result of these three effects, the rheological properties of the biobased latex containing coatings vary accordingly.

For instance, comparing the viscosity shear dependence of coatings containing petro-based extensional viscosity modifier, it can be seen that replacing 25% petro-based latex with biobased latex reduced the coating shear viscosity over the detected shear rates, which probably resulted from the impact of petro-based latex reduction (EX-1 *vs.* XSB-3) (Figure 2.3). By contrast, increasing the replacement to 35% or 45% (EX-2 or EX-3 *vs.*XSB-3), the two effects originated from the addition of biobased latex became so great that their shear viscosity increased (Figure 2.3) and their wet structures were more elastic than the control coating (Figures 2.4-2.6).

(a)

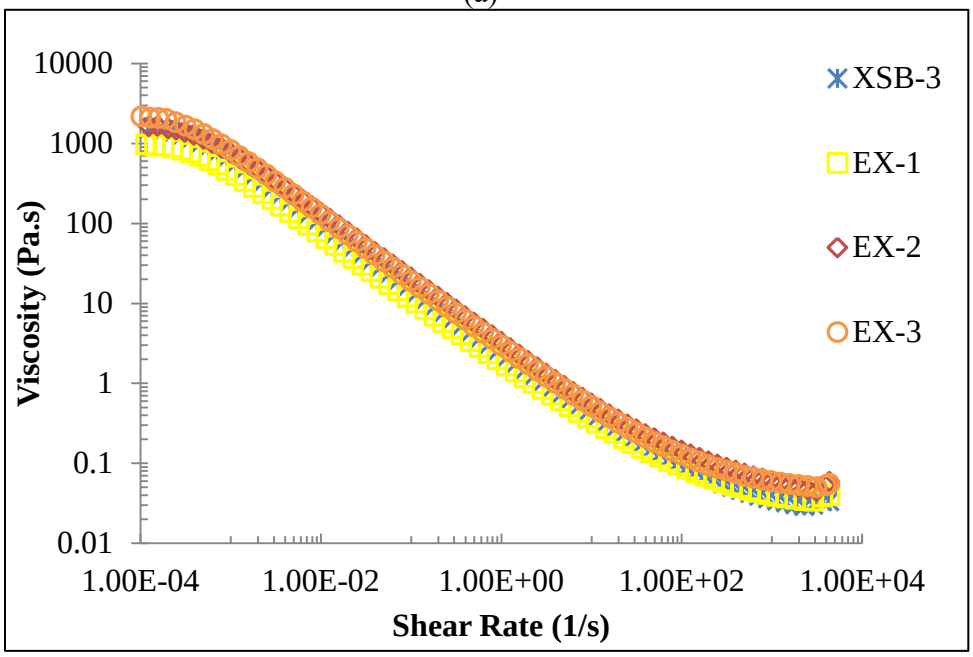
10000
1000
100
10
1
0.1
0.01
Viscosity (Pa.s)
1.00E-04
1.00E-02
1.00E+00
1.00E+02
1.00E+04
Shear Rate (1/s)
XSB-3
EX-1
EX-2
EX-3

(b)

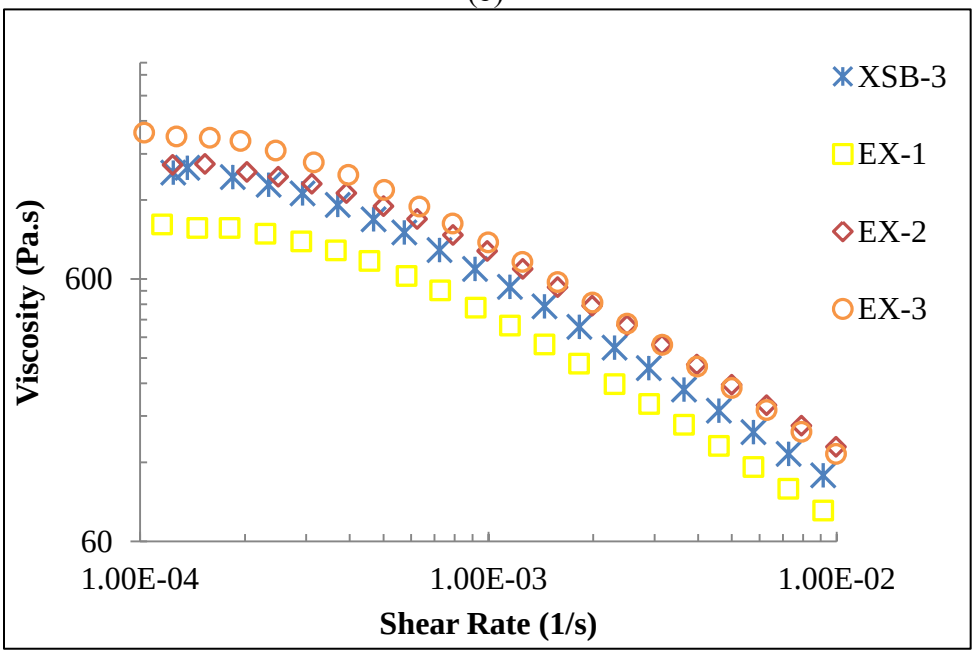
600
60
Viscosity (Pa.s)
1.00E-04
1.00E-03
1.00E-02
Shear Rate (1/s)
XSB-3
EX-1
EX-2
EX-3

(c)

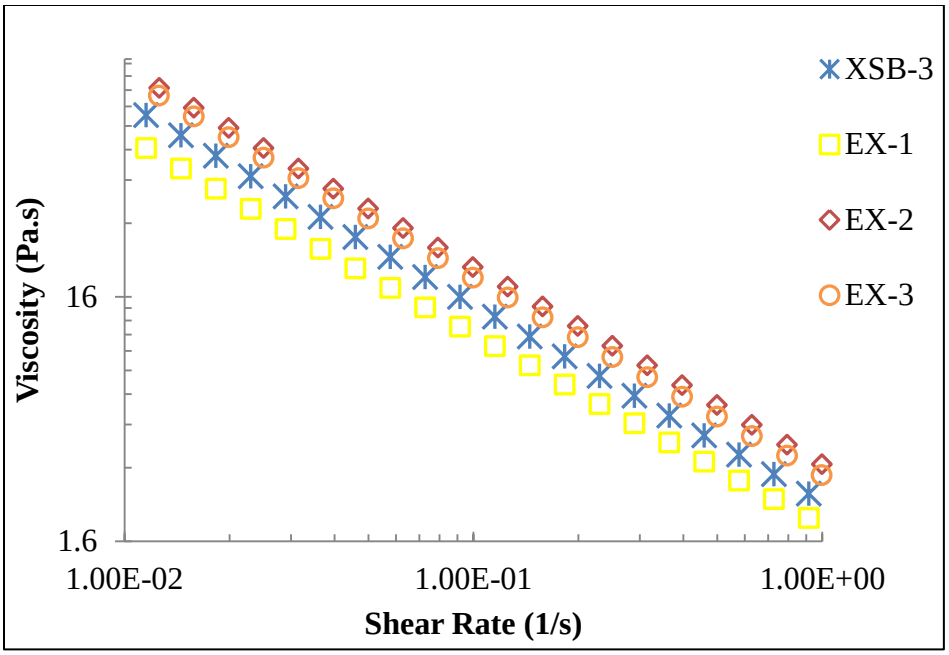
XSB-3
EX-1
EX-2
EX-3
Viscosity (Pa.s)
16
1.6
1.00E-02
1.00E-01
1.00E+00
Shear Rate (1/s)

(d)

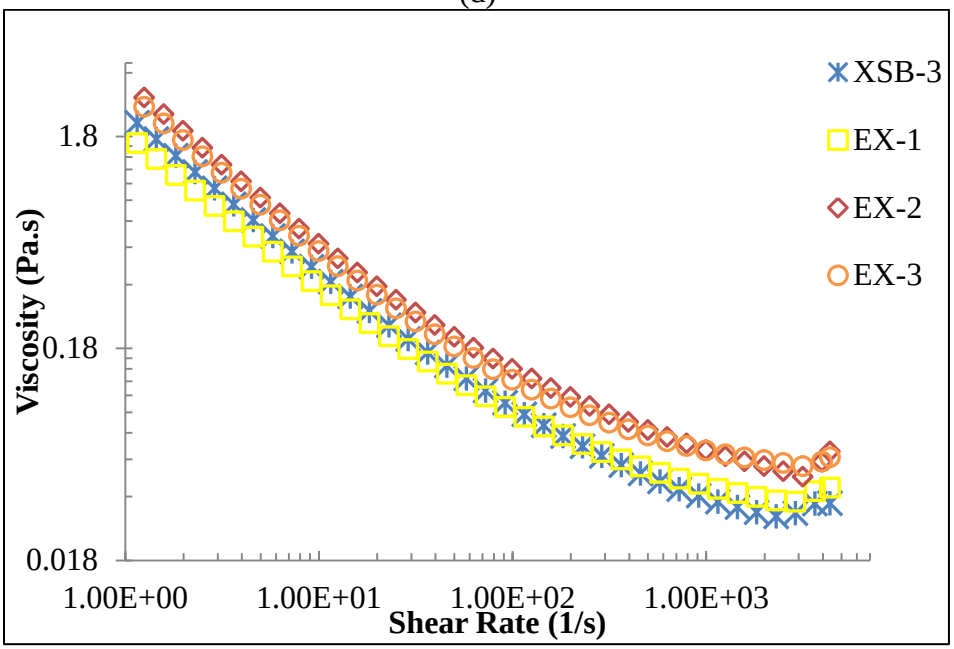

Figure 2.3: Steady state flow results of coatings with petro-based extensional viscosity modifier: a. viscosity changing with shear rates ranging from 10^{-4} to 10000 s^{-1}; b. viscosity changing under the shear rates from 10^{-4} to 10^{-2} s^{-1}; c. viscosity changing under the shear rates from 10^{-2} to 1 s^{-1}; d. viscosity changing under the shear rates from 1 to 10000 s^{-1}.

2. Frequency sweeps

After the linear viscoelastic regime (LVR) of each coating was determined by a stress sweep, a frequency sweep was conducted under the selected oscillation stress. The values of tan δ = G"/G' are shown in Figure 2.4 which indicates the viscoelasticity of all the coatings. Clearly, all coating structures are more elastic than viscous in the lower range of frequency (tan δ<1). As frequency increased, their elastic structures were enforced by the increasing particle interactions at higher deformation rates, which

resulted in the reduction of tan δ [36]. After that, the increasing tan δ suggests that the coating structures became less stable under oscillatory stress, some of which even became viscous (EX-1, EX-2, EA-2, EA-3, EB-1). On the contrary, coatings XSB-3, EX-3, EA-1, EB-2 and EB-3 seem to possess more stable elastic structures than the others.

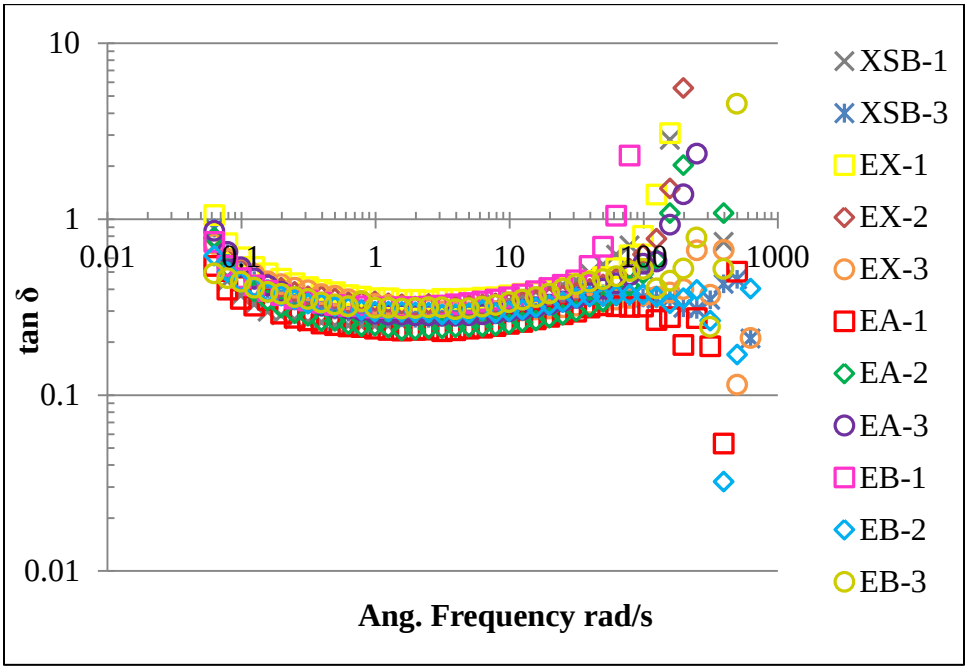

Figure 2.4: Viscoelasticity (tan δ) of all coatings obtained from frequency sweeps.

Figure 2.5 compares the viscoelasticity (tan δ) of coatings with and without petro-based extensional viscosity modifier and Figure 2.6 shows the different contributions of their elastic components to the viscoelasticity (G'). Obviously, the addition of petro-based extensional viscosity modifier generated more elastic structures in the all-synthetic latex coating (XSB-1 *vs.* XSB-3), while its effect on the biobased latex coatings varied with replacement levels, which was explained previously.

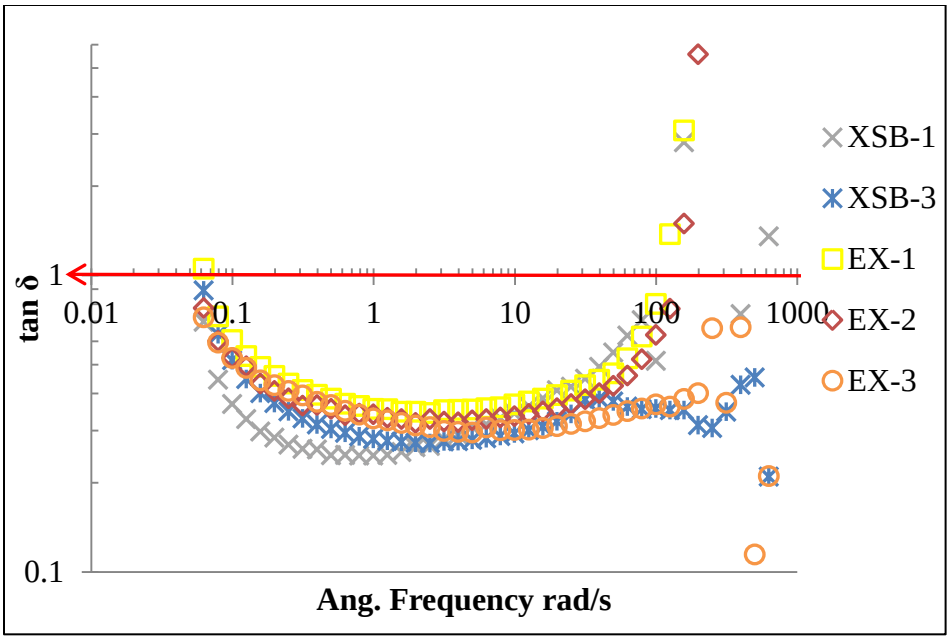

Figure 2.5: Viscoelasticity (tan δ) of coatings with and without petro-based extensional viscosity modifier changing with frequency.

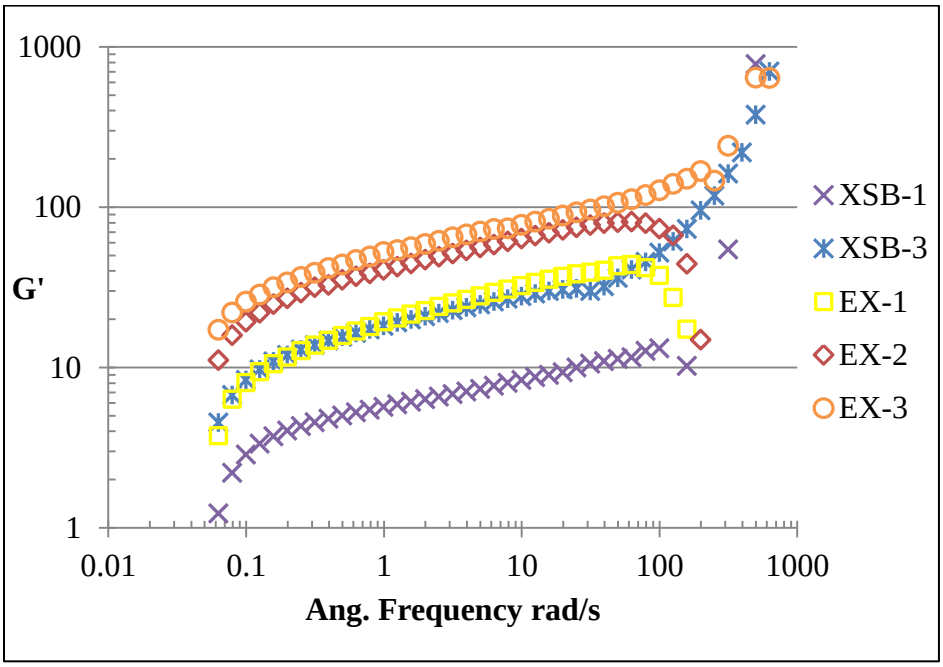

Figure 2.6: Elastic moduli (G') of coatings with and without petro-based extensional viscosity modifier changing with frequency.

It is believed that the interactions between the inorganic rheology modifiers and the biobased latex can result in unique coating rheology (Figures 2.2, 2.7-2.10). As mentioned before, increasing the replacement of latex with biobased latex can reduce the amount of free water in the coating due to the swelling of biobased latex particles. Together with the incremental amount of biobased latex, the resultant increase in the concentration of biobased latex allows the coatings to maintain or improve their rheological properties with fewer amounts of inorganic rheology modifiers. In other words, the relative effects of the biobased latex concentration and the amount of the inorganic rheology modifiers determine the rheological properties of the biobased latex containing coatings.

The comparisons of the viscoelasticity and elastic moduli in Figures 2.7 and 2.8 show that the addition of inorganic rheology modifier A imparted comparable or higher elastic components to the viscoelasticity of the biobased latex containing coatings (EA-1, EA-2 and EA-3) than the petro-based extensional viscosity modifier did to the all-synthetic latex coating (XSB-3). However, this effect in coatings EA-2 and EA-3 weakened as the angular frequency increased over 100 rad/s, likely because these coatings contained proportionally less inorganic rheology modifier available for the interactions with biobased latex. Instead, the existing agglomeration and/or crosslinking network disrupted under high shear which made the coatings transit to a more viscous wet structure (tan $\delta > 1$) (Figure 2.7).

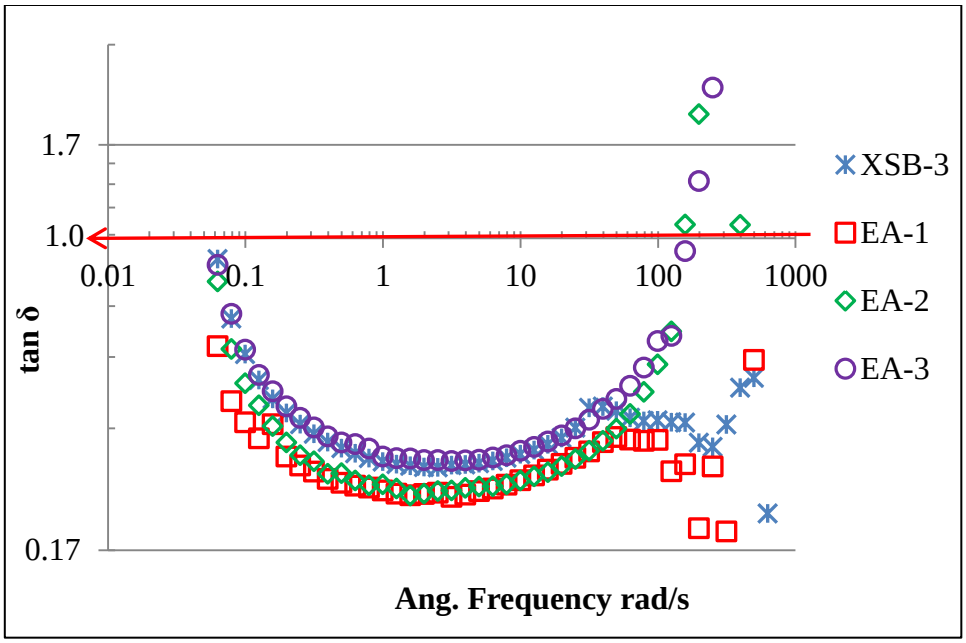

Figure 2.7: Viscoelasticity (tan δ) of the control coating XSB-3 and coatings containing inorganic rheology modifier A changing with frequency.

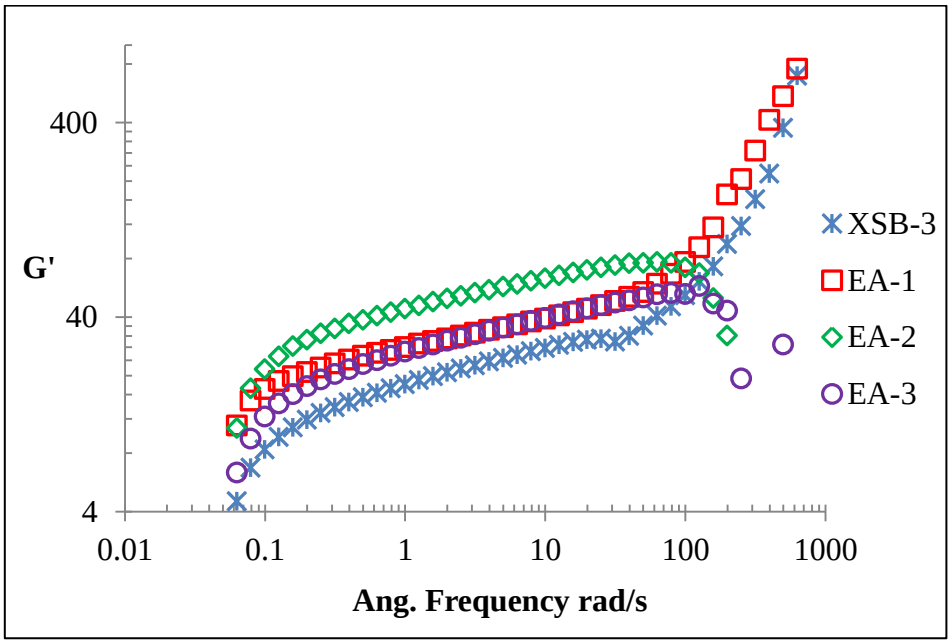

Figure 2.8: Elastic moduli (G') of the control coating XSB-3 and coatings with inorganic rheology modifier A changing with frequency.

The influences of inorganic rheology modifier B on the viscoelasticity (tan δ) and the elastic moduli (G') of coatings with biobased latex binders are shown in Figures 2.9-2.10. It was validated that adding inorganic rheology modifier B in the biobased latex coatings can maintain similar viscoelastic coating structures as the control XSB-3. Again, the aforementioned relative effects of changing biobased latex concentration and the amount of inorganic rheology modifier B resulted in the viscoelasticity of coatings EB-1, EB-2 and EB-3. The increase in the coating elastic components of EB-2 and EB-3 as the shear rate increased further indicates the enforced agglomeration and/or crosslinking in these coatings. Given that the amounts of inorganic rheology modifier B are lower than those of modifier A in these coatings, it is reasonable to speculate that the interactions between biobased latex and inorganic rheology modifier B are stronger than with A. Besides, coatings EB-2 and EB-3 behaved very similarly under oscillatory stress as control XSB-3, regardless of some outliers (Figures 2.9-2.10).

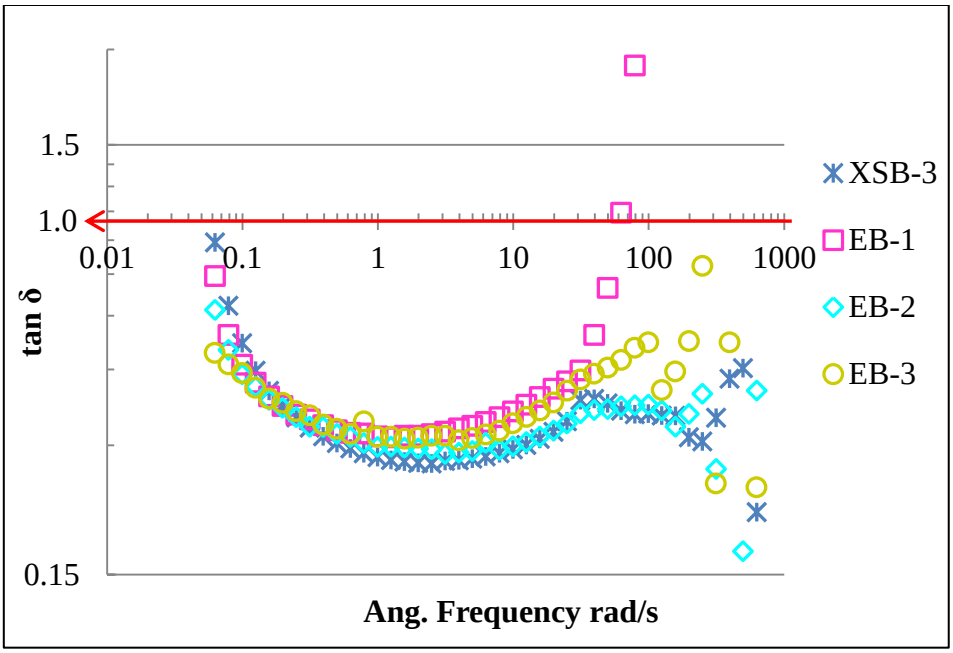

Figure 2.9: Viscoelasticity (tan δ) of the control coating XSB-3 and coatings containing inorganic rheology modifier A changing with frequency.

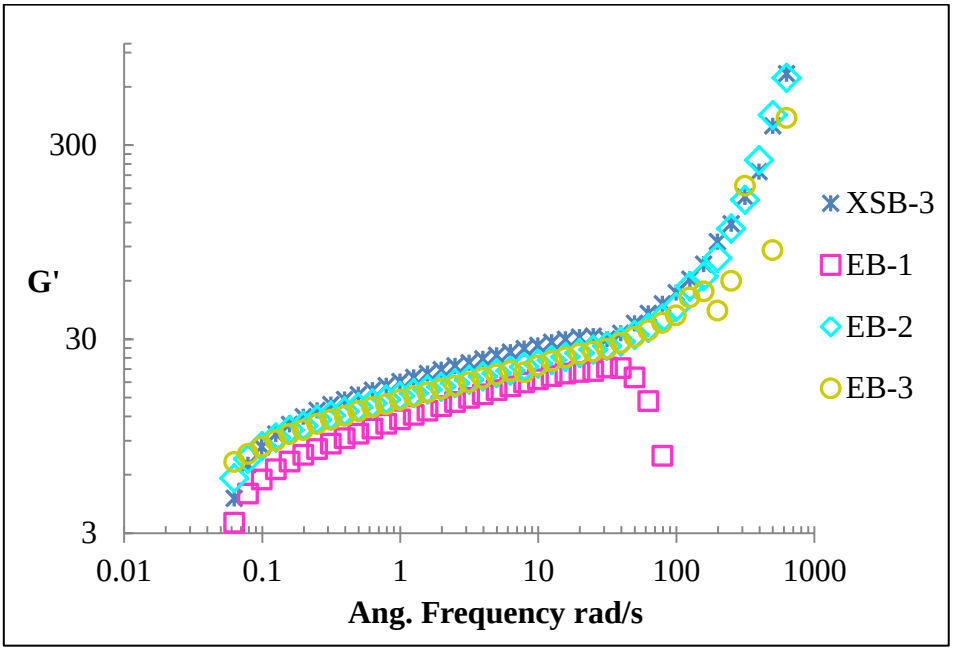

Figure 2.10: Elastic moduli (G') of the control coating XSB-3 and coatings with inorganic rheology modifier A changing with frequency.

Extensional Rheometry

1. Squeeze/pull-off tests (SPOT)

As a quick and effective check for the relative extensional viscosity behavior of the coatings (i.e. their “stretchability”), Squeeze/Pull-off tests (SPOT) were run. The control coating XSB-3 containing the petro-based extensional viscosity modifier has acceptable “stretchability” while control coating XSB-1, which contains no extensional viscosity modifier, does not. Comparing the results in Figure 2.11, it can be seen that the higher normalized delta gap values of all experimental coatings demonstrate that the addition of the two inorganic rheology modifiers at the various biobased latex levels was able to increase the coating stretchability within the range of the positive control. Except for coating EX-2, which was even significantly higher, the normalized delta gap values of all coatings were determined to be around 6000 μm/g (Figure 2.11). The recorded data can be found in Appendix A.

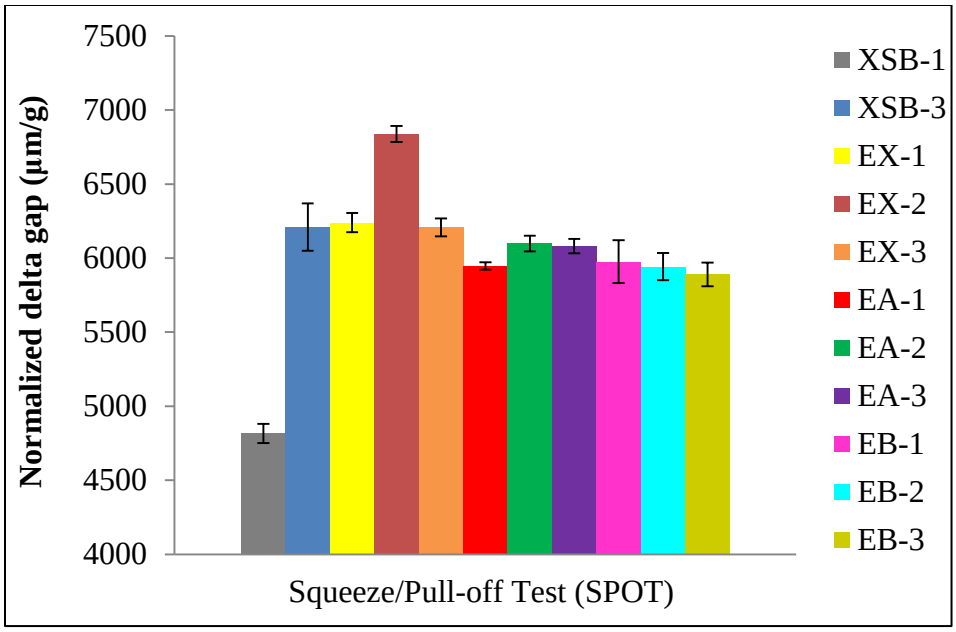

Figure 2.11: SPOT Results of all the coatings.

2. Capillary Breakup Extensional Rheometry (CaBER)

The extensional properties of coatings were further characterized by CaBER. The resulted time dependence of the filament midpoint diameter is shown in Figures 2.12-2.15, where time t = 0 is defined when the upper plate reaches the final height. All of these curves were generated using the same CaBER settings (Geometry: initial gap h = 3.00 mm, plate diameter d = 6 mm, and final height f = 11.36 mm; Linear stretch for 60 ms at speed 0.14 mm/ms). The evolution of filament is known to be driven by the capillary force that is related to the liquid surface tension, and to be resisted by the viscoelasticity, so a further interpretation of the CaBER data will be discussed in Chapter III with the results of surface tension [34].

Figure 2.12 provides the CaBER results of the control coatings with and without petro-based extensional viscosity modifier (XSB-3 *vs.* XSB-1) , which illustrate that the filament lifetime was increased substantially because of the petro-based extensional viscosity modifier, indicating a significant increase in the extensional viscosity like the SPOT results of coating XSB-3. The results in Figures 2.13-2.15 show that the extensional viscosity of experimental coatings was also increased, but it varies depending on the type of rheology modifier and amount of biobased latex in the formulation. The detailed mechanisms behind these results were discussed in Chapter III.

Figure 2.13 shows that for the same amount of petro-based extensional viscosity modifier, the coating filament lifetime is not detrimentally affected, but instead increases at increasing petro- *vs.* biobased latex levels. This impact was stronger for the coatings with 25% and 35% petro-based latex replacement than the all-synthetic latex coatings (t_{EX-1} = 0.105 s and t_{EX2} = 0.147s *vs.* t_{XSB-3} = 0.095 s), while coating with 45% biobased latex (t_{EX-3} = 0.085 s) resulted in similar filament lifetime as the control (t_{XSB-3} = 0.095 s). This indicates that the function of petro-based extensional viscosity modifier can be facilitated by the replacement of biobased latex to a certain degree, but then drops off as it likely primarily acts on the petro-based latex. In other words, the replacement of petro-based latex with biobased latex binder in the curtain coating formulation can reduce the amount of petro-based extensional viscosity modifier needed to achieve desired extensional properties, while maintaining the shear viscosity and viscoelasticity in the required range. Moreover, lower usage or elimination of the petro-based extensional

viscosity modifier can also reduce the time required for coating makedown given the practical challenges with fully dispersing the petro-based extensional viscosity modifier reported in the field by paper mills. This practical challenge was also confirmed in coating makedown during our lab and pilot studies.

In the study of inorganic rheology modifier A, it was found that increasing the latex level from 25% to 35% in the coatings (EA-1 and EA-2) prolonged the filament lifetime from 0.033 s to 0.044 s, but this effect did not continue at the higher replacement level (Figure 2.14). Although the filament lifetime is still shorter than t_{XSB-3} = 0.095 s, it can be reasonably expected that adding more inorganic rheology modifier A into coatings with 35% or 45% latex replacement can achieve this goal concomitant, however, with a certain increase in Brookfield viscosity.

With the addition of inorganic rheology modifier B, 25% replacement of XSB latex with biobased latex binder (EB-1) resulted in the longest filament lifetime (t_{EB-1} = 0.050 s), i.e. the highest extensional viscosity in this group, whereas the higher replacement levels (EB-2 and EB-3) showed slightly shorter filament lifetimes (t_{EB-2} = 0.041 s and t_{EB-3} = 0.037 s) (Figure 2.15). Given that the pH values of coatings with 25% and 35% latex replacement are above 9, it is expected that adding more inorganic rheology modifier B in the coating with 45% biobased latex results in an increase in its extensional viscosity if needed.

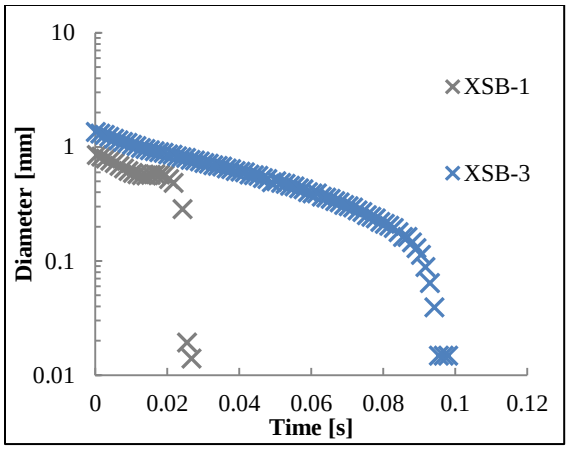

Figure 2.12: The time dependence of filament midpoint diameter of control coatings.

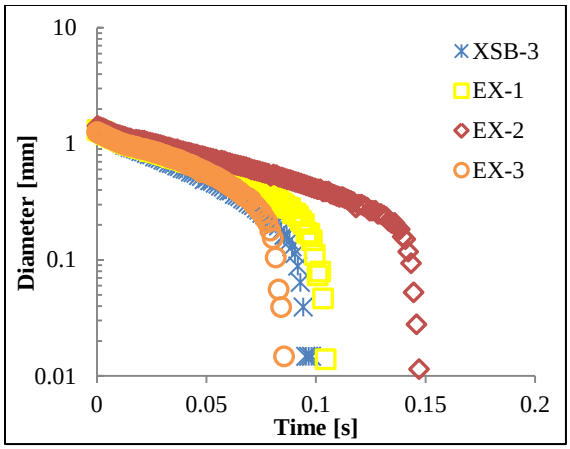

Figure 2.13: The time dependence of filament midpoint diameter of coatings containing petro-based extensional viscosity modifier.

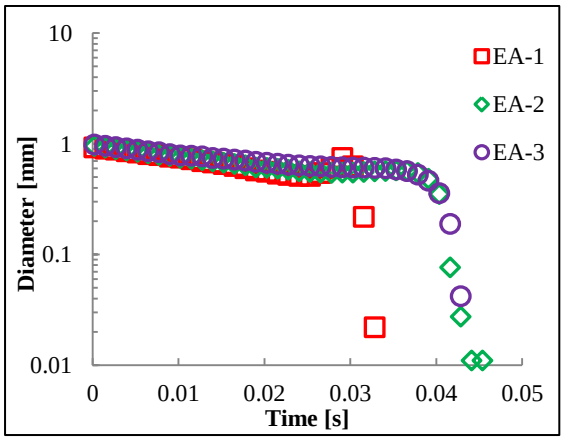

Figure 2.14: The time dependence of filament midpoint diameter of coatings with inorganic rheology modifier A.

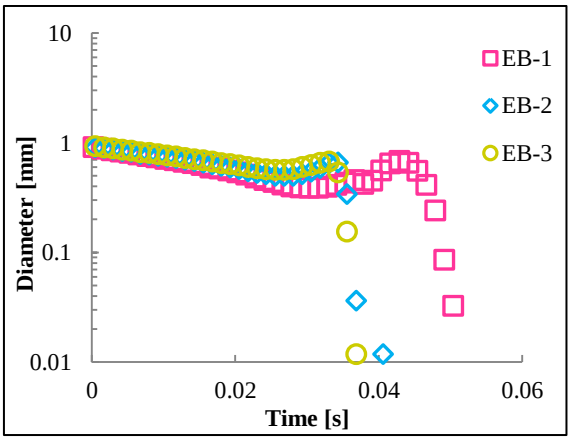

Figure 2.15: The time dependence of filament midpoint diameter of coatings with inorganic rheology modifier B.

Nevertheless, it is worth mentioning that the diameter profiles of coatings with inorganic rheology modifiers A and B indicated that axial asymmetric liquid bridges were formed, which was amplified during the initial separation and stretching, as also observed

for other systems reported in the literature (Figure 2.16) [37]. This behavior leads to a bead or droplet near the midpoint of the filament, which results in a sudden increase in filament diameter before its dramatic decrease (Figures 2.14-2.15). However, the results from the CaBER still provide a valid indication of the enhanced extensional viscosity of the coatings containing different rheology modifiers and the results correlated reasonably well to the results form SPOT.

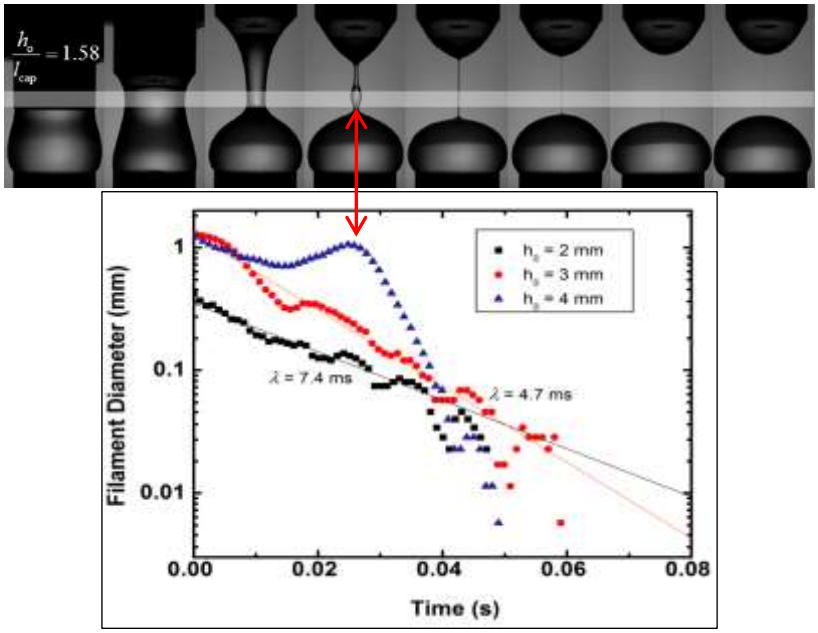

Figure 2.16: An example of the axial asymmetric initial liquid bridge formed and amplified during the initial stretching [36].

Conclusions

In this study, it was confirmed that the conventional petro-based extensional viscosity modifier function differently in the all-synthetic latex coatings and partial

biobased latex coatings. Although this type of modifier is known to react only with the petro-based latex, its function on the rheology of biobased latex coating was found to depend on the swellability of biobased latex as well.

By comparing the rheological properties of biobased latex coatings containing inorganic rheology modifiers with the all-synthetic latex coatings containing petro-based extensional viscosity modifier, it was concluded that the inorganic rheology modifiers both have the capabilities to improve the rheological properties the biobased latex containing coatings. Moreover, it was also found that the functions of these modifiers not only depend on their type, but also the ratio of them *vs.* biobased latex in the coating.

We also highlighted the effects of different rheology modifiers on the extensional viscosity of all the coatings by using CaBER technology. In addition, a new and simple method called SPOT (Squeeze/Pull-off Test) was explored using a dynamic stress rheometer. This was demonstrated to be convenient and effective for the evaluation of coating extensional viscosity. A detailed discussion of the extensional viscosity behavior of all the coatings can be seen in Chapter III. With the results of this chapter, it can help us predict curtain stability and coater runnability, and eventually optimize these new coating formulations for the commercial production on a curtain coater.

References

1. Schweizer, P. (2003): "Curtain coating-stability a critical operating parameter", 4th and 5th PITA Coating Conference, Edinburgh, UK.

2. Miyamoto, K. and Katagiri, Y. (1997) “Curtain Coating”, Chapter 11c in “Liquid film coating: scientific principles and their technological implications”, ed. Kistler, S.F. and Schweizer, P.M., Chapman & Hall, London.
3. Klass, C. (2013): “Blade, rod and contour coaters”, Coating Short Course, Western Michigan University.
4. Tripathi, P., Joyce, M., Fleming, P.D. and Sugihara, M. (2009): “A statistical study of process variables to optimize a high speed curtain coater-Part I”, TAPPI J., 8(1): p. 20-26.
5. Tripathi, P., Joyce, M., Fleming, P.D. and Sugihara, M. (2009): “A statistical study of process variables to optimize a high speed curtain coater-Part II”, TAPPI J., 8(2): p. 29-32.
6. Kistler, S.F. (1983): “The fluid mechanics of curtain coating and related viscous free surface flows with contact lines”, Ph.D. thesis, University of Minnesota, Minneapolis and University Microfilms International, Ann Arbor, MI.
7. Brown, D.R. (1961): “A study of the behavior of a thin sheet of moving liquid”, J. Fluid Mech. 10: p. 297-305.
8. Taylor, G.I. (1959): “Disintegration of fluid sheets”, Part III in “The dynamics of thin sheets of fluid”, Proc. Roy Soc. A., p.253-313, London.
9. Triantafillopoulos, N., Grön, J., Luostarinen, I., and Paloviita, P. (2004): “Operational issues in high-speed curtain coating of paper, Part 1: The principles of curtain coating”, TAPPI J., 3(11): p.6-10.

10. Alleborn, N., Suenderhauf, G., Raszillier, H., and Durst, F. (2001): “Edge retraction on a planar liquid sheet”, Proceedings of the 4th European Coating Symposium, Bruxelles, Belgium.
11. Lin, S.P. (1981): “Stability of a viscous liquid curtain”, J. Fluid Mech.104, p. 111-118.
12. Lin, S.P., Lian, Z.W. and Creighton, B.J. (1990): “Absolute and convective instability of a liquid sheet”, J. Fluid Mech. 220: p. 673-689.
13. Triantafillopoulos, N.G. (1996): “Paper coating viscoelasticity and its significance in blade coating”, TAPPI Press, Atlanta, GA.
14. Macosko, C.W. (1994): “Extensional rheometry”, Chapter 7 in “Rheology: Principles, Measurements and Applications”, ed. Macosko, C.W., Wiley-VCH, New York.
15. Petrie, C.J.S. (2006): “Extensional viscosity: A critical discussion”, J. Non-Newtonian Fluid Mech., 137: p. 15-23.
16. James, D.F. and Walters, K. (1994): “A critical appraisal of available methods for the measurement of extensional properties of mobile systems”, in: A.A. Collyer (ed.), Techniques of Rheological Measurement, Elsevier, New York.
17. Kheirandish, S., Guybaidullin, I, Wohlleben, W. and Willenbacher, N. (2008): “Shear and elongational flow behavior of acrylic thickener solutions. Part I: Effect of intermolecular aggregation”, Rheologica Acta, 48(4): p. 397-407.
18. Alleborn, N., Sünderhauf, H., and Raszillier, H. (2001): “High-speed curtain coating of paper”, PTS Coating Symposium Proceedings, Munich, Germany.

19. Kokko, A., Kettle J., Rautkoski, H., Shen, Y. (2010): “Characterization of curtain coating colors”, TAPPI 11th Advanced Coating Fundamentals Symposium, Munich, Germany.
20. van Leeuwen, J. (2006): “Paper coating - SBR latex replacement technology”, 2006 TAPPI Coating and Graphic Arts Conference, Atlanta, GA.
21. Klass, C. P. (2007): “New nanoparticle latex offers natural advantage”, Paper360°Magazine, p. 30-31.
22. van Leeuwen, J. (2007): “Update on biopolymer nanoparticle latex development and applications”, TAPPI Coating and Graphic Arts Conference, Miami, FL.
23. Bloembergen, S., McLennan, I., Lee, D.I., and van Leeuwen, J. (2008): “Paper binder performance with nanoparticle biobased latex™: EcoSynthetix develops EcoSphere® biobased latex for replacement of petroleum based latex binders”, ACFS, Montreal, Canada.
24. Bloembergen, S., McLennan, I. J., Lee, D. I., and van Leeuwen, J. (2008): “Paper binder performance with biobased nanoparticles. A starch-based biobased latex can replace petroleum-based latex binders in papermaking”, Paper360ºMagazine, p. 46-48.
25. Figliolino, F.C., Rosso, F., van Leeuwen, J. and Klass, C.P. (2009): “Mill experiences with biobased latex in Brazil”, TAPPI PaperCon Proceedings, Section 19-1.

26. Figliolino, F.C. and Rosso, F., (2009): “Reducing carbon footprint with biobased latex”, Paper360º Magazine, p. 25-28.
27. Lee, D. I, Bloembergen, S., van Leeuwen, J. (2010): “Development of new biobased emulsion binders”, TAPPI PaperCon, Atlanta, GA.
28. van Ballegooie, P., Greenall, P., Bloembergen, S. and DeJong, R., “EcoSphere® biobased latex® binders: Next generation solutions for today’s paper coating industry”, World Pulp & Paper, The International Review for the Pulp and Paper Industry, 2012, 100.
29. Bloembergen, S., McLennan, I.J., van Leeuwen, J., and Lee, D.I. (2010): “Specialty biobased monomers and emulsion polymers derived from starch”, PTS Advanced Coating Fundamentals Symposium, Munich, Germany.
30. Bloembergen, S., VanEgdom, E., Wildi, R., McLennan, I.J., Lee, D.I., Klass, C.P., and van Leeuwen, J. (2010): "Biobased latex binders for paper and paperboard applications", J. of Pulp and Paper Sci., 36(3-4), p. 1-11.
31. Shin, J.Y., Jones, N., Lee, D.I., Fleming, P.D., Joyce, M.K., DeJong, R. and Bloembergen, S. (2012): “Rheological properties of starch latex dispersions and starch latex-containing coating colors”, TAPPI PaperCon, New Orleans, LA.
32. Shin, J.Y., Jones, N., Lee, D.I., Fleming, P.D., Joyce, M.K., DeJong, R. and Bloembergen, S. (2013): “Dynamic water retention properties of biobased latex containing coating colors”, TAPPI PaperCon, Atlanta, GA.

33. Bloembergen, S. (2013): “Advances in Organic Based Binder Chemistries”, Coating Short Course, Western Michigan University.
34. Chen, T., Joyce, M., Fleming, P.D., Bloembergen, S. (2016): “Pigmented formulations containing biobased nanoparticle binders for curtain coating applications; Part 2: curtain stability analysis”, Paper submitted for presentation and publication to TAPPI PaperCon2016.
35. Anna, S., McKinely, G.H. (2001): “Elasto-capillary thinning and breakup of model elastic liquids”, J. Rheol. 45:115-138.
36. Triantafillopoulos, N., Grankvist T. (1994): “Coating viscoelasticity and blade coating defects”, Paperi ja Puu-Paper and Timber, Vol. 76, No 10, p663-667, 1994.
37. Rodd, L.E., Scott, T.P., Cooper-White, J.J., and McKinley, G.H. (2005): “Capillary breakup rheometry of low-viscosity elastic fluids”, Appl. Rheol. 15(1): p. 12–27.

CHAPTER III

PIGMENTED FORMULATIONS CONTAINING BIOBASED NANOPARTICLE BINDERS FOR CURTAIN COATING APPLICATIONS; PART 2: CURTAIN STABILITY STUDY

Abstract

This chapter continued to characterize the surface tension of control coatings containing a petro-based latex binder and a petro-based extensional viscosity modifier, as well as experimental coatings containing partial biobased latex binder and one of two inorganic rheology modifiers as complete replacement of the petro-based extensional viscosity modifier. The unique effects of biobased latex and different rheology modifiers on the coating properties were further discussed. A significant correlation between the surface tension and CaBER filament lifetime was also found in different coating groups.

The curtain stability of these coatings at the flow rates from 20 to 65 mL/s was studied using a slot-fed die set-up equipped with a controlled coating recirculation loop. It was found that the curtain stability was significantly enhanced by the addition of the petro-based extensional viscosity modifier, as well as by the inorganic rheology modifiers when biobased latex was present. By impinging the curtain exiting the slot-fed die set-up and determining the Mach angle at the point of impingement, which angle relates to the surface tension of the coating, the corresponding Weber numbers were calculated as a known and accepted measure of curtain stability. Among all the coatings, the ones containing 35% and 45% (wt. %) latex replacement plus inorganic rheology modifier

resulted in the most stable curtains, while the stability of the other coating formulations was lower but still comparable to the all-synthetic latex control coating. The findings showed the relative importance of coating surface tension, shear rate dependence of viscosity, viscoelasticity and elastic component, as well as extensional viscosity to the curtain stability at different flow rates. A coating with relatively low surface tension (< 40 mN/m) and shear viscosity required a more elastic structure and/or higher extensional viscosity to form a stable curtain, especially at higher flow rates, where shear thinning plays a more critical part. For the coatings with similar surface tension and shear thinning behavior, the coating with a low shear viscosity more readily deforms so it requires a more elastic coating structure and/or high extensional viscosity to maintain curtain stability, especially at high curtain flow rates.

This paper discusses some of the trade-offs necessary for optimizing curtain stability and helps to advance coating formulation knowledge towards the optimization of biobased latex binder containing coatings for scale-up to pilot and mill operations.

Introduction

Over the past ten years, curtain coaters have regained popularity by adapting to the high-speed production of various paper grades, such as paperboard, specialty, printing, and graphic papers, etc. [1, 2]. On a curtain coater, the coating goes through a slot-fed or slide-fed die to form a smooth curtain that falls freely onto the substrate where the coating creates a contour profile (Figures 1.13, 1.5). This process creates excellent

coating coverage regardless of coat weight, and the thickness of the coating layer is more uniform than that of the blade or rod coated paper [3]. A curtain coater is also a superior contour coater in comparison to an air knife, due to its ability to run at higher coating solids, apply higher coat weights, run at higher machine speeds, as well as its ability to run better with less noise [4]. A curtain coater can run at high speed with fewer web breaks and lower maintenance cost than the other contact coating processes [5, 6]. Another advantage is that no coating recirculation is needed, which helps maintain a high quality of coating and a clean system.

The major component of a curtain coater is the die whose internal design is so critical as to supply a uniformly distributed coating flow. Figure 1.13 shows a simple slot die design that has been modified to enable a two-layer coating to be applied simultaneously. In comparison, a slide die is more flexible and productive owing to its ability to coat a theoretically unlimited number of layers to the substrate (Figure. 1.5) [2]. Different dies inherently generate different flow profiles, but they all can be divided into three flow zones for analysis, i.e. sheet forming zone, curtain flow zone, and impingement zone (Figure1.13). To optimize the productivity of a curtain coater, extensive research has been done over the past decade [1-2, 4-14].

It has been well accepted that inertial, viscous, capillary and external forces act together on the curtain and their interactions must be properly managed to maintain a stable curtain. Some basic requirements were concluded, for instance, low dynamic surface tension (30 mN/m), air bubble free, high shear stability, good wetting ability on

the basesheet, viscosity 100-300 cP and so on [3]. In each flow zone, different parameters need to be controlled in order to achieve stable curtain formation and a high quality coated surface with desired coat weight.

In the sheet forming zone, a set of phenomena in which the static contact lines spontaneously advance, retreat, and seemingly attach at the sharp edge of the lip is called "teapot effect" [14]. It is of most concern, especially on the slide-fed dies, because it is associated with down-web striations and streaks on the coated layer when uneven wetting underneath the lip forms dried-out deposits in the dead flow zone and causes the deviation of the curtain from the vertical trajectory [7]. However, it was also claimed that small deflection caused by the teapot effect is beneficial at a high flow rate, as it forms a bowed-shape dynamic contact line that actually drives small bubbles toward the edges thereby reducing the air entrainment downstream [15].

In the curtain flow zone, how to maintain a stable curtain is challenging. Early studies concluded a criterion that the curtain stability could be related to the Weber number of the material [6, 16]. To obtain a stable curtain, the fluid's inertial forces need to be larger than its surface tension, i.e. the resultant tension ($\rho {V_c}^2 H_c$) that needs to be destroyed at the boundary has to be larger than the surface tension, i.e. $\rho {V_c}^2 H_c > 2\sigma$ (Figure 1.16) [8]. On the other hand, if a disturbance creates a free circular edge in the curtain, which evolves and propagates until the curtain ruptures, a stable curtain can be achieved by ensuring the propagation velocity (V_d) at the free edge smaller than the main velocity (V_c) of the falling curtain [1]. Both approaches above conclude that a Weber

number at least larger than 2 can maintain a stable curtain. The Weber number can be further expressed with different parameters as follows (Table 3.1).

$$We = \frac{\rho {V_c}^2 H_c}{\sigma} = \frac{\rho V_c Q}{\sigma} = \frac{\rho \sqrt{2gx}\, H_{wet} U}{\sigma} > 2 \quad (3.1)$$

Table 3.1: A list of symbols used in Chapter III.

σ	surface tension of the fluid	μ	fluid viscosity
ρ	density of the fluid	Q	volumetric flow rate
H_c	local thickness of the curtain	V	impinging velocity
		U	web speed
H_{wet}	wet film thickness on the web	x	the length of the curtain measured from the die lip
V_c	main velocity of the falling curtain	Re	Reynolds number
V_d	propagation velocity of the free edge in the curtain (It could be in any direction) $V_d = \sqrt{\frac{2\sigma}{\rho H_c}}$	Ca	Capillary number

Some guidelines can be concluded from equation (3.1). These are that the curtain stability can be improved with a thicker curtain, faster curtain velocity, higher volumetric flow rate per unit width, and lower surface tension [6]. According to practical experience, two rules of thumb are: (a) volumetric flow rate per width should be above a minimum of 1.0 cm^2/s, and (b) the surface tension needs to be below the maximum 40 mN/m [1].

Surfactant is usually added to stabilize a curtain coating by reducing its interfacial tension and free energy, and to facilitate its wetting on a solid surface. Due to its diffusion-controlled adsorption process, surfactant needs time to reach its equilibrium state where the static surface tension is achieved. The adsorption rate is determined by the surfactant mobility, which determines the surface tension of fluids. For the curtain coating process, measuring the local tension instead of static surface tension in a flowing solution or on a deforming surface, i.e. the dynamic/non-equilibrium surface tension, makes more sense due to the high speed of the process.

Various techniques can measure the liquid static/dynamic surface tension. Among them, the maximum bubble pressure and falling curtain/Mach angle methods are the most common ones for curtain coating. In the method of maximum bubble pressure, one end of a capillary is immersed in the testing liquid that introduces air bubbles at a certain rate. The surface tension can be calculated with the bubble pressure using Laplace law for any time when the corresponding radius is known [16]. By introducing a perturbation into the curtain, an angle is formed by the Mach wave, half of which is defined as Mach angle (α) (Figure 1.19) [8]. In accordance to the aforementioned guidelines, the critical condition of a stable curtain is where the fluid's inertial forces ($\rho {V_c}^2 H_c$) equal its surface tension (2σ) (Figure 1.16). Given the direction of velocity and the equation (3.1), the relation between Mach angle and Weber number can be expressed as equation (3.2) (Table 3.1).

$$We = \frac{2}{sin^2(\alpha)} = \frac{\rho H_c {V_c}^2}{\sigma} \tag{3.2}$$

Thus, the Weber number of a curtain coating at a certain height can be attained in this way for the analysis of curtain stability.

Another quantity of significance is the final curtain velocity at which the curtain impinges onto the substrate, because the relative difference of the final curtain velocity and the web velocity has a significant impact on the curtain behavior and the properties of the coated substrate in the impingement zone. Several empirical formulas were conjectured for its estimation, but none has succeeded due to the complex curtain flow arisen from the complex forces' interactions. When impinging onto the moving web, the coating curtain is usually considered as viscous free surface flows with dynamic wetting lines where the liquid/gas interface appears to intersect the substrate as the liquid continually lands on the solid substrate. Much research has been done here to avoid runnability problems, such as heel formation and air entrainment, but also to define the operational window for a curtain coating process [1, 7, 10, 17]. It was reported that when the viscous stresses overwhelm the capillary pressure, i.e. Ca >>1 (it is also the industrially relevant limit), Reynolds number (Re) and speed ratio (U/V) are the only relevant dimensionless groups for macroscopic impingement flow (Table 3.1). Accordingly, an operational window of the Reynolds number (Re) as a function of the speed ratio (U/V) can be drawn for a curtain coater (Figure 1.24).

However, so far the effects of coating rheology on the curtain stability and operability have not been taken into account. In order to form a stable curtain and avoid a web break in the impingement zone, a coating curtain should endure a certain degree of

stretching without oscillatory effects or breakage, i.e. maintain good stretchability. It has been emphasized that extensional viscosity, as well as shear viscosity and viscoelasticity, impacts curtain runnability and coatability. In Chapter II, the rheological properties of coatings containing biobased latex binder and different types of rheology modifiers were characterized. Together with the surface tension results revealed in this chapter, the contributions of these coating properties to curtain stability were determined, which clarified the influences of biobased latex binder and rheology modifiers on the stability of a curtain.

Experimental

Coatings were formulated according to Tables 2.1-2.3. A combination of GCC (Hydrocarb 90 from OMYA) and clay (KaMin Hydragloss 90) was added as the pigment system in the coatings. The petroleum-based styrene-butadiene-acrylonitrile (XSB) latex binder used in this study was Prostar 5405 (formerly Dow, then Styron, now Trinseo), and the petro-based extensional viscosity modifier was Sterocoll DF 3 from BASF. The biobased latex used was EcoSphere® X202 from EcoSynthetix. BASF Lumiten ISC was added as a surfactant and the dispersant used was BASF Dispex N40. As shown, two control coatings containing all-synthetic latex were prepared (Table 2.1). In addition, three groups of coatings were formulated with different rheology modifiers, i.e. petro-based extensional viscosity modifier, inorganic rheology modifiers A and B (Tables 2.2 and 2.3). The petro-based extensional viscosity modifier is a common additive used in

conventional curtain coatings. To determine its effect on biobased latex binder, the first group of coatings was studied (Table 2.2). The two inorganic rheology modifiers were investigated to determine if their interactions with the biobased latex binder could eliminate the need for the petro-based extensional viscosity modifier in the curtain coatings (Table 2.3). The weight percentages of latex replaced with biobased latex binder were 25%, 35%, and 45%, which are respectively denoted as EX-1, -2 and -3. The amount of inorganic rheology modifier added to each formulation was determined by matching the Brookfield viscosity for the control coating XSB-3. The target ranges of pH, %solids, and Brookfield viscosity of the coatings at 100 RPM were 8.5-9.0, 60.45-60.60%, and 200-300 cP, respectively. Note, the %solids were determined using a CEM Smart System 5 Microwave Analyzer.

To measure coating surface tension, the maximum bubble pressure method was applied by using a SITA pro line t15 tensiometer. For each coating, the dynamic surface tension at bubble lifetime from 0.1 s to 20 s was first detected. Consequently, the equilibrium bubble lifetime was found from the resultant curves to determine the static surface tension. Rheological analysis has been introduced in Chaper II. Based on all the coating characteristics attained, coatings XSB-3, EX-1, EA-1, EA-2, EA-3 and EB-2 were selected for the curtain stability analysis.

A curtain stability tester was assembled with a slot-fed die (Figure 3.1). In each test, 7 L of coating was pumped at different flow rates through the die of constant gap, 1.32 mm. During its running, the mass flow rate of coating was measured at each pump

setting. Meanwhile, the density and Brookfield viscosity of coating was measured at a certain time interval to make sure that air entrainment to the curtain was controlled to a minimum. At each flow rate, a Mach angle at the same height (5 cm) was created by a small round intruder and the angle was captured by use of a video camera every 1/30 s. Using imaging capturing software, the initial Mach angle was selected and measured. The average Mach angle of three replicates was used to calculate the Weber number using equation (3.2). As a result, the curtain stability of each coating was determined from the Weber numbers obtained at different volumetric flow rates. This is based on the theory that coatings of higher Weber numbers form more stable curtains.

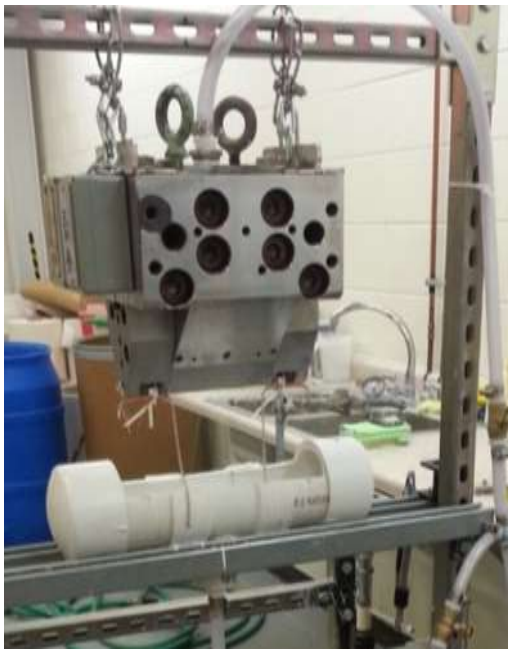

Figure 3.1: Curtain stability tester with a slot-fed die.

Results and Discussion

The basic properties of coatings have been discussed in Chapter II (Tables 2.4, 2.5). Figures 3.2-3.7 show the surface tension of all the coatings obtained by using maximum bubble pressure method. As we know, the dynamic surface tension of a liquid containing surfactant is determined by the concentration and mobility of the surfactant. In the all-synthetic latex coatings, the increase in viscosity by adding petro-based extensional viscosity modifier retards the surfactant mobility, which explains the different surface tension between two controls (XSB-1 and XSB-3) (Table 2.4 and Figures 3.2, 3.3). As is stated in Chapter II, the swelling of biobased latex particles can reduce the amount of free water in the coating, which increases the concentrations of coating components. Hence, for the coatings containing different levels of biobased latex and the same amount of petro-based extensional viscosity modifier and surfactant, the surface tension depends on the coating viscosity, as well as the replacement level of biobased latex. Therefore, it is not surprising to see that coatings with biobased latex resulted in higher surface tension than the controls in Figures 3.2 and 3.3 (EX1-3 *vs.* XSB-3, XSB-1). Given the results, it suggests that the biobased latex coatings need more surfactant than the all-synthetic latex coatings to achieve a low surface tension (<40 mN/m) in the presence of petro-based extensional viscosity modifier. Furthermore, increasing the latex replacement can affect the latex concentration through the reductions of both latex and free water, which can either increase or decrease the degree of agglomeration between latex and petro-based extensional viscosity modifier. It is also

reasonable to suspect that the formation of agglomeration can also immobilize some water that further affects the concentrations of latex and surfactant. Consequently, the surface tension of coatings EX-1, EX-2, and EX-3 differs from one another with the same amount of surfactant added (Figures 3.2, 3.3).

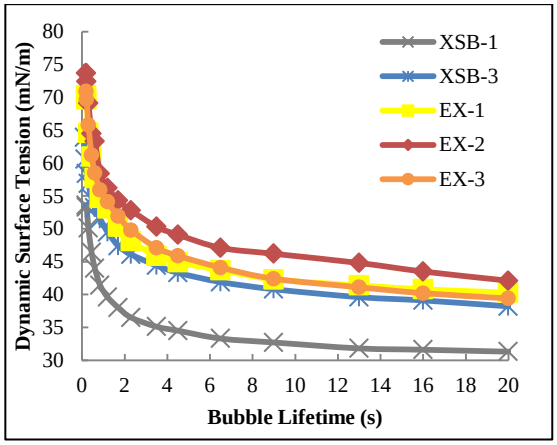

Figure 3.2: Dynamic surface tension of controls and coatings with petro-based extensional viscosity modifier.

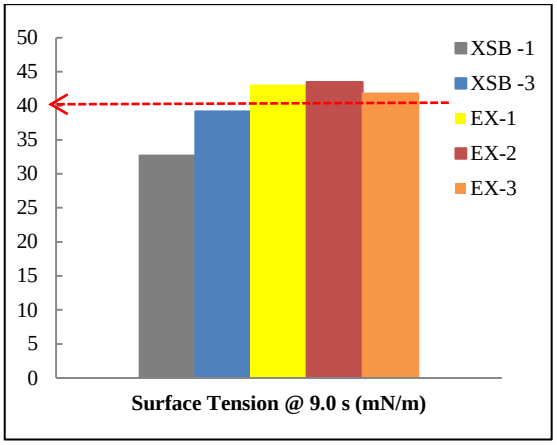

Figure 3.3: Surface tension of controls and coatings with petro-based extensional viscosity modifier at bubble lifetime of 9.0 s.

In the coating groups containing inorganic rheology modifiers, similar mechanisms can be applied, but the amount of the inorganic rheology modifier adds to another variable that affects the concentrations of coating components. The inorganic rheology modifier can form a network with biobased latex the degree of which is determined by their concentrations. Thus, not only their absolute amounts, but also the amounts of water absorbed by biobased latex and immobilized by the network determine their concentrations. Although the comparison of coating viscoelasticity and elastic components can indicate the network formation in a degree, it is still difficult to quantify

it to determine the actual amount of immobilized water in each coating. Therefore, the surface tension of coatings with inorganic rheology modifier A at different levels of latex replacement varied accordingly (Figures 3.4, 3.5).

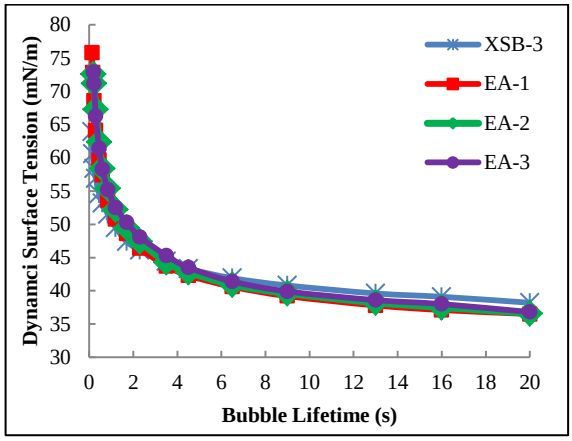

Figure 3.4: Dynamic surface tension of controls and coatings with inorganic rheology modifier A.

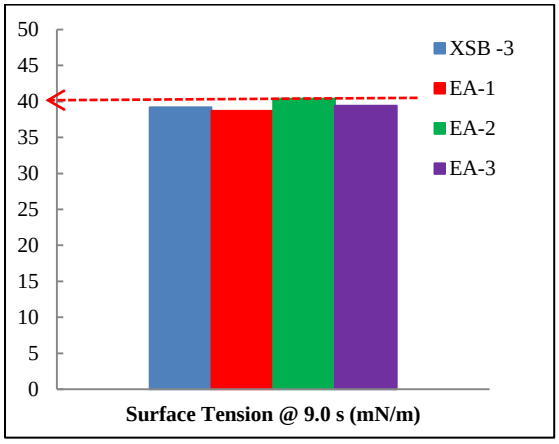

Figure 3.5: Surface tension of controls and coatings with inorganic rheology modifier A at bubble lifetime of 9.0 s.

However, the degree of network formation determined by the concentration and functionality of the inorganic rheology modifier becomes the only factor that contributes to the difference in the surface tension when comparing the coatings with different inorganic rheology modifiers at the same latex replacement level, i.e. EA *vs.* EB. Although coating EB-1 has similar surface tension as EA-1, the other coatings that consist of less inorganic rheology modifier B show lower surface tension than those with more modifier A. This indicates that the surfactant concentrations of the former ones were higher due to more networks formed to immobilize more water in them than the latter ones (EA-2 *vs.* EB-2, and EA-3 *vs.* EB-3) (Figures 3.4-3.7). In addition, the fact

that the surface tension of coatings with inorganic rheology modifier B decreases with the increase of the latex replacing levels suggests that the effect of the biobased latex swelling plays stronger part in the surface tension within this coating group (Figures 3.6, 3.7).

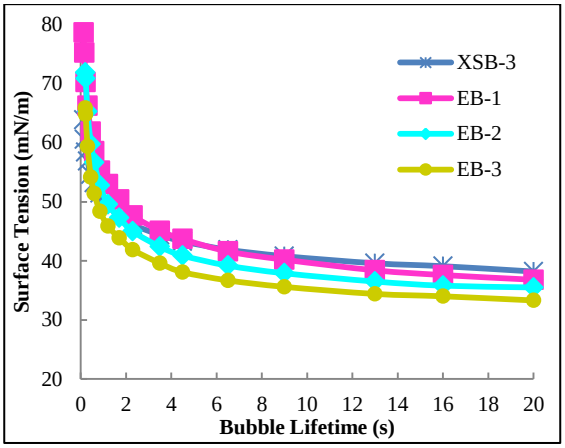

Figure 3.6: Dynamic surface tension of controls and coatings with inorganic rheology modifier B.

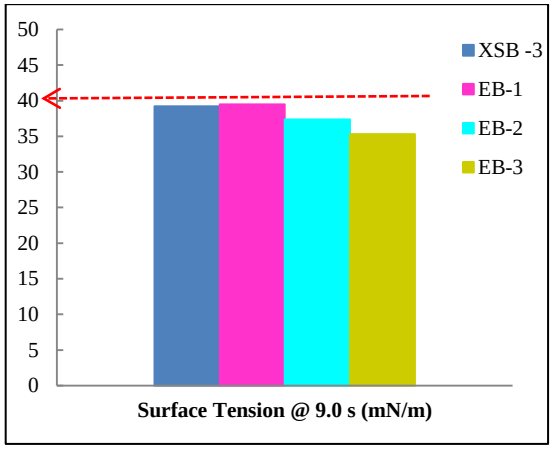

Figure 3.7: Surface tension of controls and coatings with inorganic rheology modifier B at bubble lifetime of 9.0 s.

In Chapter II, the extensional viscosity of all coatings was obtained from the CaBER measurements [18]. In principle, the evolution of the filament formed on the CaBER is driven by the capillary force, which is related to the surface tension, and is resisted by the viscoelasticity. Thus, it is interesting to see an obvious correlation between the surface tension and CaBER filament lifetime in these four groups of coatings in Figures 3.8-3.11. However, no significant correlation was found between the filament lifetime and tan δ values probably because the tan δ values of all coatings were obtained under an oscillatory shear rather than an extension. Also, such correlation cannot be

found by comparing the coatings from different groups, which is probably attributed to the inherently different natures of the coatings from different groups.

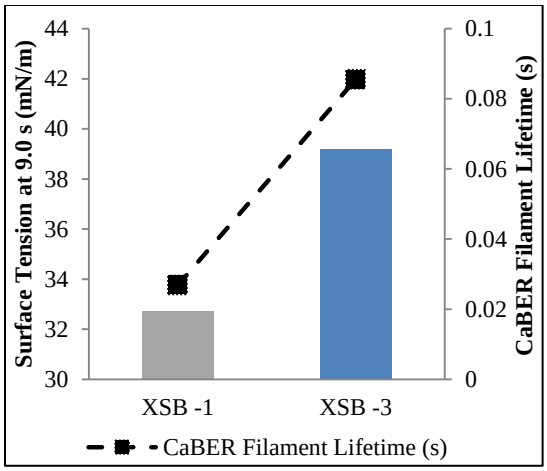

Figure 3.8: Correlation of the surface tension and CaBER filament lifetime of the control coatings.

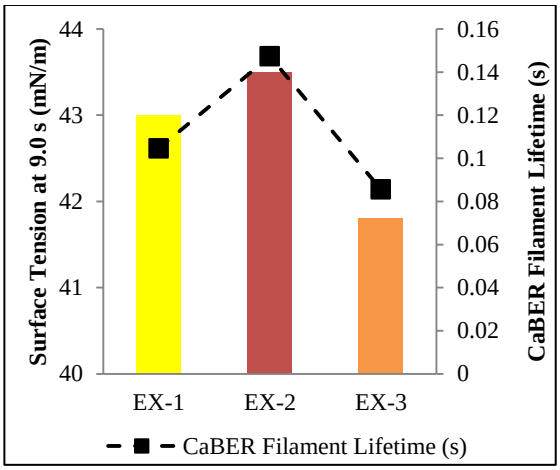

Figure 3.9: Correlation of the surface tension and CaBER filament lifetime of coatings with biobased latex and petro-based extensional viscosity modifier.

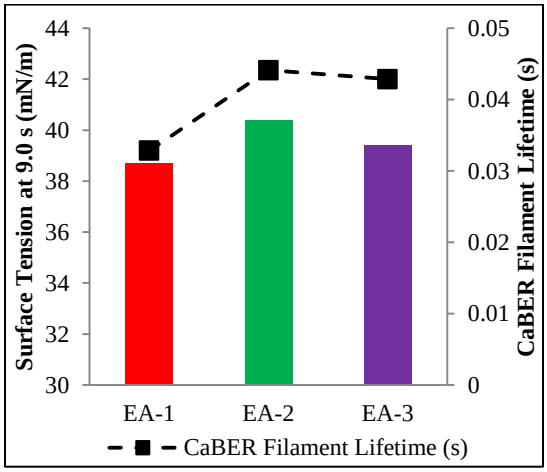

Figure 3.10: Correlation of the surface tension and CaBER filament lifetime of the coatings with biobased latex and inorganic rheology modifier A.

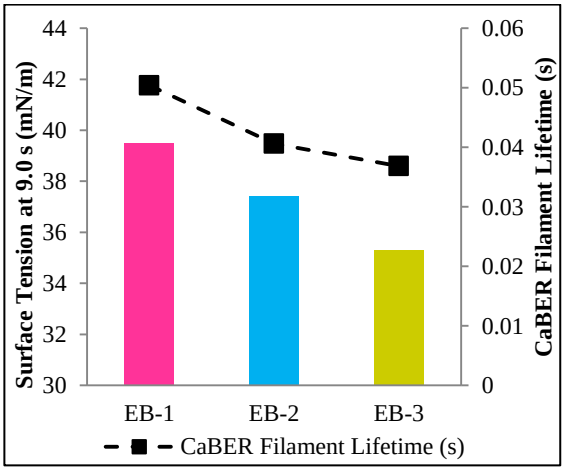

Figure 3.11: Correlation of the surface tension and CaBER filament lifetime of the coatings with biobased latex and inorganic rheology modifier B.

In Figures 3.12 and 3.13, the change of coating density and Brookfield viscosity over time implies that coatings were relatively stable during the tests.

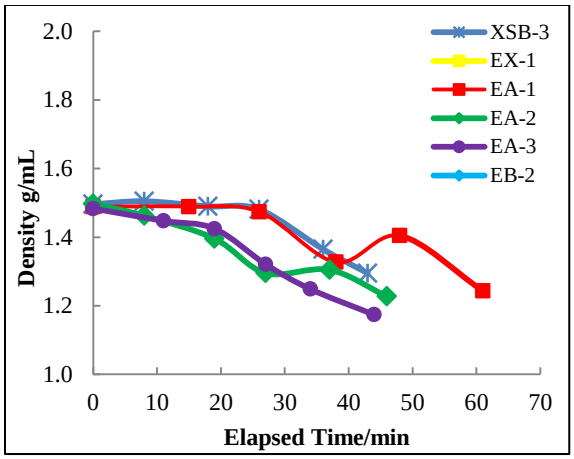

Figure 3.12: Coating density changing over time.

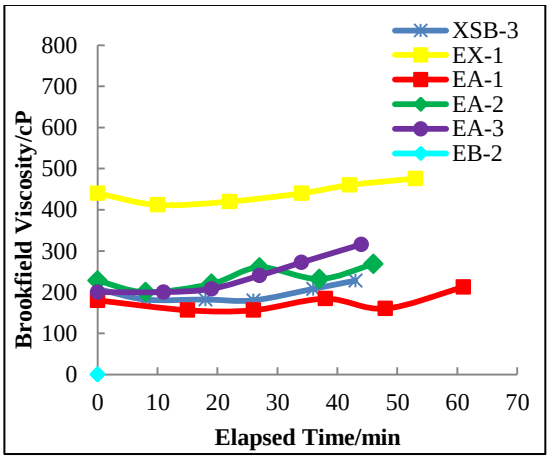

Figure 3.13: Brookfield viscosity of coating changing over time.

The linear correlation of pump setting and volumetric flow rate was plotted in Figure 3.14. It was also confirmed that the volumetric flow rate on the curtain stability test could be increased to 63 mL/s without causing severe air entrainment in the coatings.

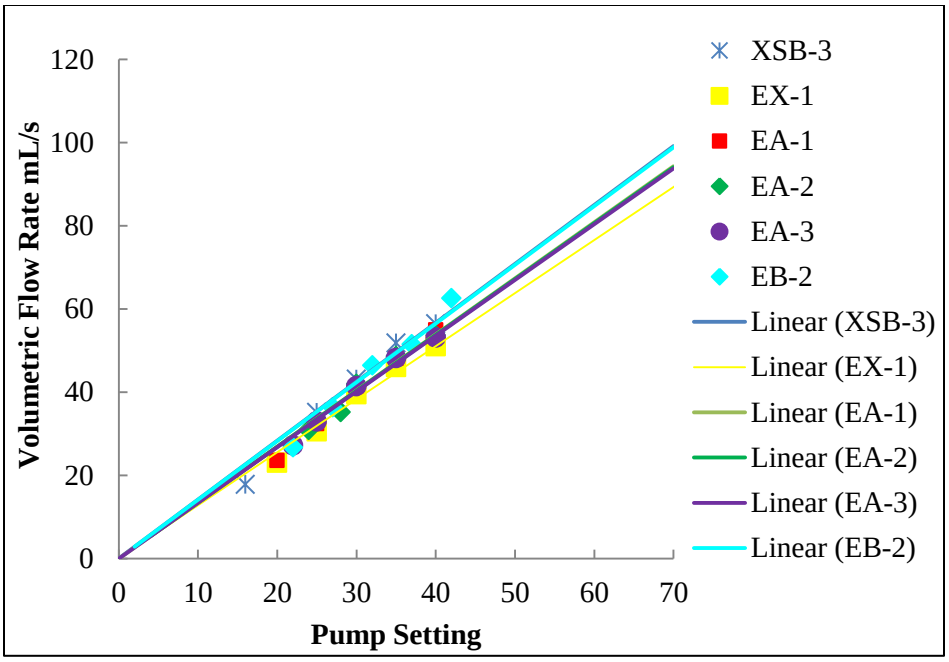

Figure 3.14: Correlation of pump setting and volumetric flow rate of curtain.

Finally, the Weber numbers of the selected coatings at five accelerated volumetric flow rates are plotted in Figures 3.15, 3.17 and 3.19. All data was fitted by cubic regression fitting with the intercept of 0. The resulted R^2 values are listed in Table 3.2. All the data attained from the curtain stability tester can be found in Appendix B. As it was expected, Mach wave was more difficult to form at higher flow rates during the tests, meaning that the curtain was more stable than that at lower flow rates. The rheological findings reported in the Chapter II are included in the discussion below.

Table 3.2: R^2 values of cubic regression fitting of the data in Figures 3.15, 3.17, 3.19.	
Sample	**R^2**
XSB-1	0.9914
XSB-3	0.9993
EX-1	0.9982
EA-1	0.9884
EA-2	0.9052
EA-3	0.9944
EB-2	0.9612

Comparing the Weber numbers of two control coatings in Figure 3.15, it can be seen that the curtain stability of the all-synthetic latex coating was slightly increased by adding the petro-based extensional viscosity modifier (XSB-1 *vs.* XSB-3). It was speculated that the ability of XSB-1 to maintain certain curtain stability at low flow rate was attributed to its relatively low surface tension and low shear viscosity (Figures 3.2, 3.3, 3.16) [18]. As the coating of lower shear viscosity is more ready to deform, the relatively low elastic component and extensional viscosity of coating XSB-1 started to affect the curtain to lose stability as the flow rates increased (Figure 3.15). Comparing the coatings with petro-based extensional viscosity modifier, biobased latex coating (EX-1) formed less stable curtain than the all-synthetic latex control one (XSB-3) at low flow rates (<30 mL/s), which was probably caused by its higher surface tension (Figures 3.3, 3.15). As the flow rates increased, the slower shear thinning, comparable elastic structure

and extensional viscosity of coating EX-1 enabled itself to achieve a better curtain stability than the control (Figures 3.15, 3.16) [18]. However, a reducing tendency of curtain stability appeared when the flow rates continued to increase which is probably caused by the fact that the coating structure became viscous when the flow rates increased to a certain degree (Figures 2.5, 3.15).

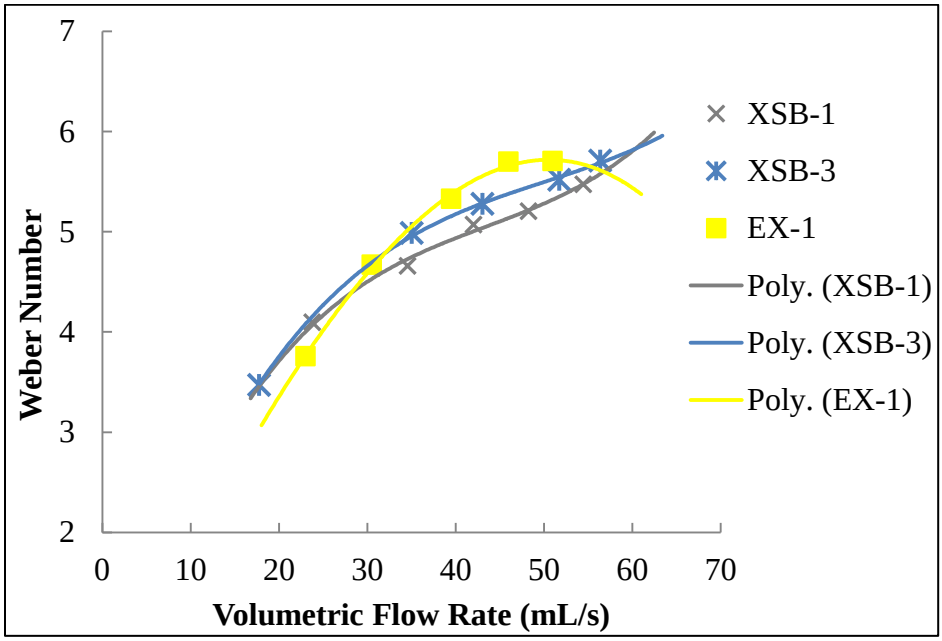

Figure 3.15: Weber numbers of coatings XSB-1, XSB-3 and EX-1 changing with curtain volumetric flow rates.

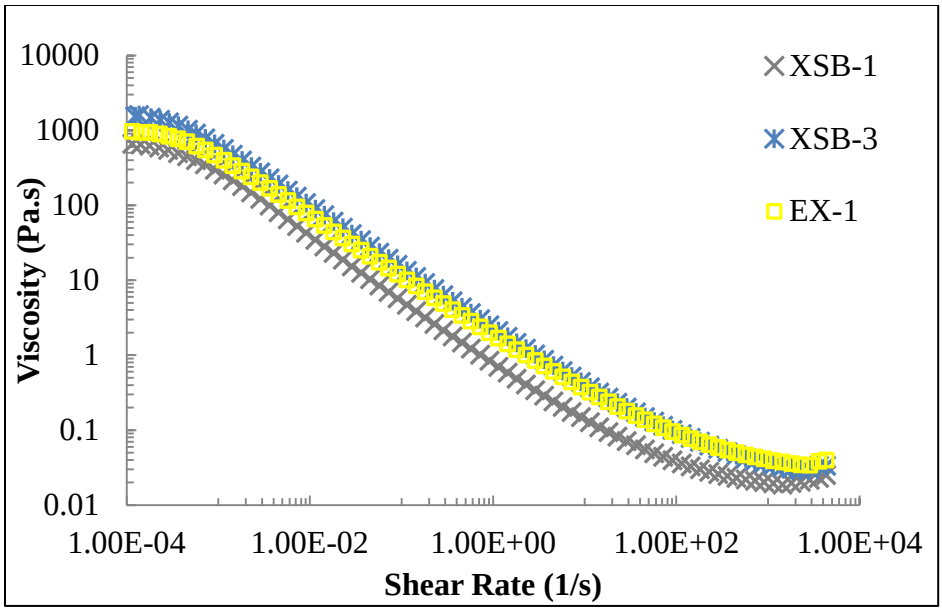

Figure 3.16: Comparison of shear thinning behavior of coatings XSB-1, XSB-3 and EX-1 [18].

In the comparison of the coating group containing biobased latex and inorganic rheology modifier A with the control XSB-3, it shows that replacing more petro-based latex with biobased latex can reduce the amount of inorganic rheology modifier A needed to achieve a comparable or even better curtain stability especially at high flow rates (EA-1, EA-2 and EA-3) (Figure 3.17). Among them, coating with 25% latex replacement (EA-1) shows very similar curtain stability as the control XSB-3 (Figure 3.17). Their comparable surface tension, shear viscosity and shear thinning behavior certainly contribute to this similarity (Figures 2.2, 3.4, 3.5). Moreover, the incremental elastic moduli (G') and reductive tan δ (<1) of them also imply a formation of more and more elastic structures as the frequency increased and the structure of coating EA-1 was more

elastic than that of the control XSB-3, which compensated for the impact of its lower extensional viscosity on the curtain stability (Figures 2.7, 2.8, 3.10).

Among all the coatings analyzed, the coatings consisting of 35% and 45% latex replacement and inorganic rheology modifier A formed the most stable curtains according to their Weber numbers (Figure 3.15, 3.17, 3.19). Their similarity in surface tension and extensional viscosity resulted in the similar curtain stability at low flow rates. Although coating EA-2 has more elastic structure than EA-3, the former exhibits more shear thinning than the latter, which retarded its increment in the curtain stability as the flow rates increased (Figures 3.17, 3.18).

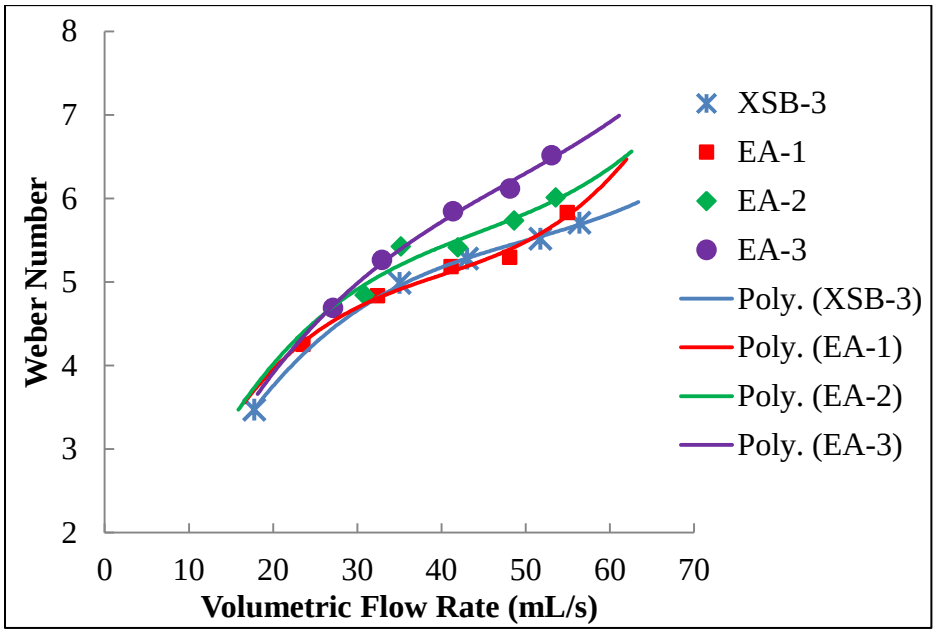

Figure 3.17: Weber numbers of coatings containing biobased latex and inorganic rheology modifier A, and control coating XSB-3 changing with curtain volumetric flow rates.

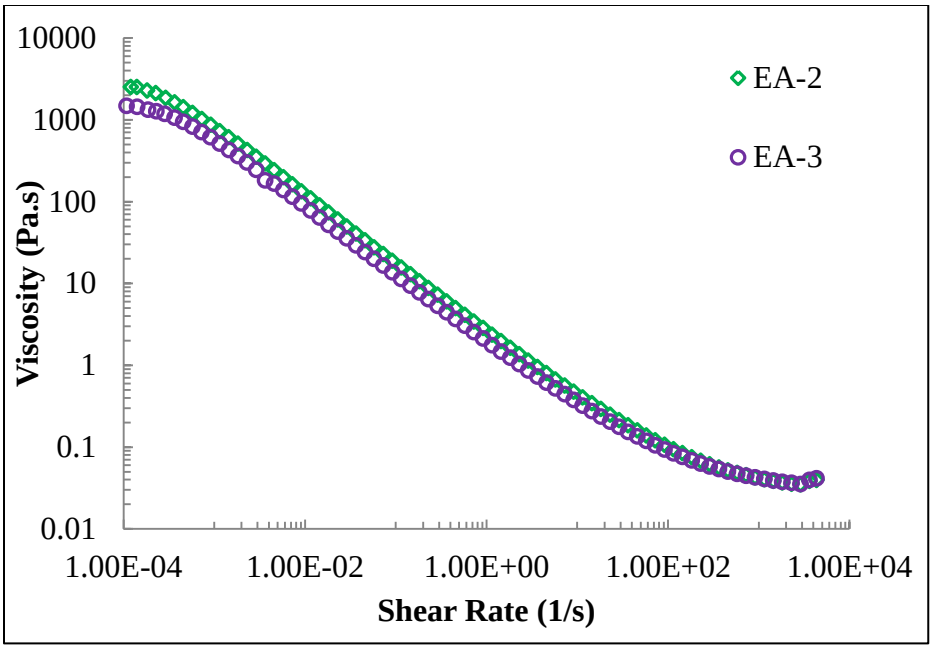

Figure 3.18: Comparison of shear thinning behavior of coatings EA-2 and EA-3 [18].

The Weber numbers in Figure 3.19 indicate that coating with inorganic rheology modifier B at 25% latex replacement level showed very similar curtain stability as the control XSB-3. Given their similar surface tension and viscoelasticity (Figures 2.9, 2.10, 3.6, 3.7), it can be speculated that the similarity was attributed to the slower shear thinning behavior of coating EB-2 which compensated for its lower extensional viscosity than the control (Figures 3.8, 3.11, 3.20).

Besides, coatings EB-2 and EB-3 manifested very similar characteristics in terms of viscoelasticity, shear rate dependence of viscosity, and extensional viscosity, so it can be predicted that the curtain performance of EB-3 could be very similar or even better than that of EB-2 due to its lower surface tension (Figures 2.9, 2.10, 3.11).

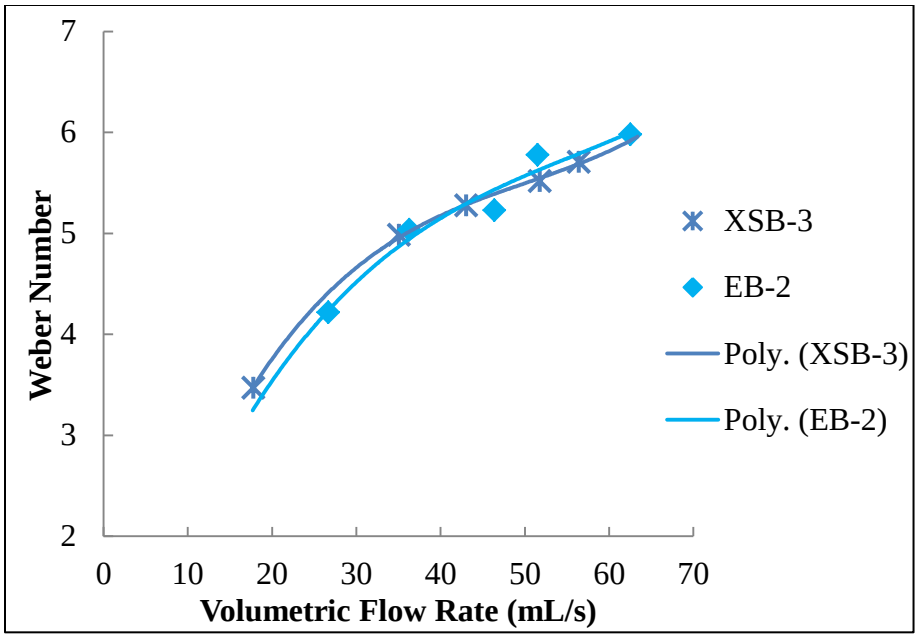

Figure 3.19: Weber numbers of coatings with 35% latex replacement and inorganic rheology modifier B, and control coating XSB-3 changing with curtain volumetric flow rates.

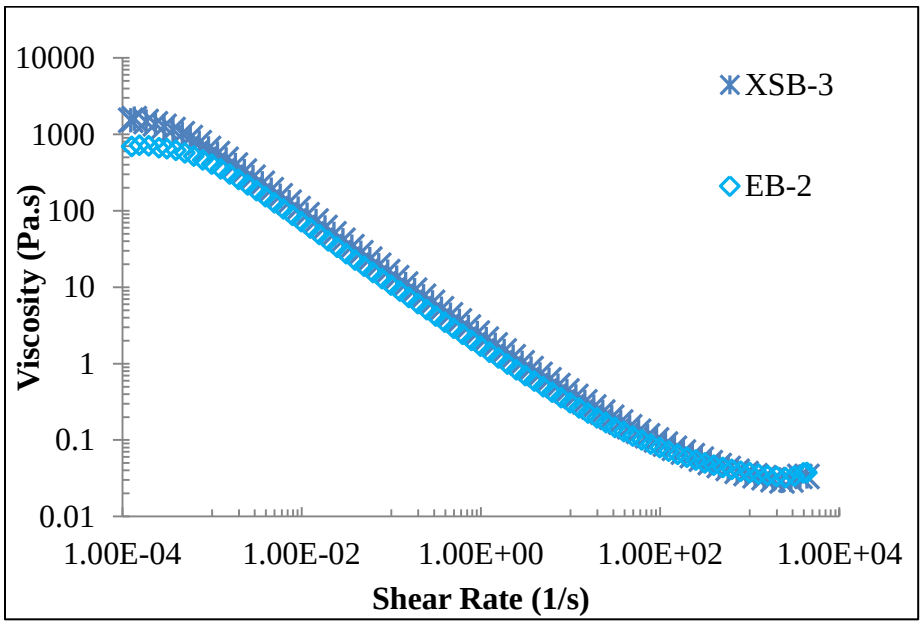

Figure 3.20: Comparison of shear thinning behavior of coatings XSB-3 and EB-2 [18].

Conclusions

This study continued to characterize the curtain coatings with different levels of biobased latex and different types of rheology modifiers in terms of dynamic/static surface tension. The effects of different interactions among different coating components on the surfactant concentration, which determines the surface tension of these coating, were revealed. In addition, a significant correlation between the surface tension and the CaBER filament lifetime was found in different coating groups.

Six coatings were selected for the curtain stability analysis on a slot-fed curtain tester. Based on the changes of Weber numbers over the flow rates from 20 to 65 mL/s, it was found that replacing latex with biobased latex and petro-based extensional viscosity modifier with inorganic rheology modifiers in the coating can generate comparable or even better curtain stability. Among them, coatings with 35% and 45% (wt. %) latex replacement and inorganic rheology modifier A formed the most stable curtains.

By interpreting the results of curtain stability with coating properties obtained, it can be concluded that the relative importance of coating surface tension, shear rate dependence of viscosity, viscoelasticity and elastic component, as well as extensional viscosity determines the curtain stability at different flow rates. A coating with relatively low surface tension (< 40 mN/m) and shear viscosity required a more elastic structure and/or higher extensional viscosity to form a stable curtain, especially at higher flow rates, where shear thinning plays a more critical part. For the coatings with similar surface tension and shear thinning behavior, the one of low shear viscosity is more ready to

deform which requires more elastic coating structure and/or high extensional viscosity to maintain the curtain stable, especially at high curtain flow rates.

In conclusion, this chapter discussed some necessary trade-offs for in the coating formulations in order to optimize curtain stability. Several promising coating formulations were selected for the analysis of coating coatability. It is believed that the findings of this study can help advance coating formulation knowledge towards the optimization of biobased latex binder containing coatings for commercial mill operations in the future.

References

1. Schweizer, P. (2003): "Curtain coating-stability a critical operating parameter", 4th and 5th PITA Coating Conference, Edinburgh, UK.
2. Miyamoto, K. and Katagiri, Y. (1997) "Curtain Coating", Chapter 11c in "Liquid film coating: scientific principles and their technological implications", ed. Kistler, S.F. and Schweizer, P.M., Chapman & Hall, London.
3. Klass, C. (2013): "Blade, rod and contour coaters", Coating Short Course, Western Michigan University.
4. Schmid, M. (2011): "Curtain coater as air knife replacement", TAPPI PaperCon, New Orleans, USA.

5. Tripathi, P., Joyce, M., Fleming, P.D. and Sugihara, M. (2009): “A statistical study of process variables to optimize a high speed curtain coater-Part I”, TAPPI J., 8(1): p. 20-26.
6. Tripathi, P., Joyce, M., Fleming, P.D. and Sugihara, M. (2009): “A statistical study of process variables to optimize a high speed curtain coater-Part II”, TAPPI J., 8(2): p. 29-32.
7. Kistler, S.F. (1983): “The fluid mechanics of curtain coating and related viscous free surface flows with contact lines”, Ph.D. thesis, University of Minnesota, Minneapolis and University Microfilms International, Ann Arbor, MI.
8. Brown, D.R. (1961): “A study of the behavior of a thin sheet of moving liquid”, J. Fluid Mech. 10: p. 297-305.
9. Taylor, G.I. (1959): “Disintegration of fluid sheets”, Part III in “The dynamics of thin sheets of fluid”, Proc. Roy Soc. A., p.253-313, London.
10. Triantafillopoulos, N., Grön, J., Luostarinen, I., and Paloviita, P. (2004): “Operational issues in high-speed curtain coating of paper, Part 1: The principles of curtain coating”, TAPPI J., 3(11): p.6-10.
11. Alleborn, N., Suenderhauf, G., Raszillier, H., and Durst, F. (2001): “Edge retraction on a planar liquid sheet”, Proceedings of the 4th European Coating Symposium, Bruxelles, Belgium.
12. Lin, S.P. (1981): “Stability of a viscous liquid curtain”, J. Fluid Mech.104, p. 111-118.

13. Lin, S.P., Lian, Z.W. and Creighton, B.J. (1990): “Absolute and convective instability of a liquid sheet”, J. Fluid Mech. 220: p. 673-689.
14. Kistler, S.F. and Scriven, L.E. (1994): “The teapot effect: sheet-forming flows with deflection, wetting and hysteresis”, J. Fluid Mech. 263: p. 19-62.
15. Suga, Y., Kobayashi, K., Sasahara, T. and Miyamoto, M. (1991): “Coating method”, European Patent EP 426122 A2.Simon, M. (1851): "Recherches Sur La Capillarité", Ann. Chim. Phys., 32: p.5-41.
16. Simon, M. (1851): "Recherches Sur La Capillarité", Ann. Chim. Phys., 32: p.5-41.
17. Kokko, A., Kettle J., Rautkoski, H., Shen, Y. (2010): “Characterization of curtain coating colors”, TAPPI 11th Advanced Coating Fundamentals Symposium, Munich, Germany.
18. Chen, T., Joyce, M., Fleming, P.D., Bloembergen, S. (2016): “Pigmented formulations containing biobased nanoparticle binders for curtain coating applications; Part 1: rheological study”, Paper submitted for presentation and publication to TAPPI PaperCon2016.

CHAPTER IV

PIGMENTED FORMULATIONS CONTAINING BIOBASED NANOPARTICLE BINDERS FOR CURTAIN COATING APPLICATIONS; PART 3: COATABILITY STUDY

Abstract

This Chapter continues to investigate the curtain stability and coatability of biobased latex containing coatings on a pre-coated linerboard using a laboratory slide-fed curtain tester. Based on the coating properties reported in the Chapters II and III, the coatings consisting of 25% and 35% latex replacement and one of two inorganic rheology modifiers were selected for this study. To adjust the coating properties for the slide-fed curtain tester, a new type of synthetic latex was used. For comparison, two control coatings containing a synthetic latex and a petro-based extensional viscosity modifier were formulated as well. The properties of coated samples were measured in terms of coat weight, brightness, gloss and IGT dry pick strength.

It was found that all coatings resulted in good curtain stability on the slide-fed coater. The curtain stability was improved by increasing the biobased latex substitution in the coatings with an inorganic rheology modifier, although the addition of petro-based extensional viscosity modifier in the coatings provided a larger range of operational pump settings. The addition of petro-based extensional viscosity modifier improved the gloss of the coated samples. Replacing it with an inorganic rheology modifier in the biobased latex coating resulted in comparable IGT dry pick strength to the control and the

amount of biobased latex binder and inorganic rheology modifier added impacted the brightness and gloss. Among them, coatings containing inorganic rheology modifier B are most promising for their higher brightness, gloss, and IGT dry pick strength in comparison to the control coating.

Introduction

As one of the coating technologies used in the paper industry, curtain coaters have been able to produce various paper grades at very high speed, such as paperboard, specialty, printing, and graphic papers, etc. [1, 2]. On a curtain coater, the coating goes through a slot-fed or slide-fed die to form a smooth curtain that falls freely onto the substrate where the coating creates a contour profile (Figures 1.13, 1.5). The internal design of a die is critical to the uniform distribution and flow of the coating. In comparison to a slot die, a slide die is more flexible due to its ability to coat a theoretically unlimited number of layers onto the substrate (Figure 1.5) [2]. In general, curtain flow is divided into three zones for analysis, i.e. a sheet forming zone, a curtain flow zone, and an impingement zone (Figure1.13).

Compared with other metering technologies, curtain coaters produce more uniform coating coverage, which contributes to superior printability. As no direct contact occurs between the die and the substrate, the strength requirements for the substrate are not as demanding as for a blade or rod coater. Streaking or scratching defects are also less prevalent. Although air-knife coaters can generate similar coating coverages, for

their limitations in speed and coating solids, and the requirement for frequent cleaning, curtain coaters have been displacing them in some applications [4].

To optimize the production of a curtain coater, extensive research has been done in the past decades [1-10]. It has been well accepted that inertial, viscous, capillary and external forces act together on the curtain and their interactions must be properly managed in different flow zones. Some basic requirements for coating properties were concluded, for instance, low dynamic surface tension (<40 mN/m), air bubble free, high shear stability, good wetting ability on the substrate, viscosity 100-300 cP, etc. [11]. In each flow zone, different parameters need to be controlled in order to achieve stable curtain formation and a high quality coated surface with desired coat weight.

In the sheet forming zone, especially on the slide-fed curtain coaters, undesired "teapot effects" are associated with down-web striations and streaks on the coated layer [10]. However, it was also claimed that the small deflection by teapot effects is beneficial at a high flow rate, because it forms a bowed-shape dynamic contact line that actually drives small bubbles toward the edges and thereby reduces the air entrainment downstream [12]. In the curtain flow zone, curtain stability is of utmost importance, which has been discussed in details in our last two papers [13, 14]. It is also emphasized that the final velocity of the curtain right before its impingement has great impact on the curtain performance downstream. Its theoretical estimation is so complicated that nobody has totally succeeded in describing it. In the impingement zone, the relative difference of the final curtain velocity (V) and the web velocity (U) has great impact on the curtain

behavior and the properties of the coated substrate. Together with speed ratio (U/V), several dimensionless numbers are used to analyze and predict curtain performance in this zone. It was claimed that when viscous stresses overwhelm the capillary pressure, i.e. Ca >>1 (it is also the industrially relevant limit), the Reynolds number (Re) and speed ratio (U/V) are the only relevant quantities for the macroscopic impingement flow [3]. Accordingly, an operational window can be drawn for a curtain coater. Figure 1.24 shows a general operational window plotted by the other researchers [15].

Moreover, coating curtain needs to be stretchable in a degree to resist the extension in different flow zones. Given the slot clearance of industrial interest, the flow transits from shear to extensional almost immediately after the coating exits the die slot [2, 3]. If the extensional force is too high, the curtain may break or split, and further interfere with the impingement zone. Once the curtain hits the substrate, it is deflected and undergoes extreme extension again because the velocity difference of the curtain and the moving web. The extension ratio, along with the volume stream of the coating, determines the final coat weight.

Experimental

Based on the previous findings, coating formulations were adjusted for the application of the slide-die curtain process. To clarify the effects of replacing Prostar 5405 (formerly Dow, then Styron, now Trinseo) with Litex 7110 from Synthomer on the coating properties, two control coatings containing one of these two latex and a petro-

based extensional viscosity modifier, were formulated according to Table 4.1. In the rest of coating formulations (Tables 4.2, 4.3), Litex 7110 denoted as petro-based latex-2 was used. The petro-based extensional viscosity modifier used was BASF Sterocoll DF 3. The biobased latex used was EcoSphere® X202 from EcoSynthetix. The surfactant used was BASF Lumiten ISC and the dispersant was BASF Dispex N40. The GCC used was Hydrocarb 90 from OMYA. The clay used was KaMin Hydragloss 90. The weight percentages of petro-based latex binder replaced with biobased latex binder were 25% and 35%, which are respectively denoted as ES(1) and ES(2) for example. The amount of inorganic rheology modifier added to each formulation is the same as in the previous studies. The target ranges of pH, %solids, and Brookfield viscosity of the coatings at 100 RPM were 8.5-9.0, 60.0%-61.0%, and 200-300 cP, respectively.

To make sure the surface tensions of the new coatings meet the requirement (<40 mN/m), the amount of surfactant needed for each coating was preliminarily determined by using a maximum bubble pressure tensiometer.

Table 4.1: Coating formulations for the controls.		
	XSB-3	**LAX-1**
	pph	pph
GCC	70	70
Clay	30	30
Petro-based Latex-1	12	0
Petro-based Latex-2	0	12
Petro-based Extensional Viscosity Modifier	0.25	0.25
Surfactant	0.2	0.2
Dispersant	0.2	0.2

Table 4.2: Coating formulations for the petro-based extensional viscosity modifier study.		
	ES(1)	**ES(2)**
	pph	pph
GCC	70	70
Clay	30	30
Petro-based Latex-2	9	7.8
Biobased Latex Binder	3	4.2
Petro-based Extensional Viscosity Modifier	0.25	0.25
Surfactant	0.2	0.2
Dispersant	0.2	0.2

Table 4.3: Coating formulations for the inorganic rheology modifier study.				
	Inorganic Rheology Modifier A		Inorganic Rheology Modifier B	
	EA(1)	**EA(2)**	**EB(1)**	**EB(2)**
	pph	pph	pph	pph
GCC	70	70	70	70
Clay	30	30	30	30
Petro-based Latex-2	9	7.8	9	7.8
Biobased Latex Binder	3	4.2	3	4.2
Inorganic Rheology Modifier A/B (Proprietary)	13.3% dry weight of biobased latex	7.14% dry weight of biobased latex	6.92% dry weight of biobased latex	3.0% dry weight of biobased latex
Surfactant	0.45	0.4	0.4	0.3
Dispersant	0.2	0.2	0.2	0.2

After stabilizing overnight, the curtain stability and coatability of all the coatings were evaluated using a slide-fed curtain tester as shown in Figure 4.1. The coating flow rates were adjusted by the pump settings, which were monitored by a potentiometer. The coating flow rates were set as low as possible in order to keep the coat weight reasonable, in the meantime still forming a curtain. Coatings were not recirculated as the water guides were employed to maintain a stable curtain. A pre-coated linerboard was coated at the speeds up to 300 m/min.

Figure 4.1: Curtain stability tester with a slide-fed die.

All coated samples were conditioned according to TAPPI standard T402. Then, they were tested in terms of coat weight, brightness, gloss 75°, and IGT dry pick strength. The measurements of brightness and gloss 75° followed TAPPI standards T452 and T480 respectively. The dry pick strength was measured by using the IGT pick tester in the condition of 23°C and 11.5% RH. An orange Lorilleux ink with viscosity of 44 Pa.s was used and the pick velocity was set at 3 m/s.

Results and Discussion

The basic properties of all the coatings are shown in Table 4.4. It shows that the addition of petro-based extensional viscosity modifier resulted in higher viscosity than that of the inorganic rheology modifiers. By increasing the amounts of surfactant, the surface tension of coatings containing inorganic rheology modifiers was controlled to be around 40 mN/m. The pH values of some coatings are slightly higher than the target 8-9.

Table 4.4: Basic coating properties.				
Sample	**pH**	**Solids (%)**	**Brookfield viscosity at 100 rpm (mPa.s)**	**Surface tension at 5 s (mN/m)**
LAX-1	9.2	60.1	410	41.7
XSB-3	9.0	60.5	410	49.0
ES(1)	8.5	60.6	390	43.2
ES(2)	8.5	60.5	440	43.0
EA(1)	9.3	60.7	340	42.6
EA(2)	8.9	60.7	340	36.0
EB(1)	9.0	60.7	240	33.0
EB(2)	9.4	60.5	230	35.3

On the slide-fed curtain tester, all coatings were able to form stable curtains, although the operable pump setting ranges, i.e. coating flow rate ranges, were different. Among all the coatings, coatings XSB-3 and EB(1) formed stable curtains with the largest pump setting ranges, 15-75 and 25-48 respectively. The correlation between pump setting/density and coat weights was plotted in Figure 4.2. During the tests, it was observed that the coatings containing inorganic rheology modifier formed more stable curtains at higher latex replacement level (EA(1) *vs.* EA(2) and EB(1) *vs.* EB(2)). In addition, two coat weights, 15 gsm and 20 gsm, was obtained with coating EA(2) , which were denoted as EA(2)-15 and EA(2)-20 respectively in the Figures 4.3-4.5.

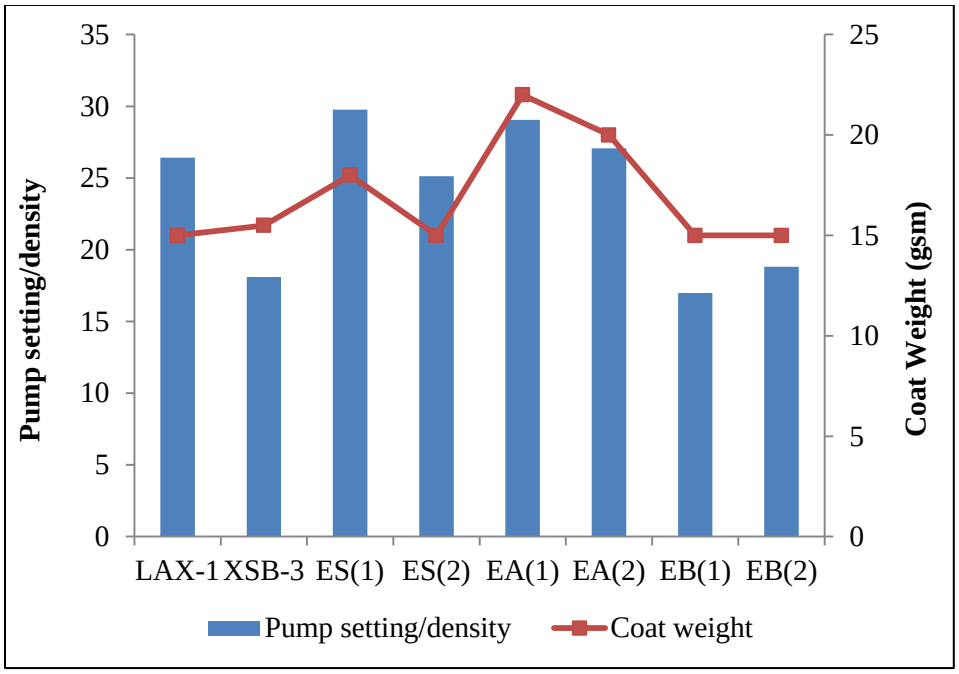

Figure 4.2: The correlation between the pump setting/density and coat weight.

The correlation between brightness and coat weights of the coated samples is shown in Figure 4.3. By applying different coatings, the brightness of the linerboard increased in different degrees. The comparison between two controls (LAX-1 *vs.* XSB-3) shows that the coating with petro-based latex-2 gave a higher brightness to the linerboard than that with petro-based latex-1. In the presence of petro-based extensional viscosity modifier, the coating with 35% latex replacement (ES(2)) resulted in higher brightness with lower coat weight than coating containing 25% latex replacement (ES(1)). However, opposite effects on the brightness were found by replacing the petro-based extensional viscosity modifier with inorganic rheology modifiers (EA(1) *vs.* EA(2)-20), (EB(1) *vs.* EB(2)). In addition, only the coatings containing biobased latex and inorganic rheology

modifier B show comparable or even better brightness than the control coating LAX-1 at the same coat weight level.

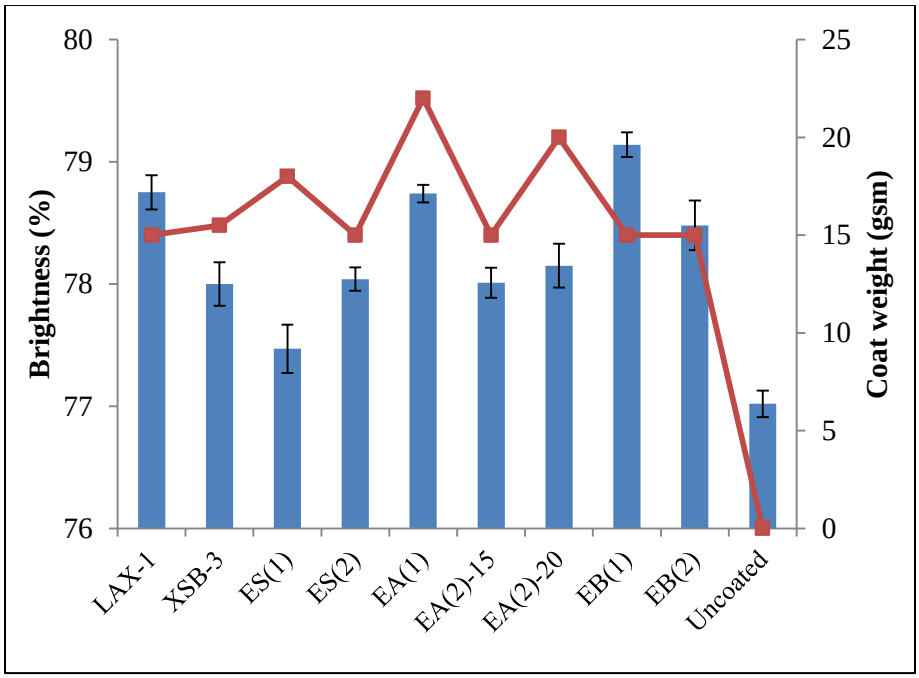

Figure 4.3: The correlation between brightness and coat weights of all coated samples.

In Figure 4.4, no significant change in gloss was caused by switching the latex type in the control coatings (LAX-1 *vs.* XSB-3) both of which lowered the gloss of the linerboard. The combination of biobased latex and petro-based extensional modifier resulted in higher gloss than the control (ES(1) and (2) *vs.* LAX-1) and this impact was enhanced by increasing the latex replacing level (ES(1) *vs.* ES(2)). In the presence of inorganic rheology modifier A, increasing the latex replacement percentage from 25% to 35% in the coatings improved the gloss of the coated samples (EA(1) *vs.* EA(2)-20), which was also found in the coatings containing inorganic rheology modifier B (EB(1) *vs.*

EB(2)). Among all the coated samples, only the two that coated by the biobased latex coatings containing inorganic rheology modifier B showed comparable gloss with the base. It is reasonable to suspect that the resultant low gloss was caused by improper coating immobilization on the linerboard, which did not allow the pigments to align and form a smooth surface.

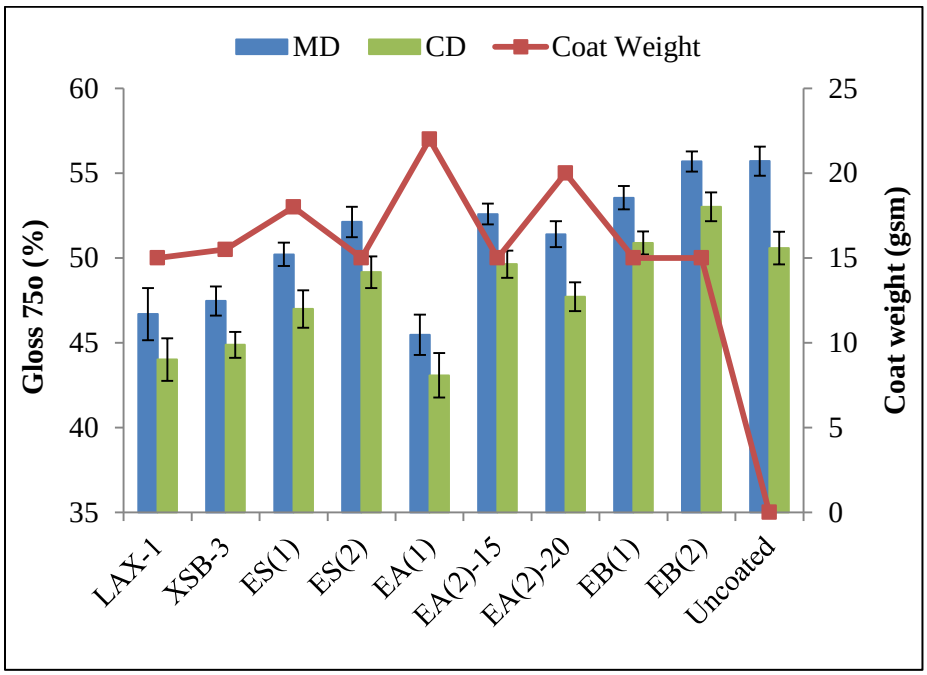

Figure 4.4: The correlation between gloss (MD and CD) and coat weights of all coated samples.

In Figure 4.5, it is obvious that petro-based latex-1 can maintain the linerboard strength better than petro-based latex-2 (XSB-3 *vs*.LAX-1). It was also found that coatings EA(2)-15, EB(1) and EB(2) provided similar strength to the linerboard as the control coating LAX-1 with similar coat weights. With the same amount of petro-based

extensional viscosity modifier, the sample coated by the coating with higher latex substitution was stronger than its counterpart (ES(1) *vs.* ES(2)). No significant difference in dry pick strength was found between the coatings containing different amounts of biobased latex and inorganic rheology modifiers.

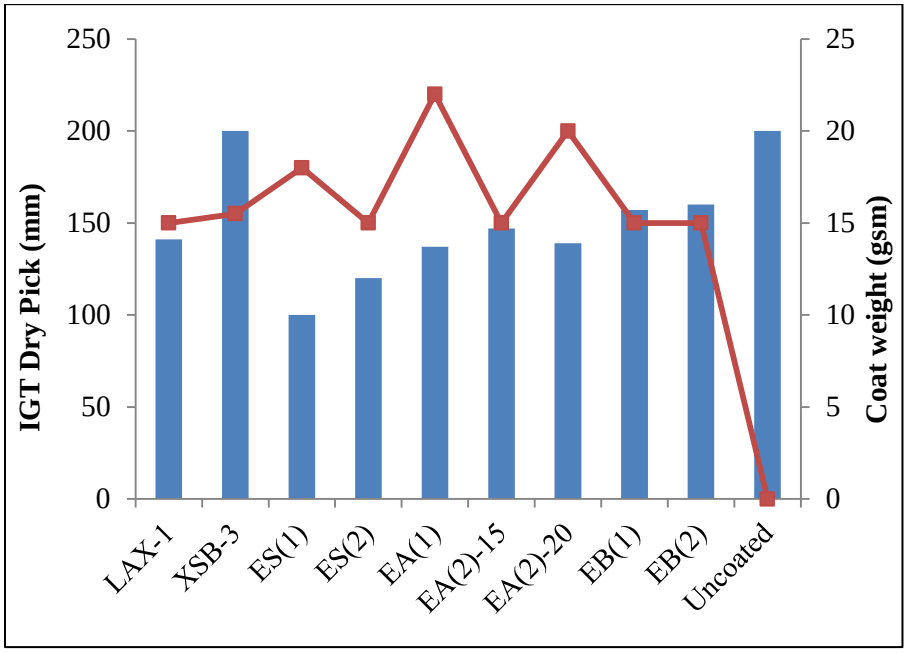

Figure 4.5: The correlation between IGT dry pick strength and coat weights of all coated samples.

Conclusions

Based on the comparable or even better curtain stability and the properties of the coated linerboard, it can be concluded that petro-based latex-1 is more compatible with biobased latex in the curtain coatings and it also requires less surfactant to achieve the coating surface tension lower than 40 mN/m.

All coatings formulated in this study formed stable curtains on the slide-fed curtain tester, wherein increasing the latex replacement in the coatings with inorganic rheology modifier can improve the curtain stability.

In the comparison of the biobased latex coatings and the control coating, the addition of petro-based extensional viscosity modifier only improved the gloss of the coated linerboard. The addition of inorganic rheology modifier A in the biobased latex binder containing coatings resulted in similar IGT dry pick strength as the control but its effects on the brightness and gloss of the coated linerboard depended on the relative amounts of the biobased latex binder and the inorganic rheology modifier. The two coatings containing inorganic rheology modifier B (EB(1) and EB(2)) are most promising due to their superior brightness, gloss, and IGT dry pick strength to their counterparts, which are also comparable or even better than the control coating.

References

1. Schweizer, P. (2003): “Curtain coating-stability a critical operating parameter”, 4th and 5th PITA Coating Conference, Edinburgh, UK.
2. Miyamoto, K. and Katagiri, Y. (1997) “Curtain Coating”, Chapter 11c in “Liquid film coating: scientific principles and their technological implications”, ed. Kistler, S.F. and Schweizer, P.M., Chapman & Hall, London.

3. Kistler, S.F. (1983): “The fluid mechanics of curtain coating and related viscous free surface flows with contact lines”, Ph.D. thesis, University of Minnesota, Minneapolis and University Microfilms International, Ann Arbor, MI.
4. Schmid, M. (2011): “Curtain coater as air knife replacement”, TAPPI PaperCon, New Orleans, USA.
5. Valmet: “Layering curtain coating”, retrieved on 4/14/2015, from http://www.valmet.com/en/products/paper_board.nsf/WebWID/WTB-090514-2256F-5B3F0?OpenDocument#.VD07d_mzHmo
6. Taylor, L.H. (1903): “Machine for production of solidification forming nutriment with whole cover as confectionery and pie”, German Patent Publication DE145517.
7. Poirier, C.C. (1966): “Curtain coating of corrugated paperboard”, TAPPI J., 49(10): p. 66-67.
8. Tripathi, P., Joyce, M., Fleming, P.D. and Sugihara, M. (2009): “A statistical study of process variables to optimize a high speed curtain coater-Part I”, TAPPI J., 8(1): p. 20-26.
9. Tripathi, P., Joyce, M., Fleming, P.D. and Sugihara, M. (2009): “A statistical study of process variables to optimize a high speed curtain coater-Part II”, TAPPI J., 8(2): p. 29-32.
10. Kistler, S.F. and Scriven, L.E. (1994): “The teapot effect: sheet-forming flows with deflection, wetting and hysteresis”, J. Fluid Mech. 263: p. 19-62.

11. Klass, C. (2013): “Blade, rod and contour coaters”, Coating Short Course, Western Michigan University.
12. Suga, Y., Kobayashi, K., Sasahara, T. and Miyamoto, M. (1991): “Coating method”, European Patent EP 426122 A2.
13. Chen, T., Joyce, M., Fleming, P.D., Bloembergen, S. (2016): “Pigmented formulations containing biobased nanoparticle binders for curtain coating applications; Part 1: rheological study”, Paper submitted for presentation and publication to TAPPI PaperCon2016.
14. Chen, T., Joyce, M., Fleming, P.D., Bloembergen, S. (2016): “Pigmented formulations containing biobased nanoparticle binders for curtain coating applications; Part 2: curtain stability analysis”, Paper submitted for presentation and publication to TAPPI PaperCon2016.
15. Triantafillopoulos, N., Grön, J., Luostarinen, I., and Paloviita, P. (2004): “Operational issues in high-speed curtain coating of paper, Part 1: The principles of curtain coating”, TAPPI J., 3(11): p.6-10

CHAPTER V

CONCLUSIONS AND OUTLOOK

This research thoroughly examined the influences of coating rheological properties, as well as surface tension, on the stability of curtain formed through a slot die. In this discussion, the effects of the interactions between different components in the coatings on these coating properties were revealed. The different functions of the conventional petro-based extensional viscosity modifier in the all-synthetic latex coatings and the partial biobased latex coatings were investigated and its replacement with two inorganic rheology modifiers in the biobased latex coatings was confirmed. It was also found that the functionality of these modifiers not only depend on their type, but also the ratio of them and biobased latex in the formulation.

By interpreting the results of curtain stability with coating properties obtained, the relative importance of coating surface tension, shear rate dependence of viscosity, viscoelasticity and elastic component, as well as extensional viscosity to the curtain stability at different flow rates was determined. It was found that a coating with relatively low surface tension (< 40 mN/m) and shear viscosity required a more elastic structure and/or higher extensional viscosity to form a stable curtain, especially at higher flow rates, where shear thinning plays a more critical part. For the coatings with similar surface tension and shear thinning behavior, the one of low shear viscosity is more ready to

deform, which requires more elastic coating structure and/or high extensional viscosity to maintain the curtain stable, especially at high curtain flow rates.

We also highlighted the effects of different rheology modifiers on the coating extensional viscosity by using CaBER technology. A significant correlation between the surface tension and the CaBER filament lifetime was found in different coating groups. A new method called SPOT (Squeeze/Pull-off Test) using a dynamic stress rheometer was demonstrated to be convenient and effective for the evaluation of coating extensional viscosity.

The experimental coatings in this study also showed comparable or even better curtain stability and coatability on a slide die. After that, the properties of coated linerboard were evaluated in terms of coat weight, gloss, brightness, and IGT dry pick strength. Two coatings containing inorganic rheology modifier B, and 25% and 35% biobased latex are most promising, due to their superior brightness, gloss, and dry pick strength to their counterparts, which are also comparable or even better than the control coating.

Based on the findings of this study, it is recommended not to overly emphasize the importance of extensional viscosity but to consider the possible trade-offs among different characteristics of the curtain coating. It is also necessary to further integrate their relative contributions in the quantified analysis of curtain stability and operability, e.g. in the operational window of a curtain coater, for a mill-scale operation. As a more

convenient method to determine the coating extensional viscosity than CaBER, the novel SPOT method is worth being promoted in the paper coating industry.

As to the formulations of biobased latex coating, it would be helpful to conduct a study with the coatings containing the same amounts of one of two inorganic rheology modifiers at each latex replacement level. By comparing their rheological properties, as well as dynamic/static surface tension, it could help researchers to further understand the various interactions between different coating components revealed in this study and to provide a guideline for the biobased latex coating formulation in the application of curtain coater.

Overall, this research has shown the big potential of biobased latex to replace synthetic latex in the application of curtain coating. It is believed that the findings not only can advance the understanding of the various coating characteristics contributing to the runnability and coatability of curtain coating, but also optimize the biobased latex coatings for the commercial mill operations in the future.

Appendix A

Data Obtained from SPOT Experiments.					
Coating	**Weight/g**	**Gap/µm**			**Normalized Delta Gap µm/g**
		Beginning	**End**	**Delta**	
XSB-1	0.6404	1262	4388	3126	4881.32
	0.6489	1201	4327	3126	4817.38
	0.6247	1198	4166	2968	4751.08
				Avg.	4816.60
				Std.	65.13
XSB-3	0.6715	1386	5517	4131	6151.90
	0.6435	1165	5278	4113	6391.61
	0.6560	1200	5194	3994	6088.41
				Avg.	6210.64
				Std.	159.91
EX-1	0.7080	1413	5853	4440	6271.19
	0.6800	1250	5442	4192	6164.71
	0.6589	1310	5450	4140	6283.20
				Avg.	6239.70
				Std.	65.22

Table-Continued					
Data Obtained from SPOT Experiments.					
EX-2	0.6619	1201	5711	4510	6813.72
	0.6423	1262	5694	4432	6900.20
	0.6521	1169	5605	4436	6802.64
				Avg.	6838.85
				Std.	53.42
EX-3	0.7089	1407	5843	4436	6257.58
	0.6813	1247	5431	4184	6141.20
	0.6600	1325	5434	4109	6225.76
				Avg.	6208.18
				Std.	60.15
EA-1	0.6739	1384	5379	3995	5928.18
	0.6740	1299	5301	4002	5937.69
	0.6688	1275	5271	3996	5974.88
				Avg.	5946.92
				Std.	24.68

Table-Continued					
Data Obtained from SPOT Experiments.					
EA-2	0.6743	1369	5449	4080	6050.72
	0.6631	1227	5266	4039	6091.09
	0.6556	1238	5273	4035	6154.67
				Avg.	6098.82
				Std.	52.40
EA-3	0.6593	1321	5323	4002	6070.07
	0.6637	1153	5161	4008	6038.87
	0.6509	1169	5162	3993	6134.58
				Avg.	6081.18
				Std.	48.81
EB-1	0.6019	1199	4833	3634	6037.55
	0.6032	1166	4834	3668	6080.90
	0.6039	1240	4749	3509	5810.56
				Avg.	5976.34
				Std.	145.19

Table-Continued					
Data Obtained from SPOT Experiments.					
EB-2	0.6076	1252	4893	3641	5992.43
	0.6050	1246	4875	3629	5998.35
	0.6147	1196	4784	3588	5836.99
				Avg.	5942.59
				Std.	91.50
EB-3	0.6909	1344	5450	4106	5942.97
	0.6803	1270	5274	3944	5797.44
	0.6754	1116	5060	4004	5928.34
				Avg.	5889.58
				Std.	80.13

Appendix B

Data Obtained from the Analysis of Slot-fed Curtain Stability.							
XSB-1	**Pump speed%**		20	25	30	35	40
	Mass flow rate g/s		35.68	49.10	57.63	59.85	64.28
	Density g/mL		1.5	1.42	1.37	1.24	1.18
	Volumetric Flow Rate mL/s		23.79	34.58	42.06	48.27	54.47
	Mach angle/degree	**Avg.**	29.24	25.43	23.23	22.61	21.44
		Std.	0.49	0.12	0.37	0.53	0.19
	Weber No.	**Avg.**	4.09	4.66	5.07	5.20	5.47
		Std.	0.06	0.02	0.08	0.12	0.05
XSB-3	**Pump speed%**		16	25	30	35	40
	Mass flow rate g/s		27.21	52.60	64.15	73.50	75.00
	Density g/mL		1.53	1.5	1.49	1.42	1.33
	Volumetric Flow Rate mL/s		17.78	35.07	43.06	51.76	56.39
	Mach angle/degree	**Avg.**	35.20	23.66	22.28	21.25	20.51
		Std.	0.37	0.57	0.59	0.22	0.25
	Weber No.	**Avg.**	3.47	4.99	5.28	5.52	5.71
		Std.	0.03	0.11	0.13	0.06	0.07

Table-Continued							
Data Obtained from the Analysis of Slot-fed Curtain Stability.							
EX-1	**Pump speed%**		20	25	30	35	40
	Mass flow rate g/s		34.30	41.52	59.25	66.67	69.36
	Density g/mL		1.49	1.36	1.5	1.45	1.36
	Volumetric Flow Rate mL/s		23.02	30.53	39.50	45.98	51.00
	Mach angle/degree	**Avg.**	32.19	25.37	22.06	20.54	20.53
		Std.	0.81	0.76	0.47	0.05	0.22
	Weber No.	**Avg.**	3.76	4.67	5.33	5.70	5.70
		Std.	0.08	0.13	0.11	0.01	0.06
EA-1	**Pump speed%**		20	25	30	35	40
	Mass flow rate g/s		32.07	48.33	61.32	67.84	74.21
	Density g/mL		1.36	1.49	1.49	1.41	1.35
	Volumetric Flow Rate mL/s		23.58	32.43	41.15	48.11	54.97
	Mach angle/degree	**Avg.**	28.06	24.43	22.70	22.20	20.06
		Std.	0.049	0.270	0.357	0.352	0.316
	Weber No.	**Avg.**	4.25	4.84	5.18	5.30	5.83
		Std.	0.007	0.050	0.077	0.080	0.088

Table-Continued							
Data Obtained from the Analysis of Slot-fed Curtain Stability.							
EA-2	**Pump speed%**		24	28	30	35	40
	Mass flow rate g/s		46.02	45.05	59.98	65.19	69.67
	Density g/mL		1.49	1.28	1.43	1.34	1.3
	Volumetric Flow Rate mL/s		30.88	35.19	41.95	48.65	53.59
	Mach angle/degree	**Avg.**	24.40	21.64	21.69	20.41	19.44
		Std.	0.266	0.198	0.251	0.247	0.231
	Weber No.	**Avg.**	4.84	5.42	5.41	5.74	6.01
		Std.	0.050	0.047	0.060	0.067	0.069
EA-3	**Pump speed%**		22	25	30	35	40
	Mass flow rate g/s		39.64	47.46	57.11	62.14	64.24
	Density g/mL		1.46	1.44	1.38	1.29	1.21
	Volumetric Flow Rate mL/s		27.15	32.96	41.39	48.17	53.09
	Mach angle/degree	**Avg.**	25.25	22.34	20.01	19.11	17.87
		Std.	0.257	0.311	0.184	0.840	0.346
	Weber No.	**Avg.**	4.69	5.26	5.85	6.12	6.52
		Std.	0.044	0.070	0.052	0.259	0.122

Table-Continued							
Data Obtained from the Analysis of Slot-fed Curtain Stability.							
EB-2	**Pump speed%**		22	27	32	37	42
	Mass flow rate g/s		40.57	52.98	64.92	71.57	75.01
	Density g/mL		1.52	1.46	1.4	1.39	1.2
	Volumetric Flow Rate mL/s		26.69	36.29	46.37	51.49	62.51
	Mach angle/degree	**Avg.**	28.34	23.41	22.49	20.26	19.54
		Std.	0.983	0.571	0.098	0.496	0.271
	Weber No.	**Avg.**	4.22	5.04	5.23	5.78	5.98
		Std.	0.136	0.115	0.022	0.134	0.080